TECHNIQUES FOR THE TOP SQUARK SEARCH AT THE FERMILAB TEVATRON

A DISSERTATION SUBMITTED TO THE GRADUATE DIVISION OF THE UNIVERSITY OF HAWAI'I IN PARTIAL FULFILLMENT OF THE REQUIREMENTS FOR THE DEGREE OF

DOCTOR OF PHILOSOPHY

IN

PHYSICS

AUGUST 2000

By
John Sender

Dissertation Committee:

Xerxes Tata, Chairperson
Sandip Pakvasa
Michael Peters
Chester Vause
Robert Joseph

We certify that we have read this dissertation and that, in our opinion, it is satisfactory in scope and quality as a dissertation for the degree of Doctor of Philosophy in Physics.

DISSERTATION COMMITTEE

Chairperson

Abstract

This dissertation addresses the question of how to detect light top squarks at the upgraded Fermilab Tevatron collider. After a brief introduction to supersymmetry, the basic phenomenology of the light stop is reviewed and the current experimental situation is surveyed. The analysis presented here is based on collider event simulations. The main decay modes accessible to the Tevatron are studied, feasible discovery channels are identified, and recipes for experimental analysis are proposed. It is found that stops with masses up to the top quark mass are liable to detection under these schemes with the data from a few years' running at the upgraded Tevatron. With such an extended run, significant portions of parameter space may be probed.

Table of Contents

List of Tables

List of Figures

Chapter 1

Introduction to Supersymmetry

This thesis investigates strategies for detecting a top squark (also referred to as the scalar top or, for short, stop) at the Fermilab Tevatron $p\bar{p}$ collider. The top squark is a representative of a new class of particles in the theory of supersymmetry. It is thought by some that the stop could be one of the most accessible particles of this class, and experimental physicists have invested a great deal of effort in the search for this particle.

We begin in this Chapter with an introduction to supersymmetry and a brief exposition of its attractions for particle physicists. We characterize the class of practical supersymmetry models and offer a synopsis of the phenomenology relevant to our study. Then we introduce the top squark and discuss its properties in Chapter 2. We present the basic formulae and indicate how the particle may be light, and also why it might be expected to be light. We summarize the production and decay modes of the stop, and include a *précis* of current experimental results on the stop and other supersymmetric particles important to our work. In Chapter 3, we describe calculational techniques and the methodology of our analysis.

Our analysis of how experiments at the Tevatron may search for the stop begins in Chapter 4 with an investigation of the decay mode $\tilde{t}_1 \to c\widetilde{Z}_1$. We review the event topology and identify physics background processes which can mask its signal. We look in several channels, and by examining key kinematical features of the stop events we are led to propose a program of experimental procedures designed to maximize the discovery potential of the stop decays via this mode. We perform a similar study for the decay mode $\tilde{t}_1 \to b\widetilde{W}_1$ in Chapter 5. Our conclusions and some summary remarks on the prospects for uncovering the stop at the Tevatron are presented in Chapter 6.

1.1 Supersymmetry as a fundamental symmetry of nature

The body of data presently available from investigations into the fundamental constituents of matter is consistent with a theoretical framework known as the Standard Model (SM) of particle physics. All observed particles and forces (apart from gravity) are encompassed by this theory. The SM is a relativistic quantum field theory which organizes elementary particles and the forces which act upon them according to the principles of gauge symmetry[95]. Despite its success, though, the Standard Model has not furnished a satisfyingly complete explanation of the realm of elementary particles. There are many *ad hoc* parameters, and difficulties arise when the theory is extrapolated to energies much beyond a TeV (in the sense explained below) without some modification. The Standard Model also affords no link between the gauge forces and the force of gravity.

Supersymmetry (SUSY)[82, 81, 65] is a proposed new symmetry of particle interactions which generalizes the symmetries of space-time. The usual space-time

symmetries are encoded in a set of commutation relations for the generators of translation P_m and rotation M_{mn}[96]:

$$\begin{aligned}[M_{mn}, M_{pq}] &= g_{np}M_{mq} - g_{mp}M_{nq} - g_{nq}M_{mp} + g_{mq}M_{np}, \\ [M_{mn}, P_q] &= g_{nq}P_m - g_{mq}P_n, \quad [P_m, P_n] = 0,\end{aligned} \tag{1.1}$$

with g_{mn} the metric tensor. These commutation relations constitute a Lie algebra for the operators, called the Poincaré algebra. With reasonable assumptions, Coleman and Mandula[45] showed that any Lie group that contains both the Lie group underlying the Poincaré algebra (the Poincaré group) and an internal symmetry group must be just a direct product of the Poincaré group and that symmetry group. There is thus no non-trivial extension of the Poincaré group, and one can say that the Poincaré algebra is the most general Lie algebra of space-time symmetries.

The notion of a Lie algebra can be extended to that of a *graded* Lie algebra by admitting anticommutators in addition to commutators. The SUSY algebra comes from adding so-called "supersymmetry" generators Q^a to the Poincaré algebra (1.1) satisfying the (anti)commutation relations

$$\begin{aligned}\left\{Q^a, \bar{Q}^b\right\} &= (\gamma^m)^{ab} P_m, \quad \left\{Q^a, Q^b\right\} = 0 \\ [P_m, Q^a] &= 0, \quad [M_{mn}, Q^a] = \tfrac{1}{2} (\sigma_{mn} Q)^a ,\end{aligned} \tag{1.2}$$

where γ and σ are the usual elements of the Dirac calculus. Haag, Łopuszanski and Sohnius[64] extended the work of Coleman and Mandula to show that the SUSY algebra of equations (1.1) and (1.2) constitutes the most general graded Lie algebra of space-time symmetries.

The SUSY generators in (1.2) are spinorial. Spinors, though non-classical, are indispensable in field theories of matter as we know it. They furnish the representation for electrons (and all matter particles), but under the algebra (1.1) they are contingent objects in space-time. SUSY builds spinors into the structure of

space-time itself and so confers on them an ontological status more befitting their fundamental role. Metaphysically, this is tidier.

In the usual SUSY scheme the transformations of equation 1.2 are global. If we promote these to a *local* symmetry then remarkably we derive the general coordinate transformations of general relativity, and find spin-2 gravitons in the theory[49][60]. Local supersymmetry necessarily leads to quantum gravity. No one has yet been able to write down a consistent field theory of quantum gravity to capitalize on this fact, but it is intriguing and suggests that SUSY may have a basic role to play in the unification of the gauge forces with gravity. The glamorous "superstring" theory, which *is* a finite theory of quantum gravity, is founded on space-time supersymmetry.

The notion of unification is on a par with symmetry as a fundamental organizational principle in physics, as exemplified by Newton's identification of terrestrial and planetary gravity, Maxwell's synthesis of electricity and magnetism into a single field, or Einstein's equivalence of gravitational and inertial mass. In particle physics we can point to the unification[1] of the electromagnetic and weak forces in Glashow, Salam and Weinberg's electroweak theory, which is a cornerstone of the Standard Model. Physicists now anticipate a Grand Unified Theory (GUT) which can unify the strong force with the electroweak theory, and a "Theory of Everything" (TOE) which will unite these with gravity.

In the simplest GUT first proposed by Georgi and Glashow[61] (following some work of Pati and Salam[84]), the gauge groups are unified as $SU(3)_C \times$

[1]Many do not count GSW theory as a proper unification, since one needs as many parameters with the theory as without; it is, however, a satisfying *conceptual* unification that puts the electromagnetic and weak forces on a common footing and serves as a model for GUT unification.

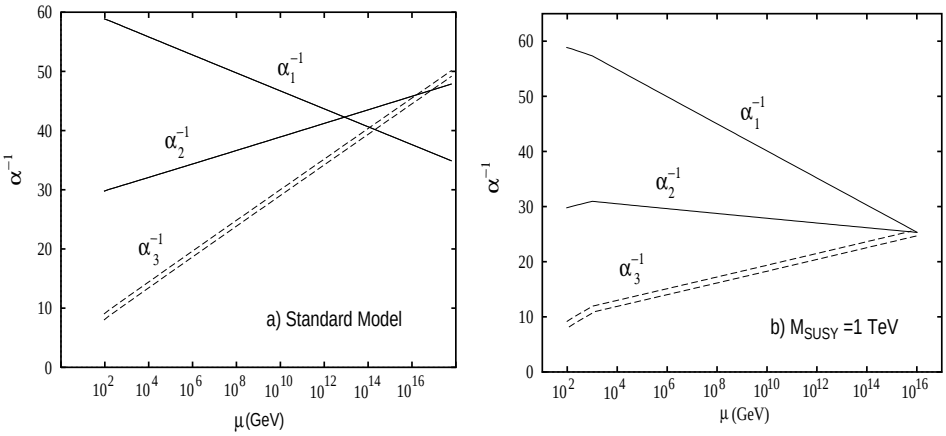

Figure 1.1: Gauge coupling unification in (a) the Standard Model and (b) the MSSM with sparticle threshold at 1 TeV. Figure reproduced from [32].

$SU(2)_L \times U(1)_Y \subset SU(5)$. The running couplings of the three low-energy gauge groups are predicted to converge at a high scale where the full SU(5) symmetry is restored. Precision measurements of the gauge couplings at M_Z by the CERN e^+e^- collider LEP are consistent with supersymmetric SU(5)[22, 32] (because of quantum corrections due to SUSY particles lying in mass between the weak and GUT scales), but not with minimal *non*supersymmetric grand unification.

This fact is suggestive. But whether or not SU(5) is the unification group, and even if nature "unifies" without grand unification, as in string models, SUSY theories generically fix a problem common to nonsupersymmetric theories. This flaw, the hierarchy problem[92], comes from quadratically divergent quantum corrections to masses of scalar particles such as the SM Higgs (since there is no symmetry in the SM to protect the scalar masses the way chiral and gauge symmetries, respectively, protect fermion and vector boson masses). This divergent contribution is due to the diagrams shown in Fig. 1.2. If there were no new physics whatsoever beyond the SM, then this divergence would be uncontrolled. So the SM must break down

at *some* scale, where new physics intervenes. Very general considerations suggest, for instance, that field theories in which gravitation is not incorporated cannot be extrapolated beyond the Planck scale ($\sim 10^{19}$GeV), where gravitational interactions are of the same strength as gauge interactions. New physics must enter here, or perhaps at the somewhat lower gauge coupling unification scale $\sim 10^{16}$ GeV.

Perturbative unitarity arguments[50, 76] require the Higgs mass to be less than a few hundred GeV. Keeping the Higgs mass at this scale while integrating the quadratic divergence up to, say, $\Lambda \sim 10^{16}$ GeV would require introducing a counterterm into the Lagrangian that must be fine-tuned to an accuracy of $(100\ \mathrm{GeV}/\Lambda)^2 \sim 10^{-26}$. While not a logical impossibility, this is repugnant to many physicists. In order to avoid an unnatural fine-tuning, the scale of new physics cannot be much larger than $\Lambda \sim 1$ TeV. If supersymmetric particles have masses at this scale, then they can do the job since by the nonrenormalization theorem of Grisaru, Rocek and Siegel[62], the scalar masses in SUSY theories are not quadratically divergent even if SUSY is spontaneously or softly broken[2]. The quadratically divergent contributions from scalars in loops are exactly cancelled by contributions from the scalars' superpartners above the SUSY restoration scale, illustrated in Fig. 1.2. Supersymmetry is the only symmetry known which offers generic protection to the scalar masses from the quadratic instability to radiative corrections.

Of course, supersymmetry is not the only extension to the SM which has been proposed. Popular alternatives in the literature include technicolor[92] and compositeness[85]. These are attractive theories but they seem to be ruled out in

[2] "Soft" SUSY breaking terms are just those that do not lead to the reappearance of quadratic divergences in the scalar masses; these include explicit mass terms for scalars (e.g., to lift the quark/squark degeneracy), trilinear scalar interactions (important in the stop sector), and others[63].

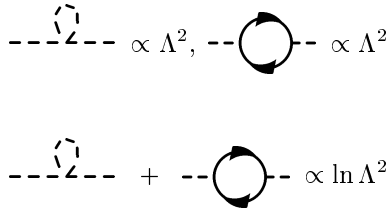

Figure 1.2: Diagrams relevant to the SUSY nonrenormalization theorem. The scalar loops diverge quadratically, as do the fermion loops. Under supersymmetry these contributions cancel, and the result diverges only logarithmically.

their simplest forms. They are strongly coupled theories, like QCD, and are often not amenable to calculation[3]. SUSY on the other hand is a weakly coupled theory whose couplings mainly derive from the SM gauge couplings in a canonical way. SUSY diagrams are calculable in perturbation theory, and in fact a wide range of computer tools exists for this purpose [27, 79, 73, 78].

That supersymmetry addresses such a wealth of physics issues with such economy brings to mind Hertz' comment on Maxwell's equations quoted by Freeman Dyson[57] (from [80]):

> One cannot escape the feeling that these mathematical formulae have an independent existence and an intelligence of their own, that they are wiser than we are, wiser even than their discoverers, that we get more out of them than was originally put into them.

1.2 The minimal supersymmetric standard model

An immediate consequence of the spinorial nature of the supersymmetry generator is that SUSY transforms bosons and fermions into each other. A supersymmetric

[3]the unreasonable *in*effectiveness of mathmatics in the natural sciences, to paraphrase Eugene Wigner[97].

	spin 0	spin 1/2	spin 1
left-handed matter	$\begin{pmatrix} \tilde{u}_L \\ \tilde{d}_L \end{pmatrix}, \begin{pmatrix} \tilde{\nu}_L \\ \tilde{e}_L \end{pmatrix}$	$\begin{pmatrix} u_L \\ d_L \end{pmatrix}, \begin{pmatrix} \nu_{eL} \\ e_L \end{pmatrix}$	
right-handed matter	$\tilde{u}_R, \tilde{d}_R, \tilde{e}_R$	u_R, d_R, e_R	
Higgs sector	$\begin{pmatrix} H_d^0 \\ H_d^- \end{pmatrix}, \begin{pmatrix} H_u^+ \\ H_u^0 \end{pmatrix}$ $\Longrightarrow h, A, H^0, H^\pm$	$\widetilde{H}_u, \widetilde{H}_d, \widetilde{B}, \widetilde{W}$ $\Longrightarrow$ $\widetilde{Z}_i \quad (i = 1, 2, 3, 4)$, $\widetilde{W}_j^\pm \quad (j = 1, 2)$	
electroweak gauge bosons			$B, \begin{pmatrix} W^1 \\ W^2 \\ W^3 \end{pmatrix}$ $\Longrightarrow \gamma, Z, W^\pm$
gluon		$\tilde{g}$	g

Table 1.1: MSSM particle content. Only the first generation of matter particles is shown; the second and third generations are replicas of this.

theory must contain for each fermion a boson with identical quantum numbers, and vice versa. Spin-$\frac{1}{2}$ matter fermions get spin-0 partners, and the spin-0 Higgs bosons and spin-1 gauge bosons get spin-$\frac{1}{2}$ partners. The minimal extension of the SM needed to do the job has the particle content listed in Table 1.1. This generic SUSY model is called the Minimal Supersymmetric Standard Model (MSSM). Supersymmetric particles are marked with tildes. By convention, fermionic superpartners of SM bosons take the suffix "ino," and scalar counterparts of SM fermions have the prefix "s" (short for "SUSY"). The term "sparticle" refers to any of these supersymmetric particles.

Matter fermions are represented by Dirac spinors and have four degrees of freedom, while (complex) scalars have only two, so each fermion f is associated with a pair of scalars. Conventionally these are chosen to be the sparticles corresponding to the fermion's two helicity states, and are written as $\tilde{f}_L$ and $\tilde{f}_R$. (This notation

is perhaps confusing since scalars of course have no chirality; it is still true, though, that only $\tilde{f}_L$ couples to the W (as also only f_L).) The particle studied in this thesis is the lighter supersymmetric partner of the top quark (a linear combination of $\tilde{t}_L$ and $\tilde{t}_R$), variously called a top squark, scalar top, or stop. For brevity, we use "stop" in the present work.

The only new non-supersymmetric content in Table 1.1 is an extra Higgs doublet, placing the MSSM in the class of Two Higgs Doublet Models (2HDMs). In the Standard Model, three of the Higgs doublet's (real) degrees of freedom go to supply longitudinal polarization for the electroweak gauge bosons, leaving a single neutral scalar Higgs. In 2HDMs similarly $8 - 3 = 5$ states remain for physical particles: two CP even Higgs bosons, a CP odd Higgs boson, and a pair of charged Higgs.

This extra Higgs doublet is a consequence of consistently applying supersymmetric field theory. The technique involved—the so-called superfield formalism—is too lengthy to go into here, but many standard treatments exist (see [70] and references therein). One writes down the most general supersymmetric Lagrangian including soft SUSY breaking terms (which lift the mass degeneracy of superpartners) consistent with Poincaré and gauge invariance. With this treatment it is easy to see that SUSY requires separate Higgs fields to couple to up-type and down-type quarks. An immediate consequence of this fact is the introduction of two new fundamental parameters. One is the ratio of the VEVs for the two Higgs scalars, $\tan\beta = v_{\mathrm{u}}/v_{\mathrm{d}}$. The other is a higgsino mixing parameter μ which parameterizes the coupling $\mu\widetilde{H}_u\widetilde{H}_d$; μ is required to be non-zero to prevent problems due to a light higgsino.

The fermionic partners of the SM photon (photino), Z boson (zino) and two neutral Higgses (higgsinos) all share the same $\mathrm{SU(3)}\times\mathrm{U(1)_{em}}$ quantum numbers and will, therefore, mix if electroweak symmetry is broken. The resulting states, called neutralinos, are denoted $\widetilde{Z}_1$, $\widetilde{Z}_2$, $\widetilde{Z}_3$ and $\widetilde{Z}_4$ in order of increasing mass[4]. For many phenomenological considerations, it is significant whether the $\widetilde{Z}_1$ has a predominantly gaugino or higgsino character. Since we typically set supersymmetric branching fractions to 100% for the decays we study here, this distinction is largely unimportant for our work. As with the neutralinos, the superpartners of the W and the charged Higgs also mix to form two chargino states, the lighter $\widetilde{W}_1$ and the heavier $\widetilde{W}_2$. The fermionic content that the MSSM adds to the SM (gauginos+higgsinos) is free of chiral anomalies.

General techniques for the construction of supersymmetric particle Lagrangians are discussed in [93]. In their most general form, these SUSY Lagrangians admit gauge-invariant renormalizable lepton- and baryon-number violating interactions, in contrast to the Standard Model. The completely unconstrained MSSM scheme is minimal with respect to particle content, but maximal in terms of parameters—106 new parameters are required in addition to the SM's 18[52]. These new parameters are strongly constrained by current data on CP violation, flavor-changing neutral currents, and lepton flavor non-conservation. Setting these possible phases are all to zero, the resulting theory has 30 new parameters. The MSSM referred to in this thesis is this 30+18 parameter model.

[4]There are two systems of notation for particles in the electroweak gaugino/higgsino sector. In this thesis we call the neutral members of this group $\widetilde{Z}_i$ ($i = 1, 2, 3, 4$) and the charged members $\widetilde{W}_j^{\pm}$ ($j = 1, 2$) (although we usually suppress the charge sign and just write $\widetilde{W}_j$) out of prejudice for the gaugino character of $\widetilde{Z}_{1,2}$ and $\widetilde{W}_1$ expected in the mSUGRA models introduced below. In other works these neutral and charged "inos" are written as $\tilde{\chi}_i^0$ and $\tilde{\chi}_j^{\pm}$, respectively.

B and L conservation leads to a further discrete symmetry of the renormalizable terms in the Lagrangian, R-parity invariance, with quantum number $R = (-1)^{3B+L+2S}$ (where S = spin). All SM particles (plus the second Higgs doublet) are R-even, and all superpartners are R-odd. If R-parity is a good symmetry then sparticles must be pair-produced by collision of SM particles, and a decaying sparticle must have an odd number of sparticles among its decay products. Therefore there must be a lightest supersymmetric particle (LSP) which is stable. Limits on long-lived colored or charged particles require the LSP to be weakly interacting and electrically neutral[54]. The $\widetilde{Z}_1$ is generally taken to be the LSP. (The only other LSP candidate is the scalar neutrino $\tilde{\nu}$, but the sneutrino is disfavored if the LSP is also to constitute the cold dark matter presumed to lie in the galactic halo[72].) In SUSY events at particle colliders, this LSP will escape the detector without interacting, leading to the classic SUSY signature of missing transverse energy $\not{E}_{\mathrm{T}}$.

If SUSY is to solve the hierarchy problem, then the masses of the superpartners of the MSSM cannot be much greater than 1 TeV, and so particle colliders currently in operation (especially the Fermilab Tevatron) or under construction (the CERN LHC) have a good chance of finding some evidence for their existence. This accessible scale of new particle states is small compared to the scale imagined for the mechanisms underlying supersymmetry (from 10^{10} to 10^{19} GeV), and these theories are generically called "low-energy supersymmetry."

1.3 Constrained SUSY models

The MSSM is completely agnostic about physics above the TeV scale of new particle states. The many parameters mentioned in the previous section are so-called "soft"

SUSY breaking parameters, and are written down from very general considerations of the supersymmetric Lagrangian. The parameter space of the general MSSM is too large for viable phenomenological studies, and one therefore turns to more restricted models. Further constraints among these parameters require a theory of physics at energies beyond 1 TeV. There being a paucity of data on physics at such scales, no complete and compelling supersymmetric theory has emerged as yet.

Constraints can be found by considering the nature of supersymmetry breaking. SUSY must of course be broken since no sparticles degenerate in mass with their ordinary partners (e.g., scalar electrons) have been observed. SUSY breaking relying only on the MSSM content of the theory (or even on just the TeV scale with more particles) seems to be infeasible, so models invoke a "hidden" sector of particles which have no SM gauge interactions. In supergravity models, SUSY is broken in this hidden sector, which communicates with the visible sector through gravitational interactions alone. One obtains a simple structure which one assumes is valid at a high energy scale ($M_{\rm GUT}$ or $M_{\rm planck}$) and uses renormalization group equations (RGE) to calculate low energy MSSM parameters. The high energy parameters are usually universal (for instance with gravity-mediated SUSY breaking), and a GUT ansatz affords further simplification by relating gaugino masses.

The minimal supergravity (mSUGRA) models widely used in phenomenological studies are prepared according to this prescription[56]. mSUGRA depends on only four continuous parameters and a sign in addition to the 18 parameters of the SM. These are generally taken to be a universal scalar mass m_0, a universal gaugino mass $m_{1/2}$, a universal trilinear interaction A_0 (sfermion-Higgs-sfermion), the Higgs VEV ratio $\tan\beta$, and the sign of the Higgsino mixing parameter μ:

$$m_0,\ m_{1/2},\ A_0,\ \tan\beta,\ \mathrm{sign}\,(\mu) \tag{1.3}$$

all input at the GUT scale except for $\tan\beta$, which is a weak-scale quantity. The Higgs bosons, which are part of chiral supermultiplets, share the common scalar mass m_0 at the high scale, and are renormalized due to gauge interactions like the doublet sleptons. The Higgs doublet that couples to the top family gets very large negative contributions to its squared mass $m_{H_u}^2$ due to the large top Yukawa coupling (discussed below) which can easily be driven to negative values leading automatically and naturally to radiative electroweak symmetry breaking (EWSB).[5] In mSUGRA the magnitude $|\mu|$ is fixed by requiring EWSB to reproduce the measured Z boson mass.

mSUGRA has many distinctive features, and its phenomenology has been studied extensively. We collect a few facts here which will be useful in our work. Because the high-scale mass parameters are universal and the RGE depend mainly on the known gauge couplings, one gets generic mass relationships such as

$$m_{\tilde{q}}^2 = m_0^2 + m_q^2 + (5-6)m_{1/2}^2 + D\text{-terms} \tag{1.4}$$

where the D-term scale is $M_Z^2/2$. The squark, slepton and gluino masses obey

$$m_{\tilde{q}}^2 = m_{\tilde{\ell}}^2 + (0.7-0.8)\, m_{\tilde{g}}^2 \tag{1.5}$$

(ignoring quark and lepton masses). The lighter neutralinos and lighter chargino are mostly gaugino (rather than higgsino) and one generally has

$$2m_{\widetilde{Z}_1} \approx m_{\widetilde{W}_1} \approx m_{\tilde{g}}/3. \tag{1.6}$$

The relations (1.6) hold because gaugino masses are assumed to unify at the GUT scale.

[5]The electroweak symmetry breaking is automatic and natural, but not miraculous; one still has to input the weak scale by hand into the high energy parameters of the theory.

mSUGRA is just one of a large and growing set of models intended to capture physics at the high scale. There are theories that are more constrained, such as certain superstring-inspired models, in which only one or two free parameters appear. There has also been recent interest in models which vary the different mSUGRA assumptions on universality at the GUT scale. For instance, this may happen if masses unify at M_{Planck} and become non-universal as they run down to M_{GUT}, or if the unifying group is larger than SU(5) and admits additional mass contributions. String models, hypercolor models, and models with novel SUSY breaking mechanisms can also exhibit non-universality. Reference [23] surveys the gross phenomenology of these models. Because the light stop sector depends on relatively few MSSM parameters, our results are not particularly sensitive to the actual physics at the high scale. Our results, as we will see, will broadly depend only on how the stop is assumed to decay.

Chapter 2

The Top Squark

2.1 The light stop

The top quark has recently been detected and its mass measured in the lepton + jets[16, 5, 9], dilepton[15, 7] and all-jets[13] channels. A concise summary of these results is presented in [71] which derives a combined value of $m_t = 174.3 \pm 3.2\,(\text{statistical}) \pm 4.0\,(\text{systematic})$ GeV. For the purpose of our calculations, we adopt $m_t = 175$ GeV.

With such an extraordinary mass, the top family Yukawa interactions are large and comparable to the electroweak gauge interactions. In renormalizing squark masses from the unification scale down to the physical mass scale, this top Yukawa coupling depresses the diagonal masses of the left and right stop states $\tilde{t}_L$ and $\tilde{t}_R$ relative to the masses of the generation 1 and 2 squarks and also allow substantial mixing between the two states[58, 69, 68]. The stop masses come from Higgs superpotential terms

$$f_{\text{MSSM}} \ni \mu \widehat{h}_u^0 \widehat{h}_d^0 + f_t \widehat{t} \widehat{h}_u^0 \widehat{T}^C \tag{2.1}$$

($\widehat{h}_u^0$ and $\widehat{h}_d^0$ are the up- and down-type Higgs superfields, $\widehat{t}$ and $\widehat{T}^C$ are left and right top superfields) and soft SUSY breaking terms

$$\mathcal{L}_{\text{soft SUSY breaking}} \ni A_t f_t \tilde{t}_L H_u^0 \tilde{t}_R^\dagger - m_{\tilde{t}_L}^2 \tilde{t}_L^\dagger \tilde{t}_L - m_{\tilde{t}_R}^2 \tilde{t}_R^\dagger \tilde{t}_R. \tag{2.2}$$

The stop masses are (assuming universality as in mSUGRA) parameterized as

$$\begin{aligned} m_{\tilde{t}_L}^2 &= \overbrace{m_0^2}^{\text{GUT-scale mass}} + \overbrace{F m_{1/2}^2}^{\text{gauge RGE}} - \overbrace{2\left(f_t^2\Delta_t + f_b^2\Delta_b\right)m_0^2}^{\text{Yukawa RGE}} + \overbrace{m_t^2}^{\text{EWSB mass}} \\ &\quad - \overbrace{(-\cos 2\beta)\left(\frac{1}{2} - \frac{2}{3}\sin^2\theta_W\right)M_Z^2}^{D\text{ term}} \\ &= m_{\tilde{u}_L}^2 + m_t^2 - 2\left(f_t^2\Delta_t + f_b^2\Delta_b\right)m_0^2, \\ m_{\tilde{t}_R}^2 &= m_{\tilde{u}_R}^2 + m_t^2 - 4 f_t^2 \Delta_t m_0^2. \end{aligned} \tag{2.3}$$

where the 1st and 2nd generation left- and right-handed squark masses at the weak scale are

$$\begin{aligned} m_{\tilde{u}_L}^2 &= m_0^2 + F m_{1/2}^2 - (-\cos 2\beta)\left(\tfrac{1}{2} - \tfrac{2}{3}\sin^2\theta_W\right)M_Z^2, \\ m_{\tilde{u}_R}^2 &= m_0^2 + F m_{1/2}^2 - (-\cos 2\beta)\left(\tfrac{2}{3}\sin^2\theta_W\right)M_Z^2. \end{aligned} \tag{2.4}$$

At the GUT scale the stops get contributions from the universal scalar mass m_0. Gauge interactions in the RGE (predominantly QCD) add the term proportional to the gaugino mass, where the coefficient F has a typical value of $5-6$. The top and bottom Yukawa couplings are

$$\begin{aligned} f_t^2 &= g^2 m_t^2 / \left(2M_W^2 \sin^2\beta\right) \approx 1.01/\sin^2\beta, \\ f_b^2 &= g^2 m_b^2 / \left(2M_W^2 \cos^2\beta\right) \approx 0.00082/\cos^2\beta \end{aligned} \tag{2.5}$$

with g the weak coupling. The quantities $\Delta_{t,b}$ are calculated from the RGE and take values on the order of 0.1. For small $\tan\beta$ the top Yukawa f_t dominates and

$m_{\tilde{t}_R} < m_{\tilde{t}_L}$ since $\tilde{t}_R$ gets twice as much depression as $\tilde{t}_L$; these two masses approach each other as $\tan\beta \to m_t/m_b$. The usual EWSB mechanism adds the top-flavor mass term m_t^2. The factor $\cos 2\beta = \left(1-\tan^2\beta\right)/\left(1+\tan^2\beta\right)$ in the D-term is negative for $\tan\beta > 1$, so the D-terms depress the diagonal masses.

The Yukawa interaction also mixes $\tilde{t}_L$ and $\tilde{t}_R$ and the stop mass matrix from interactions (2.1) and (2.2) is[40]

$$\mathcal{M}^2 = \begin{bmatrix} m_{\tilde{t}_L}^2 & -a_t m_t \\ -a_t m_t & m_{\tilde{t}_R}^2 \end{bmatrix} \tag{2.6}$$

with $a_t = A_t - \mu\cot\beta$. Diagonalizing this gives mass eigenvalues

$$\begin{aligned} m_{\tilde{t}_{1,2}}^2 &= \frac{m_{\tilde{t}_L}^2 + m_{\tilde{t}_R}^2}{2} \mp \sqrt{\left(\frac{m_{\tilde{t}_L}^2 - m_{\tilde{t}_R}^2}{2}\right)^2 + a_t^2 m_t^2} \\ &= m_{\tilde{q}}^2 + m_t^2 - \left(3f_t^2\Delta_t + f_b^2\Delta_b\right) m_0^2 \\ &\quad \mp \sqrt{\left(f_t^2\Delta_t m_0^2 - \left(1 - \frac{8}{3}\sin^2\theta_W\right)\frac{-\cos 2\beta}{4} M_Z^2\right)^2 + \left(A_t - \mu\cot\beta\right)^2 m_t^2} \end{aligned} \tag{2.7}$$

and the physically propagating eigenstates

$$\begin{pmatrix} \tilde{t}_1 \\ \tilde{t}_2 \end{pmatrix} = \begin{bmatrix} \cos\theta_t & -\sin\theta_t \\ \sin\theta_t & \cos\theta_t \end{bmatrix} \begin{pmatrix} \tilde{t}_L \\ \tilde{t}_R \end{pmatrix} \tag{2.8}$$

rotated by the stop mixing angle

$$\tan\theta_t = \frac{m_{\tilde{t}_L}^2 - m_{\tilde{t}_1}^2}{m_t\left(A_t - \mu\cot\beta\right)}. \tag{2.9}$$

In the absence of mixing, $\theta_t \to \pi/2$ and $\tilde{t}_1 = \tilde{t}_R$ in models with a universal mass at the high scale.

For moderate $\tan\beta$ the stop mass splitting is dominated by the off-diagonal terms in the mass matrix. The unification scale trilinear coupling parameter A_0 can be freely adjusted, and light stops can usually be arranged irrespective of the value of the other universal mass parameters m_0 and $m_{1/2}$; such parameter sets can

generally be made consistent with experimental constraints (particularly those on M_Z and m_H)[51]. In fact, $\tilde{t}_1$ masses can be driven low enough that model builders have to be careful to insure that the stop does not become the LSP or, worse, tachyonic leading to dangerous color-breaking minima.

2.1.1 Theoretical prejudices

We have seen that it is possible for the top squark to be light. There are also arguments that directly favor a light $\tilde{t}_1$. Chief among these is electroweak baryogenesis, a mechanism for generating the observed baryon number of the universe at the electroweak phase transition[74]. The original baryogenesis idea of Sakharov[88] involving baryon number violation, C and CP violation and thermal nonequilibrium seems not to work in the Standard Model. The CP-violating phase in the Kobayashi-Maskawa matrix is too small to allow enough baryon number production in the symmetric phase, and experiment rules out a Higgs scalar light enough to generate a strongly first order phase transition which would lock in the generated baryons. SUSY, though, has many extra CP-violating phases. And a light (scalar) stop strongly coupled to the Higgs through its large Yukawa coupling can provide for the first order phase transition while allowing the Higgs to be heavier. Detailed calculations[43, 48] indicate that the stop mass must lie in the range 100 GeV $\lesssim m_{\tilde{t}_1} \lesssim$ 160 GeV for this mode of electroweak baryogenesis to succeed. We will find that this range is quite accessible to the Fermilab Tevatron using the searches outlined in this thesis.

Let us collect here a few other theoretical considerations related to the stop. First, as mentioned above, the LSP $\widetilde{Z}_1$ is a favored candidate for the dark matter determined to be present in the halo of our galaxy. In order for these relic neutralinos

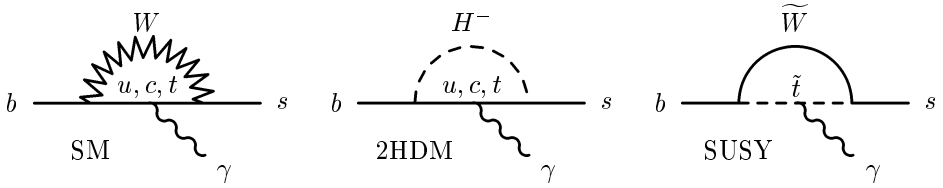

Figure 2.1: contributions to the decay $b \to s\gamma$ from the Standard Model (SM), two Higgs double models (2HDM), and supersymmetric models (SUSY).

to have an appropriate density, it is necessary that they cannot have annihilated via $\widetilde{Z}_1 + \widetilde{Z}_1 \to$ SM particles at too great a rate. If $\tilde{t}_1$ is not much heavier than $\widetilde{Z}_1$, then it is also possible to spoil the relic density through co-annihilation[38]. The authors of [38] have studied this process, and concluded that maintaining the favored relic density $0.1 < \Omega_{\widetilde{Z}_1} < 0.2$ requires a mass gap $m_{\tilde{t}_1} - m_{\widetilde{Z}_1} > 11$ to 33 GeV. Excluding the small mass gap is good news for collider experiments, where small $m_{\tilde{t}_1} - m_{\widetilde{Z}_1}$ means poor detection efficiency.

There are also constraints on the stop sector coming from precision electroweak measurements. One of these is the ρ parameter[55], which is a measure of the ratio of charged current to neutral current interaction strength. The close agreement between LEP II experimental determinations and the Standard Model $\Delta\rho = 0$ means that $\tilde{t}_L$, which couples to the W, must be quite heavy. A recent study[59] finds that in mSUGRA one needs $m_{\tilde{t}_L} > 275$ (310) GeV for $\mu > 0$ ($\mu < 0$). ρ parameter limits on the $\widetilde{W}_1$ and $\widetilde{Z}_1$ masses are weaker than the current direct experimental limits.

In 2HDM models with a light charged Higgs the rare decay $b \to s\gamma$ may require a light stop as well. This decay has been measured[21] to have a rate close to its SM predicted value. A light H^- enhances the decay by allowing a charged Higgs diagram analogous to the SM W^- diagram, as in Fig. 2.1, while a SUSY

diagram with a chargino and light stop in the loop decreases the rate and can bring it back into line with the SM rate[31, 83]. This is generally not a problem in models, as the charged Higgs is typically heavy. However, the ρ parameter data allow an mSUGRA H^- as light as 140 GeV ($\mu < 0$) [59].

2.2 Stop production and decay

Stops are color triplets, as are top quarks, and at a hadron collider such as the Fermilab Tevatron will be strongly produced in $\tilde{t}_1^*\tilde{t}_1$ pairs (to conserve R-parity) through gluon fusion and $q\bar{q}$ annihilation. The tree level production cross-section $\sigma_{\tilde{t}_1^*\tilde{t}_1}$ depends only on the mass $m_{\tilde{t}_1}$. Figure 2.2 shows this tree level $\sigma_{\tilde{t}_1^*\tilde{t}_1}$ as a function of $m_{\tilde{t}_1}$ for the Fermilab Tevatron $p\bar{p}$ collider at a center of mass energy $\sqrt{s} = 2.0$ TeV. These cross-sections were produced by the program ISAJET (see below) using the `CTEQ2L`[1] parton distribution functions[75]. For comparison, the top quark pair production cross section for 2.0 TeV $p\bar{p} \to t\bar{t}$ is $\sigma_{t\bar{t}} = 6100$ fb when calculated by the same means.

The Next to Leading Order (NLO) corrections to the tree-level $\sigma_{\tilde{t}_1^*\tilde{t}_1}$ have been calculated[36]. The authors of [36] used mSUGRA-inspired parameters to calculate higher order corrections for the Tevatron $p\bar{p}$ collider at $\sqrt{s} = 1.8$ TeV. The

[1]We have checked that our results are not affected by using more modern parton distribution functions than the `CTEQ2L` of our original analysis; this is as expected since the relatively heavy stop pairs are produced at high x.

$m_{\tilde{t}_1}$ (GeV)	K
70	1.41
110	1.30
150	1.19
190	1.11

Table 2.1: K factors for Tevatron stop pair production.

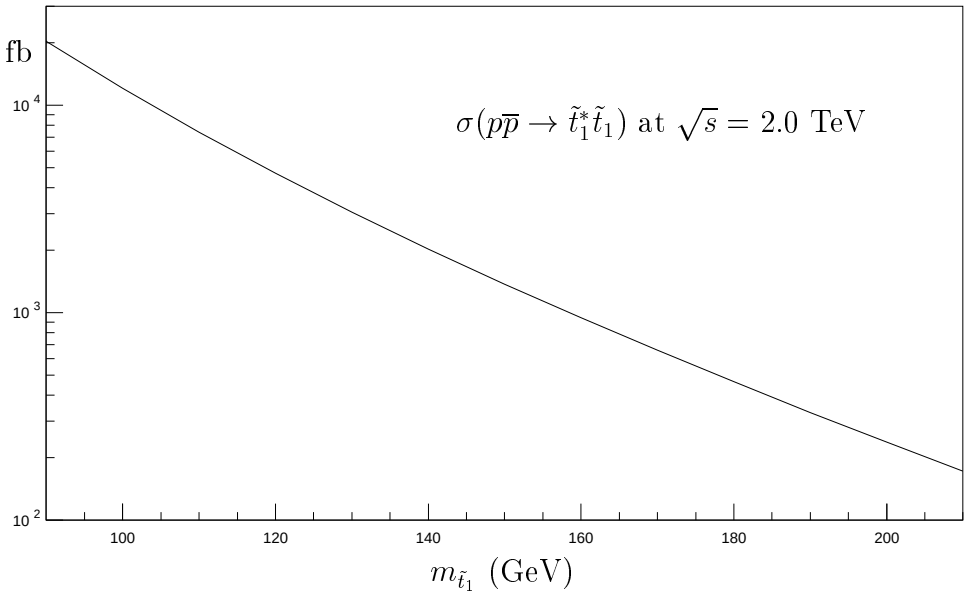

Figure 2.2: Stop pair production cross-section at the Tevatron.

corrections are positive and substantial. Table 2.1 lists the K factors they obtained. We use the lowest order cross-sections for both signal and background in the present work.

Current experimental mass limits for SUSY particles of interest here are listed in Table 2.2. These are generalized lower bounds which we will use for reference in this thesis. Many of these limits are correlated, and in some cases higher masses

particle	mass (GeV)	notes
$\tilde{q}$	220	[3, 14]
$\tilde{g}$	173	[8, 14]
$\tilde{t}_1$	90	[10, 19, 4]
$\widetilde{W}_1$	93	large m_0,[18, 11, 30]
$\widetilde{Z}_1$	32	large m_0,[18, 11]
$\tilde{e}$	92	[53]
H	108	[91]

Table 2.2: Current mass bounds for particles relevant to this study.

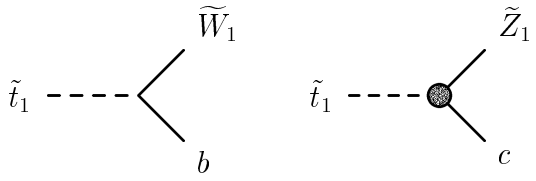

Figure 2.3: Decays of the light $\tilde{t}_1$ studied in this thesis.

have been excluded for particular combinations of other SUSY parameters. It is also possible to find corners of parameter space where these bounds may be evaded. See the indicated references for a fuller discussion. The $\tilde{t}_1$, $\widetilde{W}_1$ and $\widetilde{Z}_1$ experimental determinations are discussed briefly in Section 1.2.3.

Given these masses, the possible light $\tilde{t}_1$ decays in SUSY models without exotic particle content are [24] the 2-body tree-level modes $\tilde{t}_1 \to t\widetilde{Z}_1$ and $\tilde{t}_1 \to b\widetilde{W}_1$, the 2-body loop mode $\tilde{t}_1 \to c\widetilde{Z}_1$, the 3-body tree-level modes $\tilde{t}_1 \to bW\widetilde{Z}_1$, $\tilde{t}_1 \to b\tilde{\ell}\nu$ and $\tilde{t}_1 \to b\ell\tilde{\nu}$, and the four-body decay $\tilde{t}_1 \to bff'\widetilde{Z}_1$. Figure 2.3 diagrams the decays analyzed at length in this thesis, and Fig. 2.4 displays the others. Table 2.3 presents a summary of these modes.

We could write decays analogous to those of the preceding paragraph with a gluino $\tilde{g}$ replacing the LSP $\widetilde{Z}_1$, such as $\tilde{t}_1 \to c\tilde{g}$. The current gluino mass bound (see Table 2.2) would require a rather heavy stop to open this mode and overcome phase-space suppression enough to compete with the (loop-suppressed) $\tilde{t}_1 \to c\widetilde{Z}_1$, especially under the gaugino unification relationship $m_{\tilde{g}} \sim 6m_{\widetilde{Z}_1}$. Even if the reaction did have an appreciable branching fraction, it would be attended by the cascade $\tilde{g} \to q\bar{q}\widetilde{Z}_1$ and so would be similar the decay $\tilde{t}_1 \to c\widetilde{Z}_1$ (which we study at length) but with more jets and a softer LSP. The other possible gluino modes are even more suppressed— $\tilde{t}_1 \to bW\tilde{g}$ has too heavy a final state and

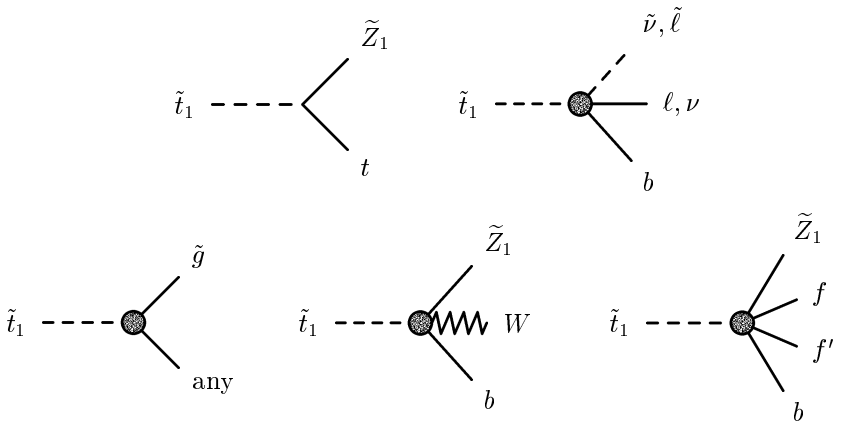

Figure 2.4: Decays of the $\tilde{t}_1$ not studied in this thesis.

$\tilde{t}_1 \to bff'\tilde{g}$ has too little phase space. We do not consider gluino decays further.[2]

When $m_{\tilde{t}_1} > m_t + m_{\widetilde{Z}_1}$ the direct 2-body decay $\tilde{t}_1 \to t\widetilde{Z}_1$ is open, but it will be strongly suppressed by phase space unless the mass gap is large. This requires $m_{\tilde{t}_1} \gg 210$ GeV. From Fig. 2.2 the production cross-section for such stops is less than 150 fb, and at 1/40th the $t\bar{t}$ production cross-section the likelihood of observing this mode is remote. We do not consider it further. We also mention in passing that the supersymmetric top decay $t \to \tilde{t}_1\widetilde{Z}_1$ can open up[89] if the stop and neutralino are light enough. See section 1.2.3 for this.

If $m_{\tilde{t}_1} > m_b + m_{\widetilde{W}_1}$, the 2-body tree-level decay $\tilde{t}_1 \to b\widetilde{W}_1$ will dominate. The chargino from $\tilde{t}_1 \to b\widetilde{W}_1$ rapidly decays to a neutralino and fermion pair, $\widetilde{W}_1 \to f'\bar{f}\widetilde{Z}_1$, so that $\tilde{t}_1$ pair production results in $\tilde{t}_1{}^*\tilde{t}_1 \to b\bar{b} + 4$ fermions $+ \widetilde{Z}_1\widetilde{Z}_1$. (We do not consider models with a slepton light enough for $\widetilde{W}_1 \to \tilde{\ell}\nu$, as explained below.) This top squark event topology is similar to the Standard Model $t\bar{t}$ pattern

[2]Models with light gluinos[25, 44] which could have evaded detection have been proposed in the literature. We do not consider such models here.

$t\bar{t} \rightarrow b\bar{b} + 4$ fermions, the main difference being the presence of the $\widetilde{Z}_1\widetilde{Z}_1$ pair. We will find that for the range of $\tilde{t}_1$ masses accessible with the luminosity upgrades at the Tevatron a real chargino cannot decay into a real W boson, which provides for another difference from $t\bar{t}$ events. (The chargino will decay to a real W only when $m_{\widetilde{W}_1} - m_{\widetilde{Z}_1} > m_W$. Given the measured W mass and the experimental limit on the neutralino mass, this requires $m_{\widetilde{W}_1} > 115$ GeV, rising to $m_{\widetilde{W}_1} > 160$ GeV as $m_{\widetilde{W}_1} \rightarrow 2m_{\widetilde{Z}_1}$ (see eqn. 1.6) and we use the $m_{\widetilde{W}_1}$ limit. As we will see in Chapter 5, such heavy charginos are not accessible at the Tevatron in $\tilde{t}_1 \rightarrow b\widetilde{W}_1$ decays.)

Phenomenologically, $\tilde{t}_1^*\tilde{t}_1$ events for the $\tilde{t}_1 \rightarrow b\widetilde{W}_1$ mode are categorized according to the leptonic or hadronic nature of the chargino decays just as $t\bar{t}$ events are categorized according to the nature of their W decays. There are (1) dilepton events $\tilde{t}_1^*\tilde{t}_1 \rightarrow b\bar{b}\ell^+\ell'^-\nu\bar{\nu}\widetilde{Z}_1\widetilde{Z}_1$ whose signature is (b)-jets + dilepton + $\not\!\!E_{\rm T}$, (2) 1-lepton events $\tilde{t}_1^*\tilde{t}_1 \rightarrow b\bar{b}q'\bar{q}\ell\nu\widetilde{Z}_1\widetilde{Z}_1$ with signature (b)-jets + lepton + $\not\!\!E_{\rm T}$, and (3) all-jet events $\tilde{t}_1^*\tilde{t}_1 \rightarrow b\bar{b}q'\bar{q}q''\bar{q}'''\widetilde{Z}_1\widetilde{Z}_1$ with (b)-jets + $\not\!\!E_{\rm T}$. The all-jets channel suffers from large QCD backgrounds; the search is difficult in this channel and we do not consider it further in this study. The leptonic channels show the same topologies as the corresponding $t\bar{t}$ channels, and thus the important backgrounds for these channels are those usually identified in $t\bar{t}$ studies, along with $t\bar{t}$ itself. These channels are considered in detail in Chapter 5.

When stop decays via the chargino $\tilde{t}_1 \rightarrow b\widetilde{W}_1$ then one also has to consider the cascade decay $\widetilde{W}_1 \rightarrow f\bar{f}'\widetilde{Z}_1$. We are particularly interested in the branching fraction to leptons, $\mathcal{B}\left(\widetilde{W}_1 \rightarrow \text{leptons} + \widetilde{Z}_1\right)$, since our detection schemes look for these leptons. When the decay proceeds predominantly via a virtual W, as in Fig. 2.5a, then the chargino branching fractions will be those of the mediating W, $\mathcal{B}(\widetilde{W}_1 \rightarrow e) = \mathcal{B}(\widetilde{W}_1 \rightarrow \mu) = \mathcal{B}(\widetilde{W}_1 \rightarrow \tau) = \mathcal{B}(W \rightarrow e) \approx 1/9$. But if some sfermion

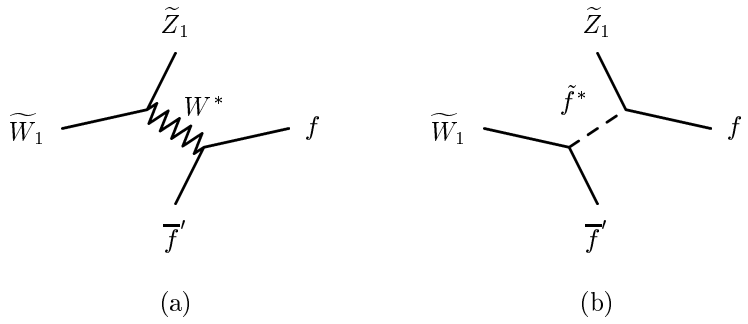

Figure 2.5: Tree-level decays of the chargino. The diagram at left is the W^*-mediated decay, which will lead to W-like fermionic branching fractions if it dominates. The sfermion diagram on the right will enhance the branching fraction to $\overline{f}'f$ when $\tilde{f}$ is light.

$\tilde{f}$ is light enough for the diagram in Fig. 2.5b to compete, then the branching fraction to the corresponding fermion and its partner $\widetilde{W}_1 \to f\bar{f}'\widetilde{Z}_1$ can be enhanced. If sleptons are lighter than squarks (but still heavier than $\widetilde{W}_1$) then we can get the branching fraction $\mathcal{B}\left(\widetilde{W}_1 \to \text{leptons} + \widetilde{Z}_1\right) \gg 1/9$. In mSUGRA (and in many other models) we can easily have $m_{\tilde{q}} \gg m_{\tilde{\ell}}$ from eqn. (1.5), and one typically finds an enhancement. This almost always works in our favor, as discussed below in Chapter 5. The $\tilde{f}^*$-mediated decay can also be important when the $W\widetilde{W}_1\widetilde{Z}_1$ coupling is dynamically suppressed.

In case $m_{\tilde{t}_1} < m_b + m_{\widetilde{W}_1}$, the stop must go via the 2-body loop decay or the 3- or 4-body decays. In mSUGRA $m_{\tilde{\ell}_L} > m_{\tilde{\ell}_R}$ and experimentally $m_{\tilde{\ell}_R} > 80$ GeV so we will not consider $\tilde{t}_1 \to b\tilde{\ell}\nu$ or $\tilde{t}_1 \to b\ell\tilde{\nu}$ here; they are treated in [47, 51].

When $m_{\tilde{t}_1} < m_b + m_W + m_{\widetilde{Z}_1}$, the remaining 3-body decay is closed, and $\tilde{t}_1$ must decay as $\tilde{t}_1 \to c\widetilde{Z}_1$ or $\tilde{t}_1 \to b\bar{f}f'\widetilde{Z}_1$. The rate for the loop decay $\tilde{t}_1 \to c\widetilde{Z}_1$ was estimated in [66], and earlier work[24, 28] had focused on the this decay. Recent calculations[39] indicate a substantial branching fraction for the 4-body decay for realistic regions of the MSSM parameter space. The event topologies for $\tilde{t}_1 \to$

$c\widetilde{Z}_1$	discussed fully in Chapter 4
$b\widetilde{W}_1$	discussed fully in Chapter 5
$bW\widetilde{Z}_1$	competes with $\tilde{t}_1 \to c\widetilde{Z}_1$ when $m_{\tilde{t}_1} \gg 165$ GeV; see [86, 87]
$b\tilde{\ell}\nu, b\ell\tilde{\nu}$	requires light slepton; not studied here; see [47, 51]
$bf\bar{f}'\widetilde{Z}_1$	may compete with $\tilde{t}_1 \to c\widetilde{Z}_1$; see [39]
$c\tilde{g}$	needs $m_{\tilde{t}_1} \gg 180$ GeV and loop-suppressed
$t\widetilde{Z}_1$	needs $m_{\tilde{t}_1} \gg 210$ GeV

Table 2.3: Light stop decay modes.

$b\bar{f}f'\widetilde{Z}_1$, but not kinematics, would be similar to those for the $\tilde{t}_1 \to b\widetilde{W}_1$ decay. It is interesting to note that Ref. [39] finds a gradual transition of dominance between the two decay modes, so that there are broad regions where *both* decays occur appreciably. This of course would greatly complicate the search strategy and make detection more difficult. In this work we only consider the loop decay $\tilde{t}_1^*\tilde{t}_1 \to c\bar{c}\widetilde{Z}_1\widetilde{Z}_1$, whose topology is c-jets + $\not\!\!E_{\rm T}$. The classic $\not\!\!E_{\rm T}$+ jets signature suffers from big backgrounds from W and Z events with jets from QCD radiation and $\not\!\!E_{\rm T}$ supplied by neutrinos. We will see below that charm tagging is necessary to develop good detection schemes. Chapter 4 is devoted to searches in this channel.

In case the $\tilde{t}_1$-$\widetilde{Z}_1$ mass difference is great enough to open up the 3-body decay, then $\tilde{t}_1 \to c\widetilde{Z}_1$ and $\tilde{t}_1 \to bW\widetilde{Z}_1$ will compete — the 2-body decay is loop suppressed and the 3-body decay is suppressed by phase space[86, 87]. Note that for the common ansatz $m_{\widetilde{W}_1} = 2m_{\widetilde{Z}_1}$ discussed earlier, the 3-body decay only opens up for $m_{\tilde{t}_1} > 165$ GeV (with $m_{\widetilde{W}_1} > 160$ GeV), and even then is strongly suppressed by phase space so this mode can only be important for $m_{\tilde{t}_1} \gg 165$ GeV. This region is difficult for either the $\tilde{t}_1 \to c\widetilde{Z}_1$ or $\tilde{t}_1 \to b\widetilde{W}_1$ search strategies we develop below for 2 fb^{-1} integrated luminosity at the Tevatron, and a direct search for $\tilde{t}_1 \to bW\widetilde{Z}_1$ would be even more problematical due to the presence of on-shell Ws

(whose rejection is key to suppressing SM backgrounds). Our preliminary analysis has indicated that this decay mode is inaccessible to the Tevatron experiments, and other investigators[86, 51] have since found the same result. We do not pursue the 3-body decay further.

Figure 2.6 shows the regions where these various decays are expected to occur. The neutralino decay mode $\tilde{t}_1 \to c\widetilde{Z}_1$ and the chargino mode $\tilde{t}_1 \to b\widetilde{W}_1$ are overlaid in this figure. The two axes will coincide if $m_{\widetilde{W}_1} = 2m_{\widetilde{Z}_1}$. The upper left region marked $m_{\tilde{t}_1} < m_{\widetilde{Z}_1}$ is ruled out because $\widetilde{Z}_1$ is the LSP by assumption.

We restrict our attention here to physics at the Fermilab Tevatron $p\bar{p}$ collider (described in Section 1.3.1). There also exists a rich stop phenomenology at e^+e^- colliders (see [35] and references therein), and proposed $\mu^+\mu^-$ colliders[34]. We do not examine R-parity violating processes for the Tevatron, which are discussed in [42] and [37].

A note on the top sector

Since we are interested in assessing the reach for the SUSY signal over Standard Model backgrounds, we assume that the top always decays via $t \to bW$ and neglect SUSY decays of tops such as $t \to \tilde{t}_1\widetilde{Z}_1$[67, 77, 89] or $t \to \tilde{t}_1\tilde{g}$[90]. If these decays are present to any extent, they could potentially add to the signal as the stops cascade via the decays discussed above. That is, a $t\bar{t}$ event where one of the tops decays supersymmetrically will be less likely to fail the cuts designed to reject the $t\bar{t}$ background, and so will improve the yield. Our assumption leads to a conservative background estimate, and if anything will underestimate the discovery potential for stops.

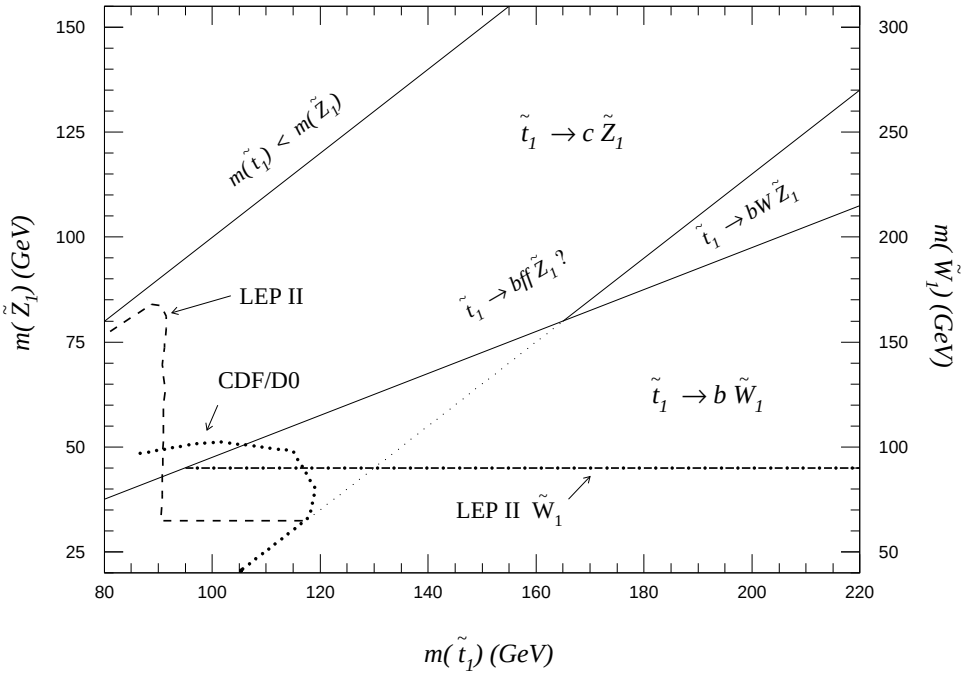

Figure 2.6: Map of decay modes and experimental results for the light stop. The vertical axis on the left is neutralino mass, and that on the right is chargino mass. In case $m_{\widetilde{W}_1} = 2m_{\widetilde{Z}_1}$, these axes coincide as illustrated. The heavy dotted line is the CDF 95% exclusion contour for the mode $\tilde{t}_1 \to c\widetilde{Z}_1$. The dashed line shows the LEP II 95% confidence limit for neutralino mass and stop mass given the decay $\tilde{t}_1 \to c\widetilde{Z}_1$. The dot-dashed line is the LEP II chargino mass limit.

2.3 Current experimental results

There are good experimental limits on the stop mass from both the CERN LEP II e^+e^- collider and the Fermilab Tevatron $p\bar{p}$ collider. LEP II results[10, 17, 29] at a collision energy $\sqrt{s} = 189$ GeV set a 95% confidence limit exclusion on stops lighter than 90.3 GeV for the decay mode $\tilde{t}_1 \to c\widetilde{Z}_1$, assuming the stop is at least 10 GeV heavier than the neutralino. This limit weakens by a few GeV when $\theta_t = 0.98$ and $\tilde{t}_1$ decouples from the Z. The LEP experiments do not report a stop mass limit for the decay $\tilde{t}_1 \to b\widetilde{W}_1$, but their chargino mass limit (see below) implies $m_{\tilde{t}_1} > 98$ GeV if stops decay via this mode.

At the Tevatron, the D0 collaboration[4] investigated the $\tilde{t}_1 \to c\widetilde{Z}_1$ mode in the $\not\!\!E_{\rm T}$ + jets channel (see Fig. 2.6 and Section 2.2) and excluded the region bounded by $m_{\tilde{t}_1} < 100$ GeV, $m_{\widetilde{Z}_1} < 40$ GeV and $m_{\tilde{t}_1} - m_{\widetilde{Z}_1} > 40$ GeV. The CDF collaboration[19] got a bigger excluded region by analyzing 88 pb^{-1} of Run I data (see Chapter 3) in the $\not\!\!E_{\rm T}$+ jet + charm jet channel for this mode and set a 95% CL exclusion for a region roughly bounded by $m_{\tilde{t}_1} < 115$ GeV and $m_{\widetilde{Z}_1} < 50$ GeV. The Tevatron collaborations also searched for the $\tilde{t}_1 \to b\widetilde{W}_1$ mode. CDF looked for a $\not\!\!E_{\rm T}$ + lepton + jets (from b-quarks)[20], and D0 looked in the dielectron channel[6]. Neither group was able to improve the existing limits (of $m_{\tilde{t}_1} > m_{\widetilde{W}_1} + m_b > 95$ GeV).

LEP II also provides the best limits on the $\widetilde{W}_1$ and $\widetilde{Z}_1$ masses. Chargino limits are generally function of m_0; small m_0 allows $\widetilde{W}_1$ and $\widetilde{Z}_1$ to be nearly degenerate in mass which seriously compromises the detection efficiency and hence the mass reach. The latest published results (for a collision energy $\sqrt{s} \leq 189$ GeV)[11, 18, 30] find $m_{\widetilde{W}_1} > 93$ GeV and $m_{\widetilde{Z}_1} > 32$ GeV for $m_{\widetilde{W}_1} \gg m_{\widetilde{Z}_1}$ (weakening to $m_{\widetilde{W}_1} > 72$ GeV, $m_{\widetilde{Z}_1} > 31$ GeV in the worst case).

Experiments at LEP II are ongoing, and limits from there are evolving even as this thesis is being written. The experiments now have accumulated data at $\sqrt{s} = 200$ GeV which will published shortly. For instance, ALEPH[53] has just released preliminary bounds of $m_{\widetilde{W}_1} > 100$ GeV, $m_{\widetilde{Z}_1} > 35$ GeV, $m_{\tilde{e}} > 92$ GeV, $m_{\tilde{\mu}} > 85$ GeV, $m_H > 92$ GeV, and $\tan\beta > 1.9$.

Chapter 3

Tevatron Simulation

3.1 Fermilab Tevatron

The Fermilab Tevatron is currently the world's premier (indeed, only) $p\bar{p}$ collider. It has two major general purpose collider detectors, CDF[12, 41] and D0[2][46]. For reference, we group Tevatron operations into three phases: Run I, Run II and Run II+. Run I refers to the data already collected during the machine's previous operating phase in 1994-1995. Run I obtained an integrated luminosity of almost 100 pb^{-1} in each detector at a center-of-mass energy of $\sqrt{s} = 1.8$ TeV. These data have already been analyzed for signatures of the light stop, and the results of these analyses are presented below. Table 3.1 lists the parameters for these runs [94].

The Tevatron is currently undergoing major machine and detector upgrades and is scheduled to resume operation in 2001. Chief among the upgrades is the

	$\sqrt{s}$ (TeV)	$\mathcal{L}$ (cm^{-2}sec^{-1})	$\int \mathcal{L}dt$ (fb^{-1})	dates
Run I	1.8	$\leq 10^{31}$	~ 0.1	1994-1995
Run II	2.0	2×10^{32}	~ 2	2001-2003
Run II+	2.0	$2 - 5 \times 10^{32}$	> 15	to 2007

Table 3.1: Tevatron run parameters.

new "Main Injector" which will store and pre-accelerate protons and antiprotons for injection into the Tevatron ring itself. The Main Injector will also recycle antiprotons from the Tevatron resulting in a tenfold increase in luminosity. Together with the new Recycler Ring, the peak luminosity is expected to rise by a factor 20 from 1×10^{31} cm^{-2}sec^{-1} to 2×10^{32} cm^{-2}sec^{-1}. Additionally, the beam energy will be raised to $\sqrt{s} = 2.0$ TeV (which will increase the $\tilde{t}^*\tilde{t}$ and $t\bar{t}$ production cross-sections by 40% over those at $\sqrt{s} = 1.8$ TeV). The primary data collection period following the Main Injector upgrade is referred to as Run II. During Run II we expect that 2 fb^{-1} of data will be accumulated at 2.0 TeV after about two years of operation.

The Tevatron is expected to continue operations for several years beyond the nominal 2 fb^{-1} Run II phase. There are also proposals on the table for further major luminosity upgrades. In anticipation of a substantially larger data sample, we also make projections for an integrated luminosity of 25 fb^{-1} at 2.0 TeV, which we call Run II+.

3.2 Event Simulation

Collisions at $p\bar{p}$ machines are messy affairs[33]. At 2 TeV the proton is a complicated assemblage of quark and gluon "partons" interacting via the strong force. In a hard-scattering event almost always just one parton from the proton and one parton from the antiproton interact. Each scattering parton has a certain probability to be of a given type (say gluon, strange quark, or whatever) and to carry a given fraction of the hadron's momentum. The set of functions which encode these probabilities for given momentum transfer in the hard-scattering sub-process are called parton distribution functions. They are fundamental inputs in any model that describes large momentum transfer hadron scattering processes..

The partons can be treated as free on their way to the hard-scattering, as are their colored reaction products. While inbound they radiate gluons freely, some of which are hard enough to be resolved as initial-state radiation (ISR). The partons being free at the collision point, the hard scattering reaction itself can be calculated in perturbation theory. After the collision the reaction products recoil from each other and the ISR. Color confinement causes the colored reaction products, any final-state radiation, the ISR, and the remnants of the initial p and $\bar{p}$ to hadronize as they flee the collision point. The usual picture is of color flux lines which stretch and break in a process called fragmentation. Each escaping colored particle will evolve into a multitude of color singlet hadrons, all moving in rough collinearity to the original particle. This concentrated shower of particles is called a "jet." (The remnants of the original p and $\bar{p}$ move down the beam axis to form "beam jets.")

The hard scattering processes are described by the underlying high energy theory. In our case , these are

$$\begin{array}{c} q\bar{q} \rightarrow \tilde{t}_1^* \tilde{t}_1 \\ gg \rightarrow \tilde{t}_1^* \tilde{t}_1 \end{array} \tag{3.1}$$

and are described by the supersymmetric model discussed in Chapter 1. The decays of the stops into SM quarks are also described by this theory. The processes by which the partons fragment and ultimately produce hadronic jets, leptons, photons and so on that are detected in the experimental apparatus is independent of the high energy theory, and phenomenological models that describe these are encoded in event generators that we outline below.

The (stable) hadrons, charged leptons, or photons produced in the collision move away from the collision point and record their passage in the surrounding detector. The detector is a complicated apparatus designed to characterize the visible

reaction products. It has components for tracking charged particles, calorimetry for absorbing and measuring the energy carried away from the collision by the hadrons as well as electromagnetic particles (mainly electrons and photons), and on the outside a system for measuring muon momenta. Modern detectors also include a sophisticated system that serves to resolve displaced secondary vertices from the decay of heavy flavors.

The fraction of the hadrons' longitudinal momentum carried by the initial hard scattering partons is unknowable, so there is an irreducible uncertainty in the longitudinal boost of the center-of-momentum frame for the colliding system. However, by forming the vector sum of all the energy deposited in the transverse direction, we get an important quantity called missing transverse energy, $\not\!\!E_{\rm T}$. A certain amount of $\not\!\!E_{\rm T}$ is due to jet and lepton mismeasurement from imperfect energy resolution, particles going into cracks in the detector, and other "non-physics" causes. A large $\not\!\!E_{\rm T}$, however, generally indicates the production of one or more high-energy long-lived weakly-interacting particles that escape the experimental apparatus without depositing energy. In the Standard Model these would be neutrinos. In SUSY searches, large $\not\!\!E_{\rm T}$ is the signature of escaping LSPs. Indeed, since a pair of LSPs are always produced in a SUSY reaction (for R-parity a good symmetry), large $\not\!\!E_{\rm T}$ is the hallmark of a supersymmetric reaction.

3.2.1 Collision simulation

We use the program ISAJET v7.29[27] with the ISASUSY[26] extension to simulate Tevatron events for both $\tilde{t}_1^*\tilde{t}_1$ and background processes. ISAJET does Monte Carlo event generation for $p\bar{p}$ (and other) collisions. It supports a wide variety of parton distribution function sets (We use the CTEQ2L set.). It incorporates lowest order

perturbative QCD cross-sections, initial- and final-state QCD radiation, independent fragmentation and final-state hadronization, and underlying event effects. It includes a phenomenological model tuned to minimum bias and hard scattering data for the beam jets. ISASUSY provides supersymmetric particle production and branching ratio calculations, and keeps track of all SUSY decay chains. A SUGRA package accepts GUT-scale input (Eq. (1.3)) and applies the RGE to produce low-energy MSSM parameters relevant for phenomenological calculations.

Because we control the relevant SUSY parameter space directly, we use the ISASUSY `MSSM` technique to set SUSY masses $m_{\tilde{t}_1}$, $m_{\widetilde{Z}_1}$ and $m_{\widetilde{W}_1}$ by hand. Events are generated with the reaction products' transverse momentum $p_{\rm T}$ ranging from 20-320 GeV (corresponding to ISAJET's `PT` and `QTW` cards). The Monte Carlo routine inefficiently samples over large $p_{\rm T}$ ranges, so each calculation is automatically broken into subranges of 20-40, 40-80, 80-160 and 160-320 GeV, and the results combined. We typically generate 50 fb^{-1} of sample for each signal and background case.

3.2.2 Detector simulation

As each event is generated, it is processed through a toy detector simulator consisting of the following elements (where η is the pseudorapidity, ϕ is the azimuthal angle, and $\Delta R = \sqrt{(\Delta\eta)^2 + (\Delta\phi)^2}$).

- Calorimeter simulator: We implement a toy calorimeter based on the ISAJET `CALSIM` subroutine. The segmentation is $\Delta\eta \times \Delta\phi = 0.1 \times 0.087$ extending to a rapidity of $|\eta| = 4$. There is a hadronic calorimeter, into which hadrons deposit their energy with a resolution of $50\%/\sqrt{E_{\rm T}}$, and an electromagnetic calorimeter which captures electrons and photons with resolution $15\%/\sqrt{E_{\rm T}}$.

We do not attempt to simulate effects of cracks or dead regions that are specific to particular detectors.

- Isolated lepton identification: We sum the hadronic transverse energy in a cone of $\Delta R < 0.4$ around each lepton. If this hadronic energy is less than 25% of the lepton's transverse energy, then the lepton is declared isolated. $p_{\rm T}$ thresholds for isolated leptons are given for the relevant channels.

- Jet identification: We use ISAJET's `GETJET` jet-finding algorithm. Jets are defined as hadronic clusters with total $E_{\rm T} > 15$ GeV falling within a cone of radius $\Delta R < 0.7$ and subject to $|\eta| < 3.5$. We do not perform jet energy corrections.

- Silicon vertex detector (SVX): We simulate a SVX detector for tagging b-jets. We identify each weakly-decaying B hadron in an event with $E_{\rm T} > 15$ GeV and $|\eta| < 2$. If $\Delta R(B, \text{jet}) < 0.5$ for some jet then that jet is tagged as a b-jet with an efficiency of 50%.

- Charge multiplicity counter: The charge multiplicity of a jet is defined as the number of charged long-lived hadrons with $E_{\rm T} > 0.5$ GeV lying within $\Delta R < 0.5$ of the jet axis. We use this for τ veto studies.

- Top mass reconstruction: For single-lepton events we perform $t\bar{t}$ event reconstruction and calculate the resulting top mass. Details of this procedure are given in Chapter 5.

Events are produced by ISAJET, passed through this detector simulator and subjected to software "trigger" cuts. Those which pass these cuts have their event

data written. This data is then post-processed to prepare ntuple files for later cut analysis using the CERN Physics Analysis Workstation (PAW) software[1].

3.3 Methodology

We study the decay modes $\tilde{t}_1 \to b\widetilde{W}_1$ and $\tilde{t}_1 \to c\widetilde{Z}_1$ separately, in each case taking the $\tilde{t}_1$ branching fraction to be 100% for the given mode. For the $\tilde{t}_1 \to c\widetilde{Z}_1$ mode, the stop signal then depends only on the two SUSY masses $m_{\tilde{t}_1}$ and $m_{\widetilde{Z}_1}$, and is independent of mixing angles in the top squark and gaugino sectors.

On the other hand, signals from $\tilde{t}_1 \to b\widetilde{W}_1$ mode events (with the cascade decay $\widetilde{W}_1 \to \widetilde{Z}_1 +$fermions) are determined by the three SUSY masses $m_{\tilde{t}_1}$, $m_{\widetilde{W}_1}$ and $m_{\widetilde{Z}_1}$, together with the branching fractions for $\widetilde{W}_1 \to e, \mu, \tau$. In most of our analysis, we collapse this parameter space from four dimensions to two. First, we generally take $m_{\widetilde{Z}_1} = m_{\widetilde{W}_1}/2$, which is approximately true in many interesting classes of SUSY models (see eqn. (1.6)). This only requires that the lighter chargino and the two lighter neutralino are gaugino-like, and that the gaugino masses obey the mass unification condition. While this occurs canonically in grand unified models, there are also many other models where this condition is obeyed but for entirely different reasons. Second, we set the chargino's leptonic branching fraction equal to the W's leptonic branching fraction:

$$\mathcal{B}(\widetilde{W}_1 \to e) = \mathcal{B}(\widetilde{W}_1 \to \mu) = \mathcal{B}(\widetilde{W}_1 \to \tau) = \mathcal{B}(W \to e) \approx 1/9, \tag{3.2}$$

as discussed earlier. We also examine how our conclusions are affected when these restrictions are relaxed.

For each channel investigated, we generate event data sets for a grid over the appropriate parameter space of relevant SUSY masses, together with event data

sets for the relevant background processes. The grid spacing is usually $\Delta m_{\tilde{t}_1} = 10$ GeV, $\Delta m_{\widetilde{W}_1} = 10$ GeV and $\Delta m_{\widetilde{Z}_1} = 5$ GeV. These data sets are then subjected to a variety of cuts on measurable quantities designed to maximize the discovery reach over the SUSY parameter space, using the PAW software to analyze cuts.

We consider a particular SUSY model "discoverable" if (1) there is a 5σ statistical significance

$$\frac{N_s}{\sqrt{N_b}} > 5, \tag{3.3}$$

where N_s (N_b) is the expected number of signal (background) events, (2) the expected signal level is at least 25% of background,

$$\frac{N_s}{N_b} > 25\%, \tag{3.4}$$

and (3) at least 5 signal events are expected

$$N_s \geq 5. \tag{3.5}$$

When comparing our results to those of other studies, bear in mind that many authors report their results at a 3σ level rather than our 5σ level. The 25% requirement eqn. (3.4) encodes our overall uncertainty in the calculated absolute cross-sections for background processes. And we require that at least 5 signal events be expected for protection against uncontrolled non-physics backgrounds.

A signal which fails $N_s/N_b > 25\%$ is called "background limited." Increasing the integrated luminosity $\widehat{\mathcal{L}}$ cannot help this situation, and only clever cuts can rescue the signal. When a signal fails $N_s/\sqrt{N_b} > 5$ it is "rate limited." A rate-limited signal that just satisfies $N_s/N_b = 25\%$ can be recovered by increasing $\widehat{\mathcal{L}}$ until the point $N_s/\sqrt{N_b} = 5\sigma$ is reached. At this point, where the equalities in (3.3)

and (3.4) both hold, we have $N_B = 400$ and $N_S = 100$. Writing $N_B = \sigma_B \widehat{\mathcal{L}}$, with σ_B the background cross-section, then

$$\widehat{\mathcal{L}} = \frac{400}{\sigma_B} \qquad \text{when } \frac{N_s}{\sqrt{N_b}} = 5\sigma \text{ and } \frac{N_s}{N_b} = 25\% \tag{3.6}$$

which will be useful to us in the sequel.

The observability criteria adopted here are conservative, and elaborate statistical schemes might well extend our reported reach considerably. We have, for instance, not investigated the utility of using information from the background-rich kinematical regions excluded by our cuts to get a better data-derived background estimation which would allow us to relax our 25% criterion. Also, it is worth remembering that by combining results from both CDF and D0 one can have get a stronger signal than either detector would get alone.

Chapter 4

The decay mode $\tilde{t}_1 \to c\widetilde{Z}_1$

If the top squark decays via $\tilde{t}_1 \to c\widetilde{Z}_1$, it can be searched for in the multijet + $\not\!\!E_{\rm T}$ channel, which is the standard channel for SUSY searches at hadron colliders. This channel picks out events where the two $\widetilde{Z}_1$ neutralinos escape detection in the experimental apparatus, resulting in a large net missing transverse energy. We also investigate the possibility of tagging one of the charm jets via its muon decay to further enhance the signal over SM backgrounds. We take the branching fraction for $\tilde{t}_1 \to c\widetilde{Z}_1$ to be 100%. The SUSY signal in each of these channels is then completely determined by the two quantities $m_{\tilde{t}_1}$ and $m_{\widetilde{Z}_1}$. The stop mass $m_{\tilde{t}_1}$ sets the production cross section and the two masses together determine the kinematics. We use ISAJET to simulate signal events over a grid in the $m_{\tilde{t}_1} - m_{\widetilde{Z}_1}$ plane. For each value of $(m_{\tilde{t}_1}, m_{\widetilde{Z}_1})$ we generate events, run them through our toy detector simulation and compare the resulting cross-sections with those from the SM background processes to determine the reach of the Tevatron experiments.

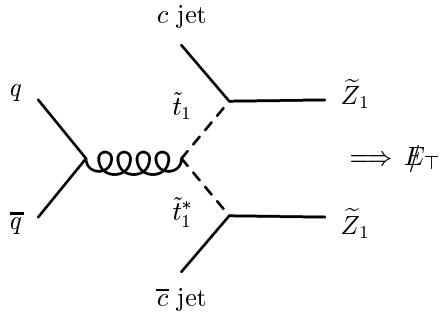

Figure 4.1: The standard event topology for the $\not{E}_{\rm T}$ + jets channel of the $\tilde{t}_1 \to c\widetilde{Z}_1$ decay mode.

4.1 Missing $E_{\rm T}$ + jets channel

The $\tilde{t}_1^*\tilde{t}_1$ event topology is exhibited in Fig. 4.1. The two LSPs combine to provide a large $\not{E}_{\rm T}$, and the two charm quarks are required to provide hard jets. Standard Model events that have hard neutrinos (to supply $\not{E}_{\rm T}$) without isolated leptons, as in Fig. 4.2, are the main physics backgrounds to this $\tilde{t}_1 \to c\widetilde{Z}_1$ search. $Z \to \nu\bar{\nu}$ is a problem when direct high $p_{\rm T}$ weak boson production is accompanied by gluon or quark radiation, and also when an outgoing quark from a QCD hard-scattering radiates a Z which decays invisibly. We use jet hardness and geometrical cuts to suppress these relative to the signal. Similarly, events with $W \to \tau\nu$ contribute to the background when the τ decays hadronically or into a non-isolated lepton and fails to be distinguished from a hadronic jet. The processes of concern are $q\bar{q}' \to W \to \tau\nu$ plus one or two QCD jets and $gq \to Wq' \to \tau\nu q'$. Ws from $t\bar{t}$ events also contribute to the background.

Note that within ISAJET, Z-production processes such as $gq \to qZ$ with final-state gluon radiation (Fig. 4.3a) are treated separately from QCD hard-scattering processes such as $gq \to gq$ or $q'q \to q'q$ with final-state Z radiation (Fig. 4.3b).

While the former are readily and efficiently simulated with the ISAJET `DRELLYAN` reaction card, the latter are treated by ISAJET as QCD processes and it is difficult to obtain a large Monte Carlo integrated luminosity for the latter due to the huge QCD hard scattering cross section. By analyzing $\sim 10^7$ events, we found that these radiative events add about 5% to the related $q\bar{q} \to gZ$ background.

4.1.1 Run I

We performed an early analysis[28] to estimate discovery prospects in this channel with the Tevatron Run I data. Based on this analysis we recommended a set of cuts: (1) $\not\!\!E_{\rm T}$> 50 GeV to reduce backgrounds from QCD heavy flavors and mismeasured jets; (2) at least two jets in the event, one of which is central ($|\eta| < 1$); (3) all jets separated by at least $30^{\rm o}$ in azimuth from $\not\!\!E_{\rm T}$, and a jet-jet separation less than $150^{\rm o}$ in case there are only two jets; and (3) no identified leptons. We also prescribed a compound cut (4) $p_{\rm T}$ (fast jet) > 80 GeV for $\Delta\phi(\not\!\!E_{\rm T}, j) > 90^{\circ}$, else $p_{\rm T}$ (fast jet) > 50 GeV. We found the dominant background after these cuts to be $W \to \tau\nu$, with the τ decaying hadronically. Depending on the ability of experimentalists to reject the $W \to \tau\nu$ background and subtract the $Z \to \nu\bar{\nu}$ backgrounds, we estimated that,

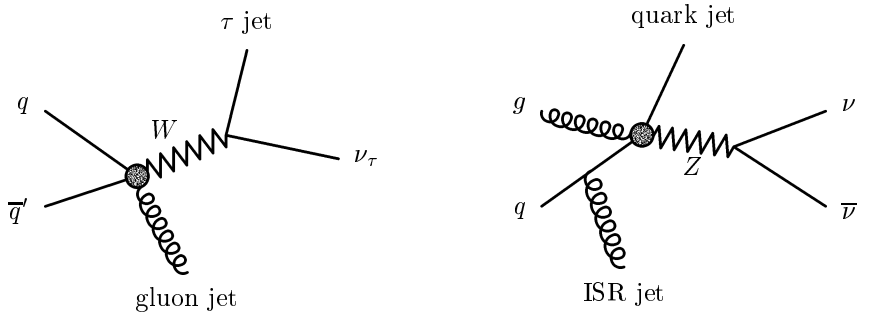

Figure 4.2: Some representative background processes for the $\not\!\!E_{\rm T}$ + jets channel.

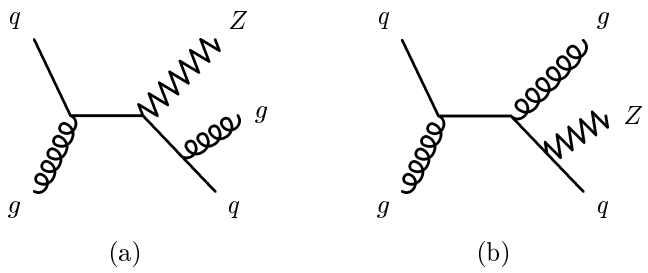

Figure 4.3: Examples of ISAJET Z radiative processes. Diagram (a) is a well-controlled ISAJET `DRELLYAN` process; processes like (b) require simulation of a very large number of ISAJET `QCD` events.

depending on $m_{\widetilde{Z}_1}$, stops as heavy as 100-125 GeV might be probed in this channel with 100 pb^{-1} of data.

So far, the full Run I data set has not been analyzed in this channel. The D0 Collaboration[4] looked at 13.5 pb^{-1} of data from the 1992-1993 run. They required $\not\!\!E_{\rm T}$> 40 GeV, two jets with $p_{\rm T} > 30$ GeV, $90^\circ < \Delta\phi(j_1, j_2) < 165^\circ$, $10^\circ < \Delta\phi(\not\!\!E_{\rm T}, j),\ \Delta\phi(\not\!\!E_{\rm T}, j) < 125^\circ$ and no identified leptons with $p_{\rm T} > 10$ GeV. They excluded a region at the 95% confidence level of $m_{\tilde{t}_1} \lesssim 90$ GeV, $m_{\tilde{t}_1} - m_{\widetilde{Z}_1} \gtrsim 35$ GeV.

4.1.2 Run II

The larger data sample anticipated in Run II enables us to sharpen the selection cuts for the stop signal. For the $\not\!\!E_{\rm T}$ + jets channel we require the following initial cuts:

(i) $\not\!\!E_{\rm T}$> 50 GeV;

(ii) at least two jets with $p_{\rm T} > 50$ GeV, one with $|\eta| < 1$;

(iii) for all jets, $\Delta\phi(\not\!\!E_{\rm T}, j) > 30^\circ$,

and if only two jets then $\Delta\phi(j_1, j_2) < 150^\circ$;

(*iv*) no identified isolated e or μ;

(*v*) no SVX b tag.

These cuts will reject QCD backgrounds from heavy flavor production ($g \to c\bar{c}, b\bar{b}$) and multijet production with mismeasured jets. Cuts (*i*) or (*ii*) may serve as triggers. Note that we require very hard jets, one of which must be central. Cut (*iii*) is designed to reduce detector-dependent backgrounds due to mismeasured QCD jets. Cut (*iv*) suppresses background events with leptons from $W \to \ell\nu$, $\ell = e, \mu$. Cut (*v*) suppresses the $t\bar{t}$ background by vetoing events with b-jets which will be efficiently tagged by the Run II Tevatron detectors. (In our simulation we ignore c contamination of SVX tags. A closer analysis which pays attention to the detailed experimental properties of the particular vertex detector, including a scheme for the outright identification of displaced charm vertices, could improve the signal yield in this channel. See the remarks at the end of the next section.) The cross sections for the backgrounds and selected SUSY signal cases after these cuts are displayed in Table 4.1 in the column labelled (*v*).

For the $Z \to \nu\bar{\nu}$ background due to Drell-Yan $q\bar{q}$ annihilation, the two hard jets come from QCD radiation recoiling against the Z boson; these jets are often close together in azimuth. The c-jets in the signal, on the other hand, come from the two $\tilde{t}_1$s which recoil mainly against each other, and hence tend to be more back to back in ϕ. Events from the $W \to \tau\nu$ background exhibit a spectrum intermediate between these two; when the two hardest jets come from QCD radiation then they are generally close, as with $Z \to \nu\bar{\nu}$, but when one of the hard jets is from a hadronically decaying τ, then the jets can have a large separation. Distributions of the azimuthal separation of the two hardest jets, $\Delta\phi(j_1, j_2)$, are displayed in Fig. 4.4

background	(v)	(vi)	(vii)	$(viii)$	$(viii')$
$W \to \tau\nu$	500	391	246	69	13.4
$Z \to \nu\bar{\nu}$	484	268	157	105	24.4
$t\bar{t}$ (175)	32	24	24	7	2.5
total	1016	683	427	181	40.3
25%	254	171	107	45	10.1
5σ @ 2fb^{-1}	113	92	73	48	(6.4)
$\tilde{t}_1$, $\widetilde{Z}_1$	(v)	(vi)	(vii)	$(viii)$	$(viii')$
120, 80	146	117	77	47	12.1
150, 80	146	120	86	58	19.7
180, 100	68	54	42	29	11.0

Table 4.1: $\not{E}_{\rm T}$ + jets channel cross-sections, in fb, after cuts as discussed in the text. The line labelled "25%" shows 25% of the total background, and the "5σ" line shows the signal level needed to produce a 5σ excess at 2 fb^{-1}. (The parenthesized 5σ value in the last column is for an integrated luminosity of 25 fb^{-1}.) For the signal cases, $\tilde{t}_1$ and $\widetilde{Z}_1$ masses are given in GeV.

for the W and Z backgrounds and a signal case of a 150 GeV $\tilde{t}_1$ decaying to an 80 GeV $\widetilde{Z}_1$. Imposing the cut

$$(vi) \quad \Delta\phi(j_1, j_2) > 90^\circ$$

eliminates about half of the $Z \to \nu\bar{\nu}$ background along with 20% of the signal and other backgrounds.

We see from Table 4.1 that while a 5σ signal is already possible even for $m_{\tilde{t}_1} = 150$ GeV, the signal to background ratio is less than 25%. To enhance the signal further, we note that these signal events generally have harder jets than the W and Z events, except when the $\tilde{t}_1 - \widetilde{Z}_1$ mass difference becomes small. Also, the $\tilde{t}_1^*\tilde{t}_1$ events may be accompanied by QCD jets. The distribution of total jet transverse energy

$$J_{\rm T} \equiv \sum_{\rm jets} E_{\rm T}\,({\rm jet}) \tag{4.1}$$

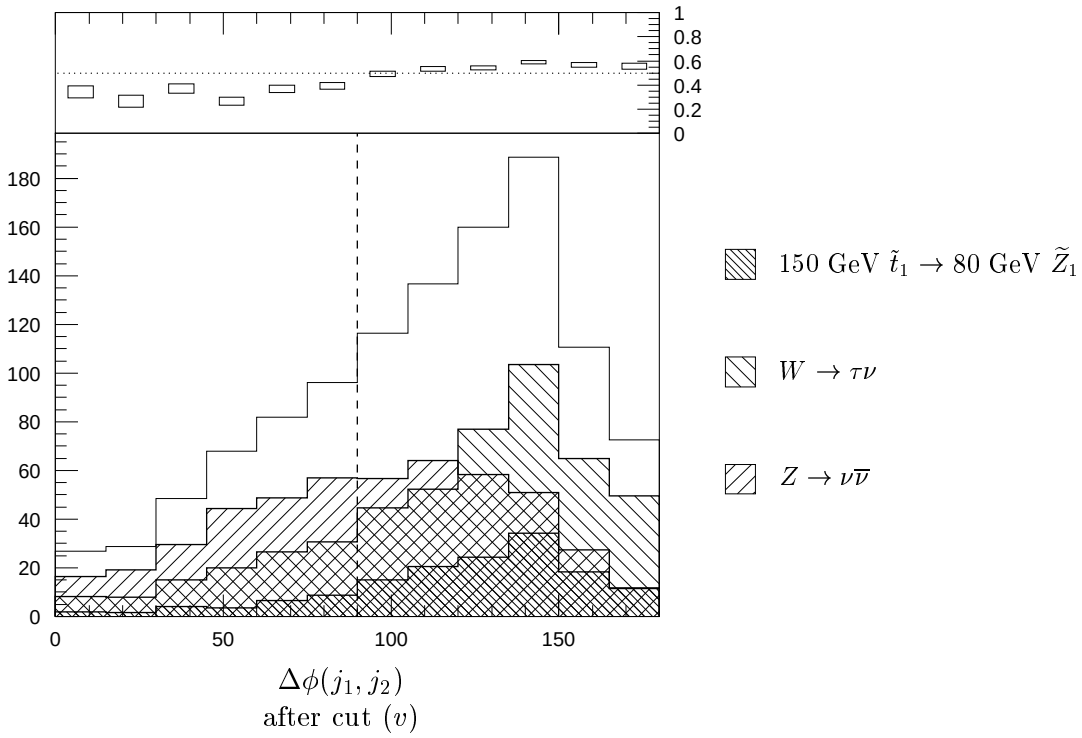

Figure 4.4: Distribution of $\Delta\phi(j_1, j_2)$ in the $\not\!\!E_{\rm T}$ + jets channel for a signal case of 150 GeV $\tilde{t}_1 \to 80$ GeV $\widetilde{Z}_1$ and backgrounds $W \to \tau\nu$ and $Z \to \nu\bar{\nu}$. The vertical axis on the main plot is in fb/bin. The top line in the histogram plot shows the sum of signal plus both backgrounds. The small subplot at the top shows the ratio of the normalized signal distribution to the normalized signal+background distribution. The box heights in this subplot are proportional to their calculated uncertainties.

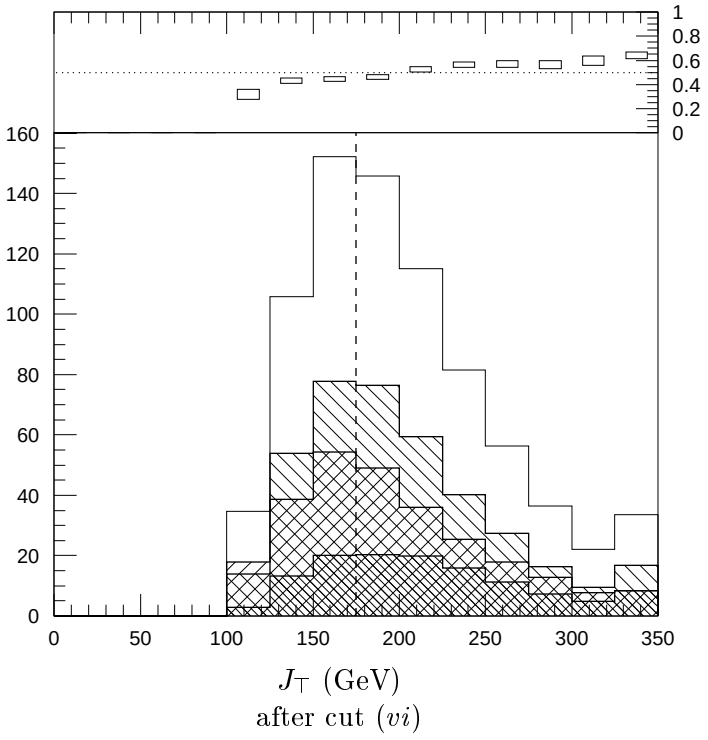

Figure 4.5: Distribution of $J_{\rm T}$ in the $\not\!\!E_{\rm T}$ + jets channel for 150 GeV $\tilde{t}_1 \to$ 80 GeV $\widetilde{Z}_1$ and backgrounds $W \to \tau\nu$ and $Z \to \nu\bar{\nu}$, after applying cut (vi). Figure elements are as in Fig. 4.4.

exhibited in Fig. 4.5 reflects this. We make the cut

$$(vii) \quad J_{\rm T} > 175 \text{ GeV},$$

which reduces the W and Z backgrounds by 40% at a cost of a fifth to a third of the signal.

Further cuts based on simple kinematical quantities do not seem to be available. In order to extend the useful discovery reach in this channel we investigate the possibility of discriminating the τs in the $W \to \tau\nu$ background. Since we have already vetoed events in this channel with an identified lepton, we expect most of these τs to decay hadronically, producing jets with low charge multiplicity. For the

purposes of our simulation, we calculate the charge multiplicity of a jet, mult(j), as the number of long-lived charged hadrons with $E_{\rm T} > 0.5$ GeV lying in the jet cone. Distributions of the minimum charge multiplicity, $\min_j$ mult(j), are shown in Fig. 4.6. Bare τs will canonically decay to one or three charged hadrons, but upon analyzing simulated events we find that a "τ-veto" requirement

$$(viii) \quad \min_j \text{ mult}(j) > 4$$

gives the best separation of signal and background over the SUSY parameter space, eliminating almost 60% of the background along with 30–40% of the signal. Note that 70% of the $t\bar{t}$ background also fails this cut since t decays with large $\not\!\!E_{\rm T}$ (from an energetic ν) and no visible leptons will usually involve $W \to \tau\nu$.

The results of applying cuts (i)–$(viii)$ are displayed as a contour plot in Fig. 4.7. This plot shows the SUSY parameter space $m_{\tilde{t}_1}$–$m_{\widetilde{Z}_1}$. The two diagonal lines indicate the kinematical boundaries of the decay $\tilde{t}_1 \to c\widetilde{Z}_1$; the upper left hand corner is excluded by the requirement $m_{\widetilde{Z}_1} < m_{\tilde{t}_1}$ that $\widetilde{Z}_1$ be the LSP, and in the lower right corner the 3-body decay $\tilde{t}_1 \to bW\widetilde{Z}_1$ opens up. The combined LEP II/Tevatron Run I excluded area (see Fig. 2.6) is denoted by the hatched region. The legend in the upper left corner shows the estimated background cross-sections, in fb, after cut $(viii)$. The contour labels are also given in fb. The heavy solid line at 48 fb represents $N_s/\sqrt{N_b} = 5\sigma$ for the Run II integrated luminosity of 2 fb^{-1}. The heavy dashed line is at 45 fb = 25% of the 180 fb total background. From the plot we see that even with our conservative criteria, experiments at the Tevatron can discover most cases with $m_{\widetilde{Z}_1} \lesssim 70 - 80$ GeV and $m_{\tilde{t}_1} \lesssim 165$ GeV in this channel.

Note that the contours of Fig. 4.7 extend into the region marked $\tilde{t}_1 \to bW\widetilde{Z}_1$, where the three-body decay is kinematically open. Above the $\tilde{t}_1 \to bW\widetilde{Z}_1$ line the

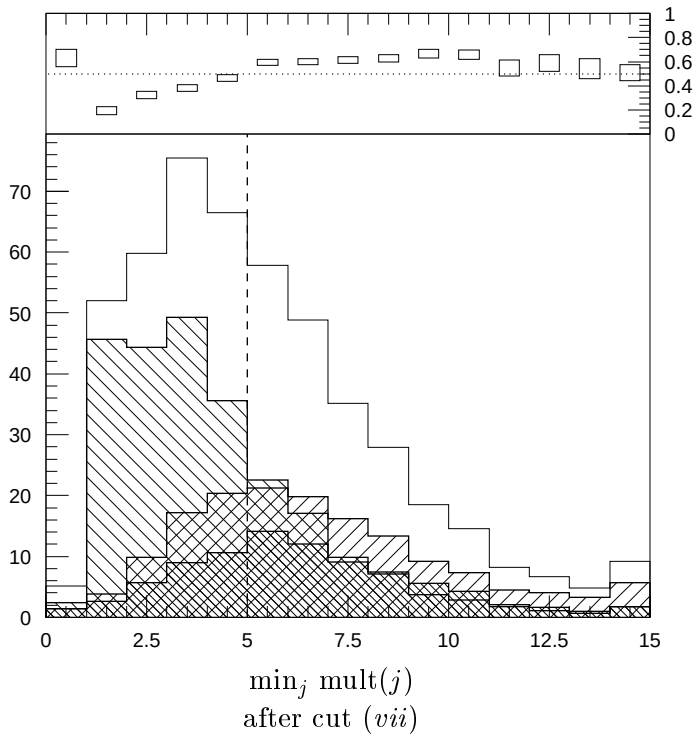

Figure 4.6: Distribution of $\min_j$ mult(j) in the $\not\!\!E_{\rm T}$ + jets channel for 150 GeV $\tilde{t}_1 \to 80$ GeV $\widetilde{Z}_1$ and backgrounds $W \to \tau\nu$ and $Z \to \nu\bar{\nu}$, after applying cut (vii). Figure elements are as in Fig. 4.4.

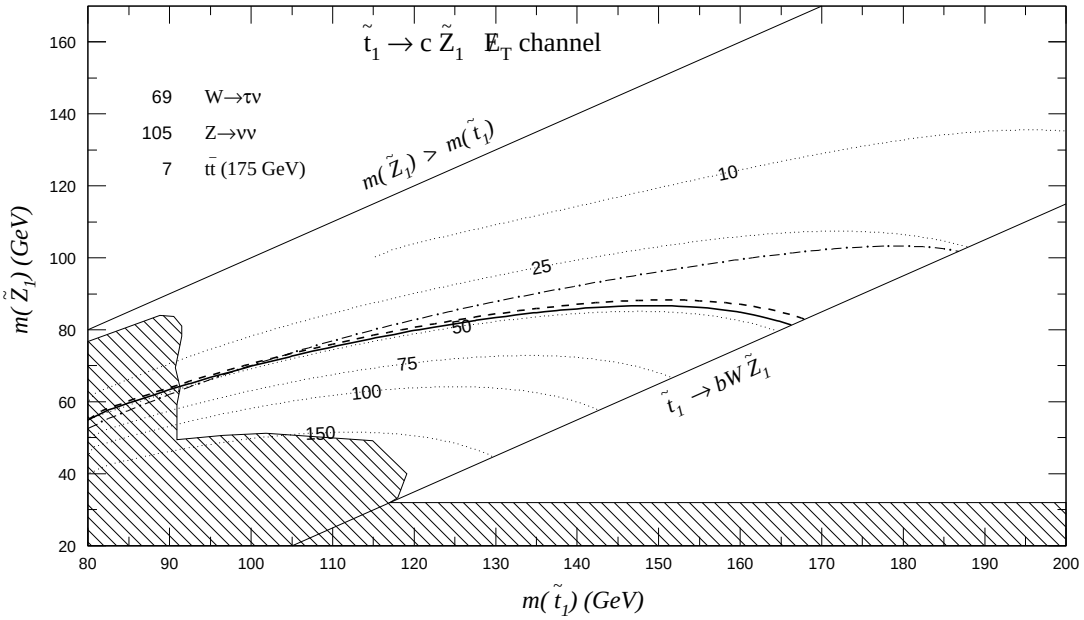

Figure 4.7: Cross-section contours, in fb, for the $\not{E}_T$ + jets channel after cut (*viii*) as described in the text. The heavy solid line at 48 fb is the 5σ discovery limit for an integrated luminosity of 2 fb^{-1}. The dashed line is 45 fb of signal, which is 25% of background. The dot-dashed line shows the reach at 25 fb^{-1} after cut (*ix*). The hatched region is experimentally excluded at the 95% confidence level.

branching fraction $\mathcal{B}(\tilde{t}_1 \to c\widetilde{Z}_1)$ is taken to be 100%, while below the line the two decay modes are expected to compete[87, 86].

4.1.3 Run II+

This channel is background limited in that even for higher integrated luminosity the search is limited by the signal to background ratio, and without refining the requirements on event topology, such as the c-tagging studied in the next section, little improvement seems available for the high luminosity scenario of the Run II+ Tevatron. The availability of more events, though, allows us to make deeper cuts and still preserve an acceptable $N_s/\sqrt{N_b}$. By tightening the previous cuts to

$$
\begin{aligned}
(vi') \quad & \Delta\phi(j_1, j_2) > 120^\circ, \\
(vii') \quad & J_{\mathrm{T}} > 225 \text{ GeV}, \\
(viii') \quad & \min_j \text{ mult}(j) > 5
\end{aligned}
$$

we can push the discovery limits at the heavy $\tilde{t}_1$ end of the parameter space, up to about 185 GeV. Our projection of the reach at 25 fb^{-1} after these cuts is shown on the contour plot of Fig. 4.7 as a heavy dot-dashed line. We see that the reach extends beyond $m_{\tilde{t}_1} = 180$ GeV.

4.2 c-tagged channel

In the c-tagged channel we attempt to identify the charm quark by looking for a jet with a soft muon due to the decay $c \to s\bar{\mu}\nu_\mu$. The backgrounds here are similar to those in the previous channel. $Z \to \nu\bar{\nu}$ contributes when accompanied by tagged heavy flavor production (e.g., $g \to c\bar{c}$ from initial state QCD radiation). $W \to e, \mu$ and $W \to \tau \to e, \mu$ are a problem when the lepton mis-tags an unrelated jet. $t\bar{t}$ events will be a reducible background when a semileptonic b-jet is tagged as a c-jet.

4.2.1 Run I

Our earlier analysis of this channel geared for the Run I[28] integrated luminosity suggests cuts as in the Run I $\not\!\!E_{\rm T}$+ jets channel (see Sect. 4.1.1), except that we here require a tagging muon with $p_{\rm T}(\mu) > 3$ GeV within $\Delta R = 0.4$ of a jet axis, and the compound cut (4) is changed to (4') $\Delta\phi(\not\!\!E_{\rm T}$,nearest jet) $\leq 90^\circ$ or $p_{\rm T}$(fast jet) > 50 GeV. We concluded that with the integrated luminosity available in Run I, the c-tagged channel would not extend the reach beyond the $\not\!\!E_{\rm T}$+ jets channel because, although it has a better signal to background ratio, the signal is severely rate limited.

The CDF Collaboration has analyzed 88 pb^{-1} of Run I data[19] looking for $\not\!\!E_{\rm T}$+ c-tagged jet with a different technique than ours, using the SVX detector to identify charmed hadrons by looking for displaced vertices. They required $\not\!\!E_{\rm T} > 40$ GeV, 2 or 3 (hard) jets with $E_{\rm T} > 15$ GeV within $|\eta| < 2$ (to reject $t\bar{t}$ events, which usually have 4 or more hard jets) but no (soft) jets with $E_{\rm T} < 15$ GeV (to suppress QCD multijet events), $45^\circ < \Delta\phi(\not\!\!E_{\rm T}, j) < 165^\circ$, $45^\circ < \Delta\phi(j_1, j_2) < 165^\circ$, and no leptons with $p_{\rm T} > 10$ GeV. Then they look for the SVX charm tag. By this means, they get a 95% confidence level excluded region bounded roughly by $m_{\tilde{t}_1} < 115$ GeV and $m_{\widetilde{W}_1} < 50$ GeV.

4.2.2 Run II

Initial cuts for the c-tagged channel are:

(i) $\not\!\!E_{\rm T} > 50$ GeV;

(ii) two jets with $p_{\rm T} > 30$ GeV, one with $|\eta| < 1$;

(iii) for all jets, $\Delta\phi(\not\!\!E_{\rm T}, j) > 30^\circ$,

and if only two jets then $\Delta\phi(j_1, j_2) < 150^\circ$;

(*iv*) one muon with $p_{\rm T} > 2$ GeV, $|\eta| < 1.7$ within $\Delta R = 0.4$ of a jet;

(*v*) no other visible leptons;

(*vi*) no SVX b tag.

Cuts (*i*) to (*iii*) are implemented for the same reasons as in the previous channel. The charm tag lets us relax our jet $p_{\rm T}$ requirement. Cut (*iv*) identifies the muon tagging a c-jet. After this cut, some background events will have genuine c-jets, others will have μ-tagged b quarks, and yet others will get fake c-tags due to miscellaneous muons accidentally coinciding with unrelated jets. Most $t\bar{t}$ events in this sample are of the $b \to \mu$ sort. Significant numbers of $Z \to \nu\bar{\nu}$ events are also of this type, since $Z \to \nu\bar{\nu}$ events which pass the initial cuts are almost all due to gluon splitting to heavy flavors, and $g \to b\bar{b}$ occurs roughly as often as $g \to c\bar{c}$ for these events after the hard cuts (*i*) and (*ii*). We veto extra isolated leptons and identified b-jets with cuts (*v*) and (*vi*).

After these cuts, we still have the reducible background from non-SVX-tagged b-jet production as well as fake c-tags, in addition to the irreducible background with real c-tags. To reduce the former, we consider the transverse momentum of the muon with respect to its tagged jet. This is

$$p_{\rm T}^{\rm rel} \equiv |\vec{p}(\mu) \times \hat{p}(j)|\,,$$

where $\hat{p}(j) = \vec{p}(j)/|\vec{p}(j)|$ is the jet direction unit vector. Since $m_b > m_c$, the average $\left\langle p_{\rm T}^{\rm rel} \right\rangle$ will be greater for b-jet samples than for c-jet samples. Figure 4.8 displays scatter plots of $p_{\rm T}^{\rm rel}$ versus the μ–jet axis separation $\Delta R(\mu, j)$ for the backgrounds together with a pair of representative signal samples. Also shown is the line $\Delta R + p_{\rm T}^{\rm rel}/5$ GeV $= 0.4$ which we have selected for our cut. The efficient separation is

Figure 4.8: Scatter plots of $p_{\mathrm{T}}^{\mathrm{rel}}$ vs $\Delta R\,(\mu, j)$ for backgrounds and selected signal points in the c-tagged channel after cut (vi). The diagonal line shows the cut (vii) line $\Delta R + p_{\mathrm{T}}^{\mathrm{rel}}/5$ GeV= 0.4.

background	(vi)	(vii)	$(viii)$
$W \to \tau\nu$	34.7	16.7	7.1
$W \to \ell\nu$	61.3	9.9	4.8
$Z \to \nu\bar{\nu}$	20.5	14.2	6.6
$t\bar{t}$ (175)	22.5	11.4	4.4
total	139.0	52.2	22.9
25%	34.7	13.0	5.8
5σ @ 2 fb^{-1}	41.7	25.5	(4.8)
$\tilde{t}_1, \widetilde{Z}_1$	(vi)	(vii)	$(viii)$
120,80	59.9	48.1	33.5
160,90	36.9	30.3	19.3
180,110	19.1	15.9	10.0

Table 4.2: c-tagged channel cross-sections, in fb, after cuts as discussed in the text. The line labelled "25%" shows 25% of the total background, and the "5σ" line shows the signal level needed to produce a 5σ excess at 2 fb^{-1}. The parenthesized 5σ value in the last column is for an integrated luminosity of 25 fb^{-1}. For the signal cases, $\tilde{t}_1$ and $\widetilde{Z}_1$ masses are given in GeV

obvious from the diagram, and we enhance the c-jet purity by requiring

$$(vii) \qquad \Delta R(\mu, j) \; + \; p_{\rm T}^{\rm rel}(\mu|j)/5 \text{ GeV} < 0.4.$$

As shown in Table 4.2, this cut eliminates 60% of the background at a typical cost of 20% in signal. The large reduction shown in the table for $W \to \ell\nu$ is due to the limit on $p_{\rm T}^{\rm rel}$, since the high-$p_{\rm T}$ muons in these events are only coincidentally associated with a jet. We have checked further cuts, such as limits on $p_{\rm T}(\ell)$, and found that they have nothing substantial to add after cut (vii).

A contour plot summarizing the result of applying cuts (i)-(vii) is shown in Fig. 4.9. The total background remaining at this level is 52.2 fb. The heavy solid line in the figure gives the 25.5 fb signal level, which corresponds to 5σ at an integrated luminosity of 2 fb^{-1}. This channel affords substantially more coverage than the $\not\!\!E_{\rm T}$ + jets channel of the previous section, and much of the parameter space $m_{\tilde{t}_1} \lesssim 170$ GeV, $m_{\widetilde{Z}_1} \lesssim 90$ GeV is accessible to detection.

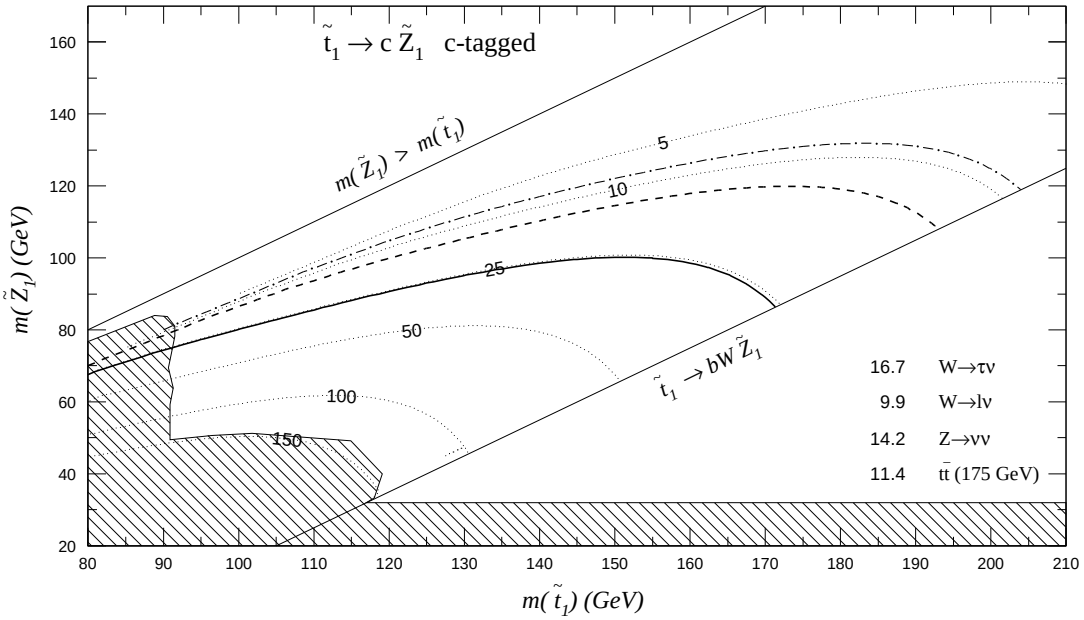

Figure 4.9: Cross-section contours, in fb, for the c-tagged channel after cut (*vii*) as described in the text. The heavy solid line at 25.5 fb is the 5σ discovery limit for an integrated luminosity of 2 fb^{-1}. The dashed line is 13 fb of signal, which is 25% of background. The dot-dashed line shows the reach at 25 fb^{-1} after cut (*viii*). The hatched region is experimentally excluded at the 95% confidence level.

Some recent analyses[19, 51] have looked at tagging charm jets directly with the SVX. The CDF Collaboration has done this for the Run I data, yielding the excluded regions shown on Figs. 4.7 and 4.9. They rely on improved resolution to identify the small impact parameters of c-decay displaced vertices. This analysis has been extended for the Run II scenario[51]. These searches proceed in a complementary channel to the one we investigate here, since they accept SVX tags and reject identified leptons (to reduce W and Z backgrounds) while we veto SVX tags and require a lepton. The CDF estimated reach with these cuts is similar in extent to ours. It may be worth investigating whether combining the two c-tagging techniques would further extend the Tevatron reach.

4.2.3 Run II+

Unlike the $\not\!\!E_{\rm T}$ + jets channel, the signal in the c-tagged channel is not background limited at 2 fb^{-1}, as indicated by the large gap between the solid 5σ line at 25.5 fb and the dashed $N_s/N_b = 25\%$ line at 13 fb. Thus, more integrated luminosity can rapidly improve the reach with these same cuts. By eqn. (3.6), 7.7 fb^{-1} will bring us to the 13 fb contour. After this point further cuts are needed for the Run II+ scenario.

To cut the background further, we note that by vetoing events with non-tagging leptons we have increased the fraction of hadronically decaying ts, so that most $t\bar{t}$ events surviving cut (*vii*) are either $t \to W \to \tau$ decays or $\ell\nu$ + 4-jet events with the lepton faking a charm tag. About 60% of these events have 5 or more reconstructed jets, as seen in Fig. 4.10, so limiting the jet multiplicity helps suppress $t\bar{t}$.

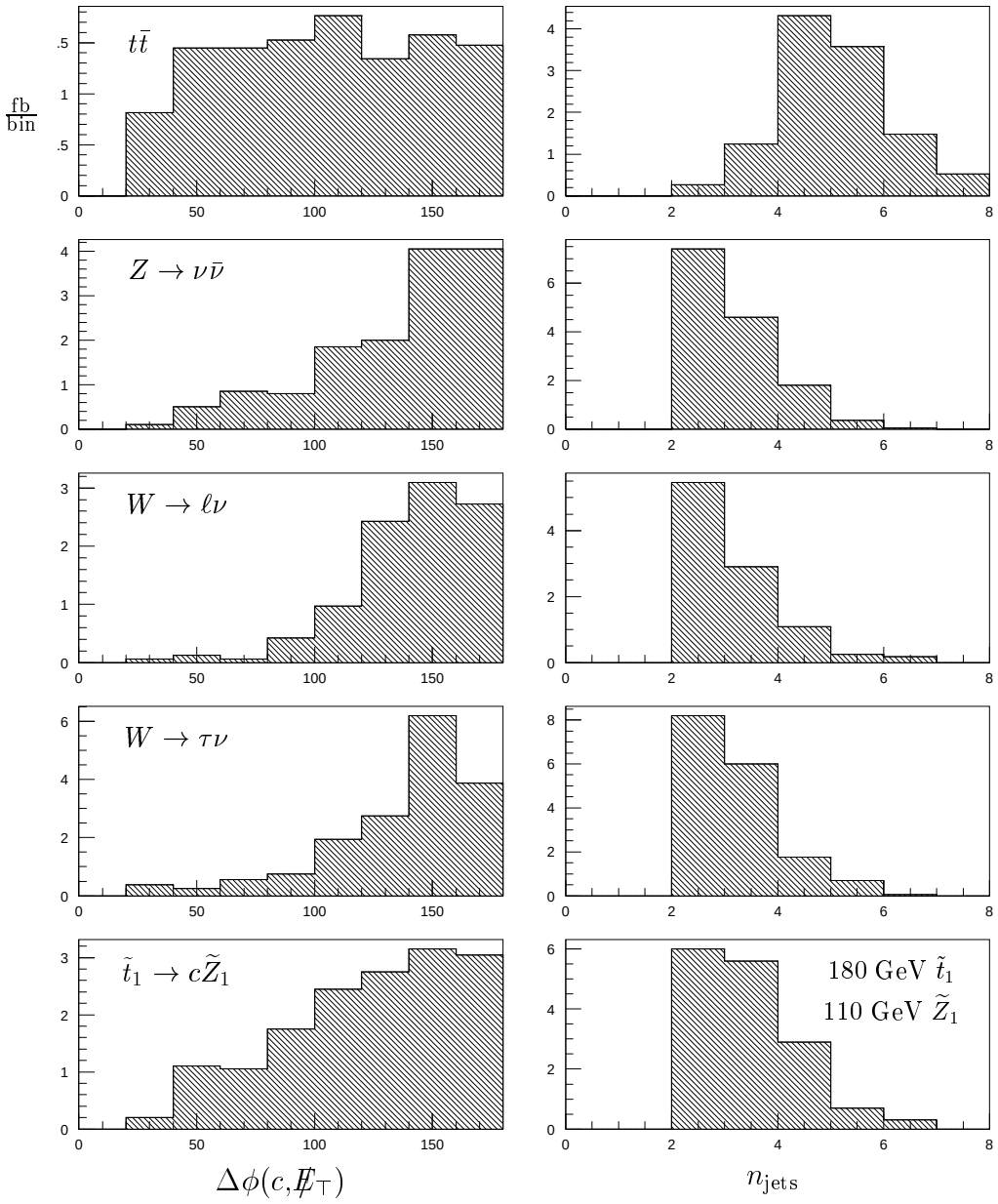

Figure 4.10: Distributions of $\Delta\phi(c,\not{E}_{\rm T})$ and $n_{\rm jets}$ in the c-tagged channel for a signal case of 180 GeV $\tilde{t}_1 \to$ 110 GeV $\widetilde{Z}_1$ and backgrounds $t\bar{t}$, $Z \to \nu\bar{\nu}$, $W \to \ell\nu$ and $W \to \tau\nu$, after cut (*vii*). The vertical axes are in fb/bin.

As in the previous channel, the jets in $Z \to \nu\bar{\nu}$ recoil against the Z boson, which itself is converted to $\not\!\!E_{\rm T}$. Thus the angle $\Delta\phi(c,\not\!\!E_{\rm T})$ between the tagged jet and $\not\!\!E_{\rm T}$ will be large. For $\tilde{t}_1^*\tilde{t}_1$ there are two c-jets recoiling independently against their two LSPs, and the distribution of $\Delta\phi(c,\not\!\!E_{\rm T})$ should be broader. This is indeed the case, as shown in Fig. 4.10. In $W \to \ell\nu$ events with $p_{\rm T}(W) \ll m_W$, the angle $\Delta\phi(\ell,\nu)$ will be large and if ℓ mistags a jet and ν supplies $\not\!\!E_{\rm T}$ then $\Delta\phi(c,\not\!\!E_{\rm T})$ will be large too. We address these points by insisting that $\not\!\!E_{\rm T}$ and the c-jet not be too back-to-back (75% of the Drell-Yan background has $\Delta\phi(c,\not\!\!E_{\rm T})$ greater than 120°). Our Run II+ optimized high luminosity cut is

$$(viii) \quad \Delta\phi(c,\not\!\!E_{\rm T}) < 145^\circ \text{ and } n_{\rm jets} < 5$$

which eliminates over half of the background events and fewer than 1/3 of the signal events. Cross-sections after this cut are shown in Table 4.2. The dot-dashed discovery line in Fig. 4.9 indicates that $\tilde{t}_1$s as heavy as 200 GeV may be accessible to the Run II+ Tevatron in this channel, even if the $\widetilde{Z}_1$ mass is well beyond 100 GeV.

It is amusing to note, with reference to Fig. 4.9, that if (1) the electroweak baryogenesis story of Section 2.1.1 is correct and $m_{\tilde{t}_1} \lesssim 160$ GeV, and (2) the galactic halo story of Section 2.1.1 is correct and $m_{\tilde{t}_1} - m_{\widetilde{Z}_1} \gtrsim 20$ GeV, and (3) we "double" the integrated luminosity by combining the CDF and D0 experimental results, and (4) the stop decays as $\tilde{t}_1 \to c\widetilde{Z}_1$ without the 4-body decay of Section 2.2 having a significant branching fraction, *then* the stop should be discovered at the Run II+ Tevatron!

Chapter 5

The decay mode $\tilde{t}_1 \to b\widetilde{W}_1$

When $m_{\tilde{t}_1} > m_b + m_{\widetilde{W}_1}$, the stop decays via $\tilde{t}_1 \to b\widetilde{W}_1$ with essentially 100% branching fraction since competing decays occur only at higher order. The $\widetilde{W}_1$ then cascades to a $\widetilde{Z}_1$ plus a SM fermion pair. Unlike the $\tilde{t}_1 \to c\widetilde{Z}_1$ mode, where the analysis depended only on $m_{\tilde{t}_1}$ and $m_{\widetilde{Z}_1}$, here we have 4 parameters: the three masses $m_{\tilde{t}_1}$, $m_{\widetilde{W}_1}$, $m_{\widetilde{Z}_1}$ and the leptonic branching fraction of the chargino, $\mathcal{B}(\widetilde{W}_1 \to e, \mu \text{ or } \tau)$ (assuming lepton universality in $\widetilde{W}_1$decays). To make the parameter space tractable, we will adopt the gaugino unification relation $m_{\widetilde{W}_1} \approx 2m_{\widetilde{Z}_1}$ (eqn. (1.6)) for most of the discussion, and separately examine the consequences of relaxing this. We also will take $\mathcal{B}(\widetilde{W}_1 \to \ell) \approx \mathcal{B}(W \to \ell)$ for the main analysis.

When both $\widetilde{W}_1$'s decay hadronically, the signal is jets plus $\not\!\!E_{\rm T}$ from the pair of $\widetilde{Z}_1$'s. This signal, with degraded $\not\!\!E_{\rm T}$ due to the two-step decay of the $\tilde{t}_1$, is difficult to discriminate from SM processes. Therefore, we focus on channels where one or both $\widetilde{W}_1$'s decay leptonically. In the case of one leptonic decay we look for a hard isolated lepton together with a b-tag along with the usual $\not\!\!E_{\rm T}$. We refer to this search as the "b-jet + lepton channel". In the "dilepton channel" we look for $\not\!\!E_{\rm T}$ plus 2 unlike-sign isolated leptons (e or μ) as the result of both $\widetilde{W}_1$'s decaying to leptons.

The dominant background in both channels is SM $t\bar{t}$ production and decay followed by the leptonic decay of one or both W's; such processes have b-jets, leptons and substantial $\not\!\!E_{\rm T}$ from the associated neutrinos. Indeed, the decays $t \to bW \to b\bar{f}f'$ and $\tilde{t}_1 \to b\widetilde{W}_1 \to b\bar{f}f'\widetilde{Z}_1$ differ only in the presence of two $\widetilde{Z}_1$'s in $\tilde{t}_1{}^*\tilde{t}_1$ events and the presence of on-shell Ws in $t\bar{t}$ events; event topologies from stop and top production are identical. The two massive $\widetilde{Z}_1$s in the final state lead to a distinctive softening of the spectra of many kinematical quantities in the signal events. The on-shell W in $t \to bW$ events implies useful kinematical constraints on its daughters $\bar{f}, f'$. This is especially helpful when only one of the Ws decays leptonically, in which case the transverse mass of the lepton and $\not\!\!E_{\rm T}$ help to discern the real W in the event. The W kinematics are also useful in suppressing other backgrounds, such as those due to Drell-Yan Ws, W radiation, and W pair production.

5.1 b-jet + lepton channel

In the b-jet + lepton channel, we look for $\not\!\!E_{\rm T}$, hard jets with a tagged b, and an isolated e or μ. In this channel we contend with two main SM backgrounds. The first is $t\bar{t}$ production, as mentioned above. The second is due to events with a leptonically decaying weak boson $W \to e, \mu, \tau$ associated with QCD radiation. This reaction has a huge cross-section, and readily delivers large $\not\!\!E_{\rm T}$ from the decay neutrino, along with a hard isolated lepton. Much of this background is suppressed by requiring a tagged b-jet in the event. The W jets that pass this criterion generally have bs from gluon splitting $g \to b\bar{b}$. A minor background comes from the process $Z \to \tau^+\tau^-$ when one of the τs decays leptonically and a real or fake b is tagged. We ignore mistagged b-jet backgrounds.

5.1.1 Run I

In our earlier pre-LEP analysis[28] of the Run I situation for this channel, we suggested the following initial cuts: (1) $\not\!\!E_{\rm T} > 25$ GeV; (2) at least 2 jets with $p_{\rm T} > 15$ GeV, one of which lies in the central region $|\eta| < 2$; (3) an isolated electron or muon with $p_{\rm T}\,(e) > 10$ GeV and $p_{\rm T}\,(\mu) > 5$ GeV; and (4) an SVX b-tag (with an efficiency estimated at 40% (in the barrel) $\times$ 30% (identified displaced vertex) = 13%)[1]. The purpose of these cuts is the same as the analogous cuts in our Run II analysis presented below. After these, we also recommended (5) no more than 4 jets (with $p_{\rm T} > 15$ GeV); and (6) the transverse mass cut $m_{\rm T}(\ell,\not\!\!E_{\rm T}) < 45$ GeV (see below for this quantity). We found that in this channel the signal dwindles as $m_{\tilde{t}_1} \to m_{\widetilde{W}_1}$, where the b becomes too soft to tag. We determined that the region $m_{\tilde{t}_1} \lesssim 90$ GeV, $m_{\widetilde{W}_1} \lesssim 60$ GeV would be accessible to this treatment with the Run I integrated luminosity of 100 pb^{-1}.

The CDF Collaboration examined this channel for 88 ± 4 pb^{-1} of their Run I data[20]. They used the cuts (1) $\not\!\!E_{\rm T} > 25$ GeV; (2) at least 2 jets with $p_{\rm T} > 12$ GeV for the hardest jet and $p_{\rm T} > 8$ GeV for the second jet; (3) an isolated electron or muon with $p_{\rm T} > 10$ GeV; and an SVX b-tag. They further required that (5) any dilepton have invariant mass $m\,(\ell^+\ell^-) < 60$ GeV; and (6) the azimuthal angles between $\not\!\!E_{\rm T}$ and each of the two hardest jets satisfy $\Delta\phi\,(\not\!\!E_{\rm T}, {\rm jet}) > 0.5$ rad. They found no evidence for $\tilde{t}_1^*\tilde{t}_1$ production, but were not able to improve the existing (LEP II) stop mass limits.

[1] In the meantime, SVX technology has improved considerably. Resolution has gone up and coverage has extended to $|\eta| < 2$. For Run II, both D0 and CDF will be equipped with SVX detectors.

5.1.2 Run II

For the higher luminosity run, our initial cuts for this channel are

- (i) $\not\!\!E_{\rm T} > 25$ GeV;
- (ii) exactly one isolated e or μ with $p_{\rm T} > 8$ GeV and $|\eta| < 2$;
- (iii) at least two jets with $p_{\rm T} > 15$ GeV and $|\eta| < 2$;
- (iv) at least one SVX b-tagged jet with $|\eta_B| < 1.4$.

Cuts (i) to (iii) are canonical for this channel. The b-tag, cut (iv), is critical to reduce the W background. The b-tagging efficiency for signal events ranges from one third to two thirds, while less than a percent of the W events get tagged. The $|\eta_B|$ distribution for W events with bs due to $g \to b\bar{b}$ is broader than that for signal events, as shown in Fig. 5.1, hence the cutoff at $|\eta_B| < 1.4$. The soft-lepton b-tagging used in SM $t\bar{t}$ studies is avoided here to avoid the large background from events like $sg \to Wc \to \ell\nu c$ or $q\bar{q} \to Wg \to \ell\nu dc\bar{c}$ where ℓ is isolated, ν provides $\not\!\!E_{\rm T}$, the c is tagged and g provides the second jet. (In the $t\bar{t}$ studies, one makes hard cuts to reject these W events; as we shall see below such hard cuts would remove too much of our stop signal.)

We expect that for $t\bar{t}$ and $W \to e, \mu$ backgrounds, where missing transverse energy is due to a single neutrino and $\not\!\!E_{\rm T} \sim p_{\rm T}(\nu)$, the transverse mass $m_{\rm T}(\ell,\not\!\!E_{\rm T})$ of the lepton and $\not\!\!E_{\rm T}$ should show a strong Jacobian peak near m_W, while the signal distribution should be a broad bump. Figure 5.2 shows that this is indeed the case. The transverse mass is the invariant mass of the $\not\!\!E_{\rm T}$ vector and the projection of the lepton's momentum in the transverse plane,

$$m_{\rm T}(\ell,\not\!\!E_{\rm T})^2 = 2p_{\rm T}(\ell)\not\!\!E_{\rm T}(1 - \cos\Delta\varphi).$$

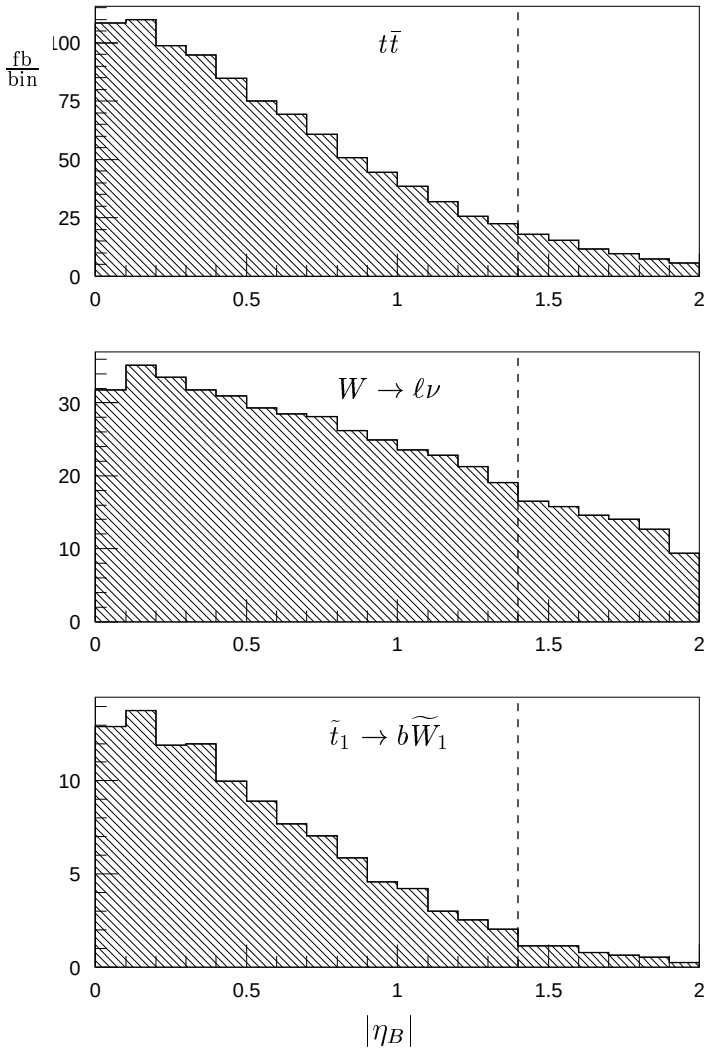

Figure 5.1: Distribution of $|\eta_B|$ in the b-jet + lepton channel for the initial cut sample. The signal case is a 160 GeV $\tilde{t}_1$ decaying to a 120 GeV $\widetilde{W}_1$ which in turn decays to a 60 GeV $\widetilde{Z}_1$. The vertical axes are in fb/bin.

background	(iv)	(v)	(vi)	(vii)	$(viii)$	(ix)
$t\bar{t}$ (175)	916	247	138	138	80	15.7
$W \to e, \mu, \tau$	387	96	88	51	48	5.2
total	1303	343	226	189	128	20.9
25%	326	86	56	47	32	5.2
5σ @ 2 fb^{-1}	128	66	53	49	40	(4.6)
$\tilde{t}_1$, $\widetilde{W}_1$	(iv)	(v)	(vi)	(vii)	$(viii)$	(ix)
140, 120	134	72	66	55	50	6.4
160, 120	106	57	50	47	40	7.4
180, 110	65	36	29	29	23	5.1

Table 5.1: b-jet + lepton channel cross-sections, in fb, after cuts as discussed in the text. Signal levels required for detection are given in the "25%" and "5σ" rows. The parenthesized 5σ value in the last column is for an integrated luminosity of 25 fb^{-1}. For the signal cases, $\tilde{t}_1$ and $\widetilde{W}_1$ masses are given in GeV, and $m_{\widetilde{Z}_1} = m_{\widetilde{W}_1}/2$. Cut (ix) is made after cut $(viii')$.

We can get even more information from this kinematical data by forming a "semi-transverse" mass which is the invariant mass of $\not{E}_{\rm T}$ and the lepton's full 4-momentum:

$$m_{\rm T+}(\ell,\not{E}_{\rm T})^2 = 2p_{\rm T}\,(\ell)\not{E}_{\rm T}\,(1/\sin\vartheta_\ell - \cos\Delta\varphi) \tag{5.1}$$

where $\vartheta_\ell = 2\arctan\exp(-\eta_\ell)$ is the lepton's polar angle. The $m_{\rm T+}$ distribution is also plotted in Fig. 5.2, where one sees that for the W-containing backgrounds it has a broader high-end tail than $m_{\rm T}$, and that the distribution vanishes in the limit $m_{\rm T+} \to 0$, unlike $m_{\rm T}$ which remains finite there. Both of these behaviors make $m_{\rm T+}$ a better discriminator than $m_{\rm T}$, as the signal distributions for the two quantities are largely the same. With a cut of

$$(v) \quad m_{\rm T+}(\ell,\not{E}_{\rm T}) < 60 \text{ GeV}$$

3/4 of the $t\bar{t}$ and $W \to \ell\nu$ background is removed with less than half of the signal lost. (In comparison, an $m_{\rm T}$ cut removes less than 2/3 of the background Ws at the same signal loss.) The results of this cut are listed in Table 5.1.

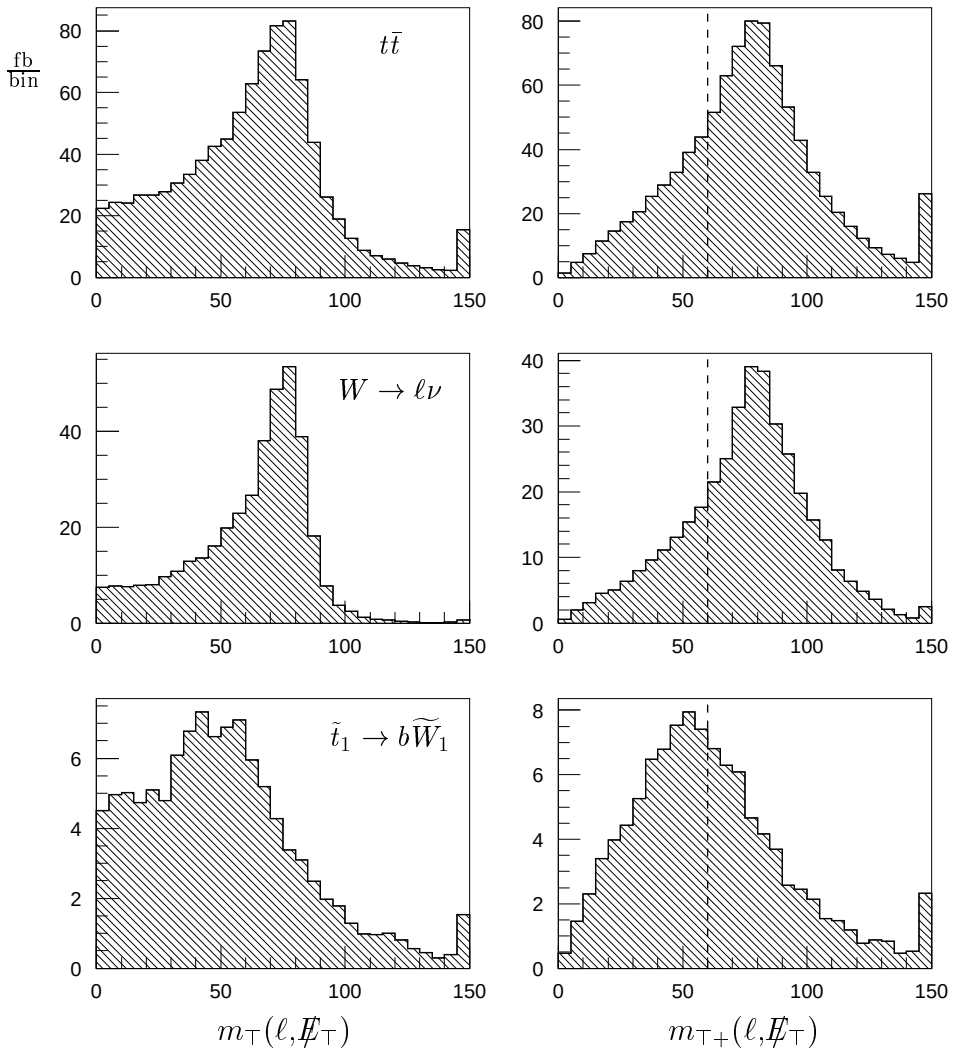

Figure 5.2: Distributions of $m_{\rm T}(\ell,\not\!\!E_{\rm T})$ and $m_{\rm T+}(\ell,\not\!\!E_{\rm T})$ in the b-jet + lepton channel, after cut (iv). The signal case is a 160 GeV $\tilde{t}_1$ decaying to a 120 GeV $\widetilde{W}_1$ which in turn decays to a 60 GeV $\widetilde{Z}_1$. The vertical axes are in fb/bin. The dashed lines show cut (v).

The $t\bar{t}$ background still dominates the signal. To reduce it further, we note that the lepton from W decay is typically more energetic than that from $\widetilde{W}_1$ decay. In the decaying W or $\widetilde{W}_1$ frame, one can crudely compare the available lepton energy, $m_W/2$ for $W \to \ell\nu$, with $(m_{\widetilde{W}_1} - m_{\widetilde{Z}_1})/2 \sim m_{\widetilde{W}_1}/4$ for $\widetilde{W}_1 \to \ell\nu\widetilde{Z}_1$ and use the fact that generally $m_{\widetilde{W}_1} < 2m_W$ for the models accessible in this channel. We have also found that the third jet tends to be harder in $t\bar{t}$ events than in our signal events. The reason is similar to that given for the lepton since, in the absence of hard QCD radiation, this third jet mainly comes from the hadronically decaying W or $\widetilde{W}_1$. We capture this feature by defining the quantity

$$W \equiv \sqrt{p_{\rm T}(\ell)^2 + p_{\rm T}(j_3)^2} \tag{5.2}$$

where $p_{\rm T}(j_3)$ is taken as 0 for those events with only two jets. Imposing the cut

$$(vi) \quad W < 60 \text{ GeV}$$

reduces the dominant background from $t\bar{t}$ by almost half and the signal by just 10–20%. W distributions are displayed in Fig. 5.3, and the results of the cut are tabulated in Table 5.1.

We turn our attention now to the W events, which are distinguished in several ways from the signal (and $t\bar{t}$) events. First, their jets come from QCD radiation so they have a lower jet multiplicity. Also, they have a low efficiency for a second b tag, a fact used in the Run II+ section below. Finally, the W and Z events are generally softer than the signal events, which is reflected in the distribution of the quantity

$$H_{T+} \equiv \not{E}_{\rm T} + p_{\rm T}(\ell) + \sum_j p_{\rm T}(j), \tag{5.3}$$

which is well-known from $t\bar{t}$ studies to provide a good separation of $t\bar{t}$ from the $W \to e, \mu, \tau$ background. Figure 5.4 shows these distributions. The $\tilde{t}_1$ distribution

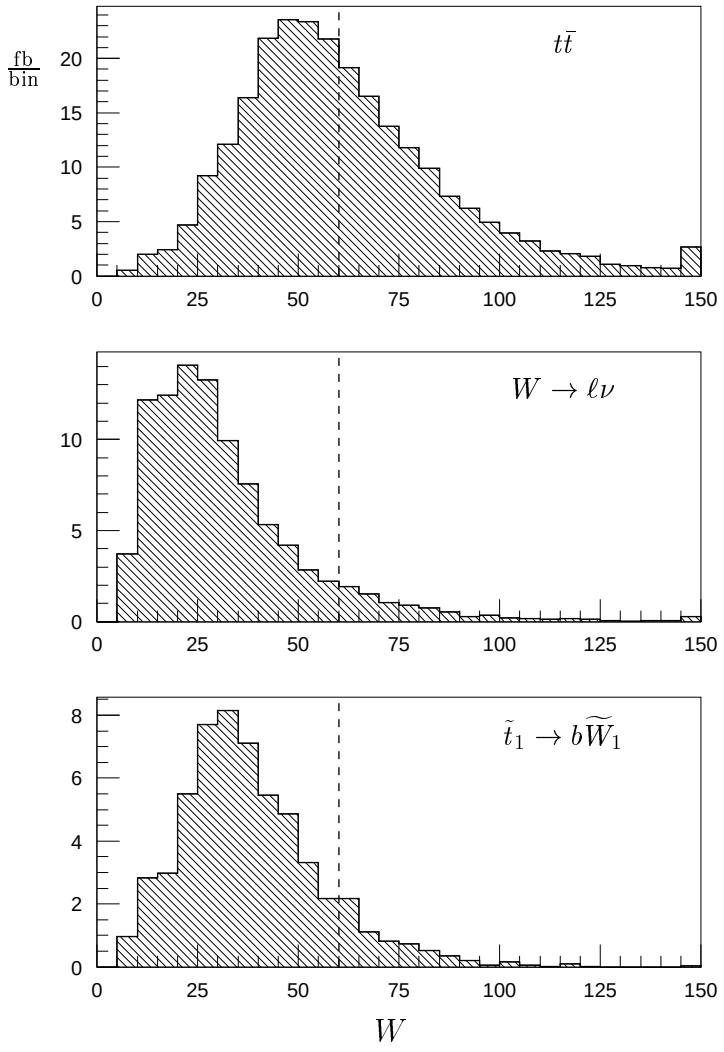

Figure 5.3: Distribution of W in the b-jet + lepton channel, after cut (v). The signal case is a 160 GeV $\tilde{t}_1$ decaying to a 120 GeV $\widetilde{W}_1$ which in turn decays to a 60 GeV $\widetilde{Z}_1$. The vertical axes are in fb/bin. The dashed lines at $W = 60$ GeV indicate cut (vi).

unfortunately falls in between the two backgrounds, a predicament which is quite general across the parameter space we have investigated for this channel. Still, the cut

$$(vii) \quad H_{T+} > 140 \text{ GeV}$$

eliminates 40% of the W background with only a few percent loss of signal, as shown in Table 5.1.

So far, we have not used the fact that elaborate techniques have been developed for reconstructing $t\bar{t}$ events. The single lepton plus b-tag channel is a primary source of $t\bar{t}$ events for Standard Model top mass reconstruction studies and our experimental colleagues will certainly subject events in this channel to a thorough characterization using these techniques. Mass reconstructions begin by assuming that the missing E_T represents the momentum of the ν from a leptonic $W \to \ell\nu$ decay (the other W is assumed to have decayed hadronically). By forcing ν and ℓ to reconstruct a real W, one gets two solutions for the longitudinal momentum of the ν. Together with combinatorics from assigning jets to the (possibly tagged) bs, the hadronic W daughters and miscellaneous QCD radiation, one gets several fitted solutions. For top mass reconstruction studies, these solutions are variously all used, used with weights, or judged to select a best solution. Although straightforward in principle, such analyses are quite complicated in practice. Results are sensitive functions of jet energy corrections, and thus depend strongly on the details of the detector simulation.

To estimate the utility of using $t\bar{t}$ characterization to suppress these events as a background, we have performed toy reconstructions on our Monte Carlo samples. We use the procedure outlined above, without applying jet energy corrections. For

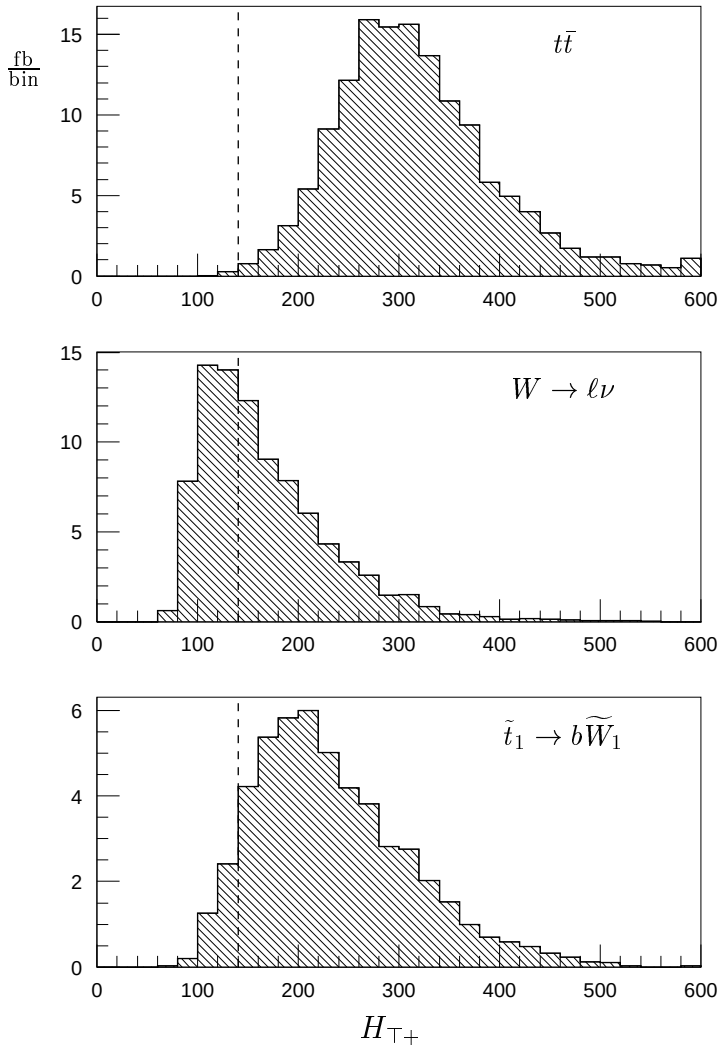

Figure 5.4: Distribution of $H_{\mathrm{T}+}$ in the b-jet + lepton channel after cut (*vi*). The signal case is a 160 GeV $\tilde{t}_1$ decaying to a 120 GeV $\widetilde{W}_1$ which in turn decays to a 60 GeV $\widetilde{Z}_1$. The vertical axes are in fb/bin. The dashed line at $H_{\mathrm{T}+} = 140$ GeV shows cut (*vii*).

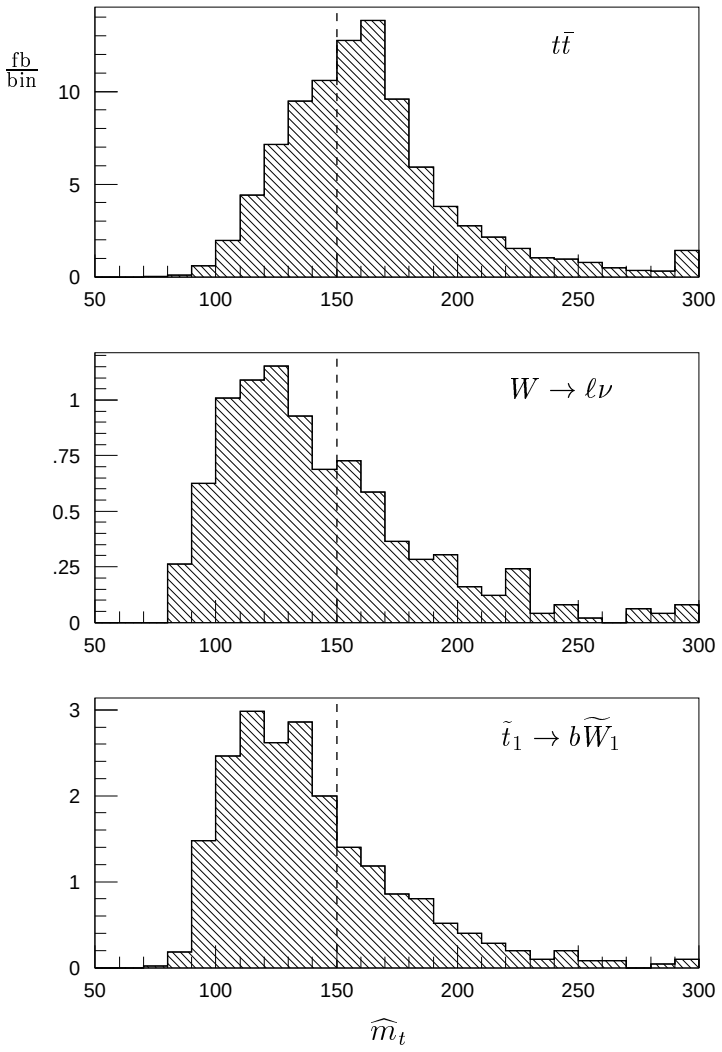

Figure 5.5: Distribution of $\widehat{m}_t$ in the b-jet + lepton channel after cut (*vii*). The signal case is a 160 GeV $\tilde{t}_1$ decaying to a 120 GeV $\widetilde{W}_1$ which in turn decays to a 60 GeV $\widetilde{Z}_1$. The vertical axes are in fb/bin. Events that are not reconstructible (for which $\widehat{m}_t = 0$) are not shown in the plots; the plotted events constitute 82% of the $t\bar{t}$ sample, 15% of the $W \to \ell\nu$ background, and 46% of the signal sample.

each event, we judge a best solution to be that which minimizes the quantity

$$(m_t^{\rm lep} - m_t^{\rm had})^2 + (m_W(jj) - m_W)^2, \tag{5.4}$$

where $m_t^{\rm lep}$ is the reconstructed mass of the semi-leptonic top, $m_t^{\rm had}$ that of the hadronic top, and $m_W(jj)$ the invariant mass of the two jets assigned to the hadronic W. From this best solution we form the quantity

$$\widehat{m}_t \equiv (m_t^{\rm lep} + m_t^{\rm had})/2 \tag{5.5}$$

which is our (crude) representation of the fitted top mass. Reconstruction is not possible for events with less than four jets, and for those events we define $\widehat{m}_t = 0$. Events with more than four jets are reconstructed with all possible jet assignments to find the best fit. The resulting $\widehat{m}_t$ distributions are shown in Fig. 5.5. The crudity of our reconstruction is manifested in the $t\bar{t}$ plot, which is asymmetric and peaks noticeably below m_t, largely due to our lack of jet energy correction. Even at this level of sophistication though we can reject almost half of the $t\bar{t}$ contamination with a penalty of less than 15% of signal by cutting

$$(viii) \quad \widehat{m}_t < 150 GeV.$$

Figure 5.6 summarizes the discovery potential of applying cuts (i)–$(viii)$ in the b-jet + lepton channel. The parameter space of this plot is $m_{\tilde{t}_1}$–$m_{\widetilde{W}_1}$, where we have taken $m_{\widetilde{Z}_1} = m_{\widetilde{W}_1}/2$ and $\mathcal{B}(\widetilde{W}_1 \to \ell) = \mathcal{B}(W \to \ell)$. The contours show signal cross-sections in fb, on a total background of 128 fb. The solid line at 40 fb indicates the 5σ reach for 2 fb^{-1} of integrated luminosity, which is an expected 80 SUSY events on top of 256 SM events. The dashed line corresponds to a quarter of the background cross section. Stops with mass up to $\sim$ 160 GeV should be

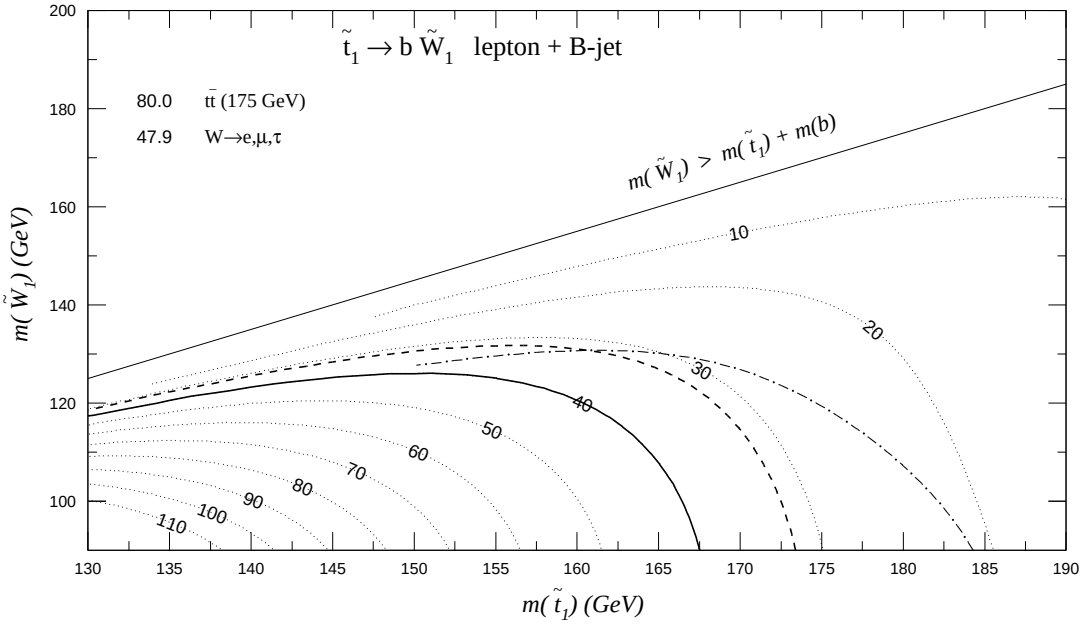

Figure 5.6: Cross-section contours, in fb, for the b-jet + lepton channel after cut (*viii*) as described in the text. The heavy solid line at 40 fb is the 5σ discovery limit for an integrated luminosity of 2 fb^{-1}. The dashed line is 32 fb of signal, which is 25% of background. The dot-dashed line shows the reach at 25 fb^{-1} after cut (*ix*). We have set $m_{\widetilde{Z}_1} = m_{\widetilde{W}_1}/2$ for the signal cases.

discoverable in this channel for charginos lighter than 120 GeV. Notice from Table 5.1 that for lighter stops cuts (*i*) - (*vi*) may give a better significance of the signal.

Relaxing the assumption $m_{\widetilde{Z}_1} = m_{\widetilde{W}_1}/2$

If we consider models more general than mSUGRA and its cogeners, which have strict gaugino unification at the GUT scale, then the relationship $m_{\widetilde{Z}_1} = m_{\widetilde{W}_1}/2$ of eqn. 1.6 may fail to hold[2]. We study this situation by performing our analysis in the $m_{\widetilde{W}_1} - m_{\widetilde{Z}_1}$ plane for the case of a 160 GeV stop. Our results are presented in the contour map of Fig. 5.7. The contours are signal cross-sections in fb after cut (*viii*) and we show the 32 fb and 40 fb reach lines, as in Fig. 5.6. The straight dot-dashed line traces $m_{\widetilde{Z}_1} = m_{\widetilde{W}_1}/2$, and indicates the slice of this plot corresponding to the $m_{\tilde{t}_1} = 160$ GeV slice of Fig. 5.6. The diagonal line cutting off the lower right corner is where $\widetilde{Z}_1$ fails to be the LSP, contrary to our hypothesis.

The straight solid line marked $m_{\widetilde{W}_1} = m_{\widetilde{Z}_1} + M_W$ indicates where the mediating W^* in the chargino decay (see Fig. 2.5a and attendant discussion) goes on-shell. The signal efficiency falls in this region as our W-rejection cuts take hold. Also, when $\widetilde{Z}_1$ is too light, the fermions from the $\widetilde{W}_1$ decay are energetic enough that the cuts (*v*) and (*vi*) designed to suppress $t\bar{t}$ background erode the signal as well. In the main part of the plot, the efficiency is fairly independent of the $\widetilde{Z}_1$ mass, but it falls again in the limit $m_{\widetilde{Z}_1} \to m_{\widetilde{W}_1}$, as the lepton becomes undetectable. In general, the $\tilde{t}_1$ detectability declines outside the region $m_{\widetilde{W}_1}/2 \lesssim m_{\widetilde{Z}_1} \lesssim 2m_{\widetilde{W}_1}/3$.

[2]Indeed, this relation is only approximately true even in the mSUGRA framework because of gaugino-higgsino mixing.

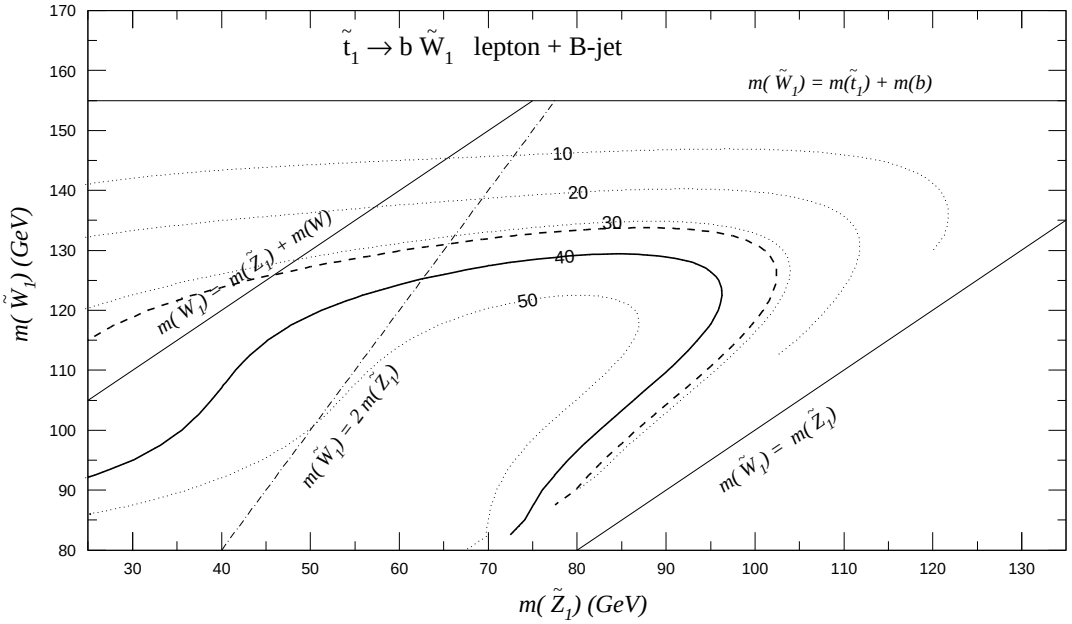

Figure 5.7: Cross-section contours, in fb, for the b-jet + lepton channel in the $m_{\widetilde{W}_1}$–$m_{\widetilde{Z}_1}$ plane after cut (*viii*) as described in the text. The top squark mass is 160 GeV. Annotations are as in Fig. 5.6.

Relaxing the assumption $\mathcal{B}(\widetilde{W}_1 \to \ell) \approx \mathcal{B}(W \to \ell)$

We can also ask what happens if the chargino's leptonic branching fraction is not W-like. As discussed in Section 2.2, this is due to $\tilde{f}^*$-mediated decays, which for models with GUT scale universal scalar masses will usually favor slepton mediation (over squark mediation) due to general features of the RGE. This will increase lepton production and for moderate values of the enhancement

$$r = \frac{\mathcal{B}(\widetilde{W}_1 \to \ell)}{\mathcal{B}(W \to \ell)} \tag{5.6}$$

the signal cross-sections should go up by the factor r (without any increase in backgrounds)[3]. Of course, in the limit that $\widetilde{W}_1$ decays *only* to leptons the signal will be lost, since we veto the second lepton in this channel. The single-lepton fraction is maximized when $\mathcal{B}(\widetilde{W}_1 \to \ell) = 0.5$, or $r \approx 2$. If r were to actually take this value, then the discovery reach at 2 fb^{-1} would extend to the 20 fb line of Fig. 5.6, finding stops as heavy as 185 GeV and charginos as heavy as 140 GeV.

5.1.3 Run II+

The $N_S/N_B = 25\%$ line at 32 fb in Fig. 5.6 is well beyond the $N_S/\sqrt{N_B} = 5\sigma$ line at 40 fb, which indicates that we can do more with cuts $(i)-(viii)$ if more integrated luminosity is available. The 5σ reach would extend out to the 32 fb line with 3.2 fb^{-1} of data (see eqn. (3.6)), revealing stops almost as heavy as the top quark. For even higher integrated luminosities, we can reduce the $t\bar{t}$ background by making a deeper cut on the reconstructed top mass

$$(viii') \quad \widehat{m}_t < 125 \text{ GeV}.$$

[3]An admixture of the sfermion-mediated diagram could also change the production kinematics. For instance, if $m_{\widetilde{W}_1} \approx m_{\tilde{\nu}_\ell} \ll m_{\tilde{\ell}}$, then the dominant $\tilde{\nu}_\ell$-mediated decay would produce very soft leptons.

Then we can attack the W background by insisting on a second b-tag. In general, the W event's tagged b jets are less distinguishable since they are due to gluon splitting ($g \to b\bar{b}$ frequently forms only one jet). This leads to a low efficiency for double-tagging; while the signal and $t\bar{t}$ events have about a 25% probability of having a second b tag, only about 8% of the W and Z events get this second tag. We require a second tag in the Run II+ scenario:

$$(ix) \quad \text{at least 2 } b\text{-tags}$$

At 25 fb^{-1} of data these cuts give the dot-dashed line in Fig. 5.6, where the reach in $m_{\tilde{t}_1}$ now extends well beyond m_t. The reach still cuts off at $m_{\widetilde{W}_1} \approx 125$ GeV though, presumably because the b-jets have to be hard enough in order to be tagged.

5.2 Dilepton channel

In the dilepton channel we look for two opposite sign hard isolated leptons, presumed to come from the leptonic decays of both $\widetilde{W}_1$s in the $\tilde{t}_1^*\tilde{t}_1$ event. The major backgrounds here are $t\bar{t}$, as usual, along with W pair production and the processes $Z \to \ell^+\ell^-$ ($\ell = e, \mu$) and $Z \to \tau^+\tau^-$. (Note that $Z \to \tau^+\tau^-$ was left out of the study [28].) As in the channels previously investigated here, the $t\bar{t}$ background is controlled by rejecting events which are too "hard." The W pair process has a modest production cross-section, but in the absence of b-tagging its event topology is quite similar to that of $\tilde{t}_1^*\tilde{t}_1$ and this background proves the most difficult to remove. Drell-Yan $Z \to \ell^+\ell^-$ has a large production cross-section, but there is no source of $\not\!\!E_{\rm T}$ in the basic reaction and those events which remain are effectively controlled by reconstructing the Z boson from the same-flavor dilepton invariant mass. Finally,

to reduce the background from $Z \to \tau^+\tau^-$ with both τs decaying leptonically we reconstruct the $\tau^+\tau^-$ invariant mass, as explained below.

5.2.1 Run I

For the dilepton channel, our Run I analysis[28] proposed the following cuts: (1) $\not\!\!E_{\rm T}$> 25 GeV;(2) at least one jet with $p_{\rm T} > 15$ GeV and $|\eta| < 2$; (3) an opposite sign $\ell^+\ell'^-$ pair with $p_{\rm T}(\ell) > 8(5)$ GeV for $\ell = e(\mu)$; and (4) an azimuthal dilepton angle satisfying $20^\circ < \Delta\phi(\ell^+, \ell^-) < 160^\circ$. We also defined a kinematical quantity called bigness, B (see eqn. (5.8)), and imposed the cut (5) $B < 100$ GeV. Our analysis, which ignored the important background $Z \to \tau^+\tau^-$, found a reach to $m_{\tilde{t}_1} \lesssim 110$ GeV, $m_{\widetilde{W}_1} \lesssim 90$ GeV. We noted that in distinction to the b-jet + lepton channel the signal here was not strongly attenuated in the limit $m_{\tilde{t}_1} \to m_{\widetilde{W}_1}$, since a b-tag was not required.

This study was undertaken by the D0 Collaboration on 75 ± 8 pb^{-1} of their Run I data, looking specifically in the dielectron channel[6], in which the signal is four times smaller than if both electrons and muons are counted. They used the RGSEARCH cut optimization method and imposed (1) $\not\!\!E_{\rm T}$> 22 GeV; (2) $E_{\rm T}(j_1) >$ 30 GeV; (3) $p_{\rm T}(e_1) > 16$ GeV and $p_{\rm T}(e_2) > 8$ GeV; and (4) $m(e^+e^-) < 60$ GeV. They also applied our bigness cut as (5) $B < 90$ GeV. Two events remained in the data set after these cuts, and the experimenters found too much $Z \to \tau^+\tau^-$ background to set a meaningful limit. Below, we outline a technique which may be used to control this background.

5.2.2 Run II

The initial cuts for the dilepton channel are

- (i) $\not\!\!E_{\rm T}$> 25 GeV;
- (ii) at least one jet with $p_{\rm T} > 15$ GeV and $|\eta| < 2$;
- (iii) an opposite-sign $\ell^+\ell^-$ pair with $p_{\rm T}\,(\ell) > 10$ GeV and $|\eta| < 2$;
- (iv) $20^\circ < \Delta\phi(\ell^+, \ell^-) < 160^\circ$;
- (v) $m\left(\ell^+\ell^-\right)$ not between 80 and 100 GeV for same-flavor $\ell^+\ell^-$.

After these cuts, less than 1 fb of $Z \to \ell^+\ell^-$ ($\ell = e, \mu$) remains, and we do not consider it any further. The other backgrounds, together with some representative signal points, are displayed in Table 5.2. As shown in the table, the largest background after the Z veto cut (v) is $Z \to \tau^+\tau^-$. Although the Z in such events cannot be reconstructed in as straightforward a manner as for $Z \to \ell^+\ell^-$, an indirect method is available.

In the Z rest frame, the τs are highly relativistic, so that the lepton and neutrinos from $\tau \to \nu_\tau \nu \ell$ are strongly boosted along the τ direction. We approximate the τ^+ 3-momentum as $\vec{\tau}^+ \sim P_+ \hat{\ell}^+$ where $\hat{\ell}^+$ is the observed ℓ^+ unit direction vector and P_+ is the (unknown) magnitude of $\vec{\tau}^+$. Now, the Z transverse momentum all comes from its recoil against QCD radiation, so we can estimate it as $\vec{Z}_{\rm T} = -\sum_{\rm hadrons} \vec{E}_{\rm T}({\rm had})$. From above, we can also write $\vec{Z}_{\rm T} = (\vec{\tau}^+ + \vec{\tau}^-)_{\rm T} = (P_+\hat{\ell}^+ + P_-\hat{\ell}^-)_{\rm T}$. Therefore after solving the two components of

$$\left(P_+\hat{\ell}^+ + P_-\hat{\ell}^-\right)_{\rm T} = -\sum \vec{E}_{\rm T}({\rm had})$$

for the two unknowns P_+ and P_- we can reconstruct the τ 4-momenta as

$$\tau^\pm = (\sqrt{(P_\pm\hat{\ell}^\pm)^2 + m_\tau^2},\, P_\pm\hat{\ell}^\pm). \tag{5.7}$$

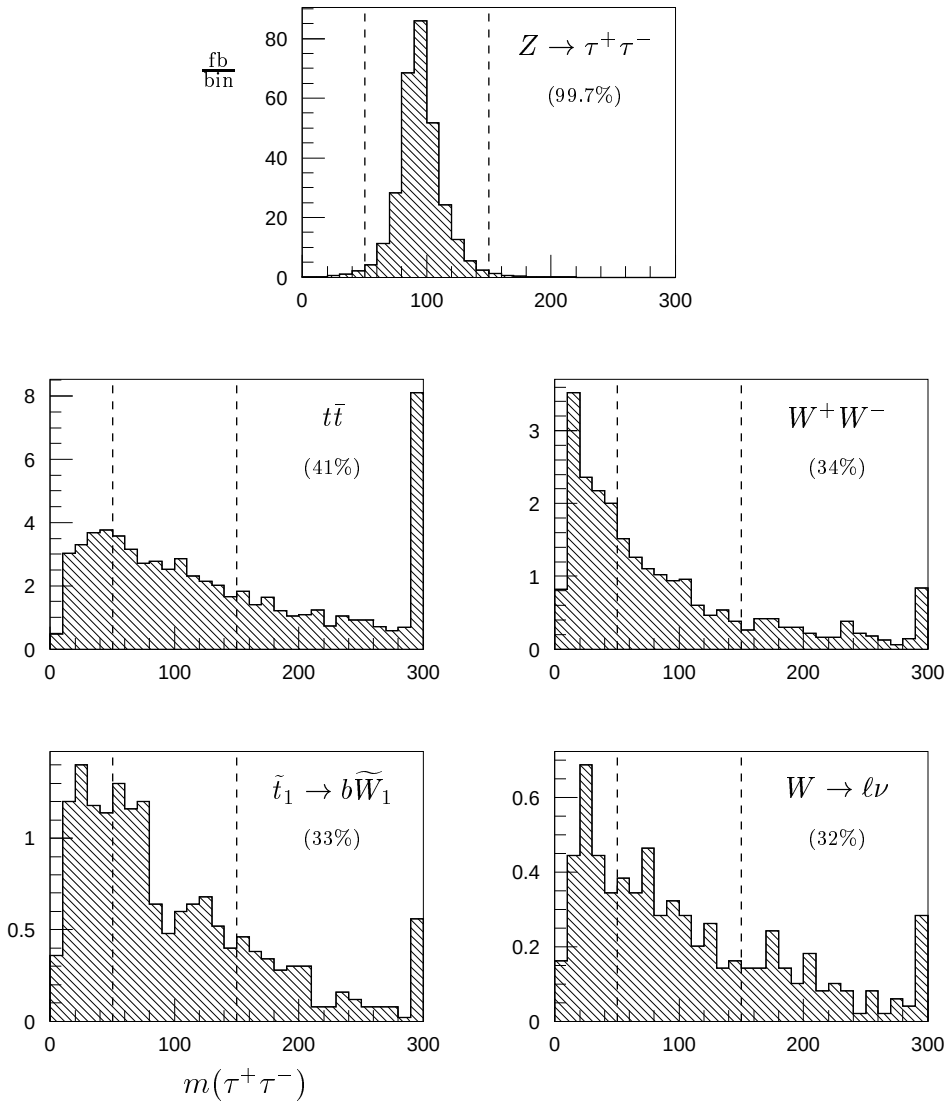

Figure 5.8: Distribution of $m(\tau^+, \tau^-)$ in the dilepton channel, after cut (v). The signal case is a 130 GeV $\tilde{t}_1$ decaying to a 100 GeV $\widetilde{W}_1$. The vertical axes are in fb/bin. Only events for which $m(\tau^+, \tau^-) > 0$ are shown; the percentage of such events is indicated in parentheses on the plots (so, 99.7% of the $Z \to \tau^+\tau^-$ events are plotted, but only 41% of the $t\bar{t}$ events). Dashed vertical lines indicate cut (vi).

background	(v)	(vi)	(vii)	$(viii)$	(ix)
$t\bar{t}$ (175)	155	129	24.7	17.0	10.7
W pair	70	61	27.8	18.5	0.1
$W \to e, \mu, \tau$	21	18	11.1	7.5	2.2
$Z \to \tau^+\tau^-$	302	7	6.9	5.7	0.2
total	548	215	70.5	48.7	13.2
25%	137	54	17.6	12.1	3.3
5σ @ 2 fb^{-1}	83	52	29.7	24.7	(3.6)
$\tilde{t}_1$, $\widetilde{W}_1$	(v)	(vi)	(vii)	$(viii)$	(ix)
130, 100	48.9	41.6	31.7	26.8	13.5
150, 110	24.9	21.1	14.2	12.6	7.2
170, 120	12.9	10.9	6.4	5.6	3.2

Table 5.2: dilepton channel cross-sections, in fb, after cuts as discussed in the text. Signal levels required for detection are given in the "25%" (of background) and "5σ" rows. The parenthesized 5σ value in the last column is for an integrated luminosity of 25 fb^{-1}. For the signal cases, $\tilde{t}_1$ and $\widetilde{W}_1$ masses are given in GeV, and $m_{\widetilde{Z}_1} = m_{\widetilde{W}_1}/2$.

Note that for this procedure to make sense for $Z \to \tau^+\tau^-$ both P_+ and P_- should be positive quantities, which is to say that neither τ should be oppositely directed to its lepton. (This condition is also equivalent to requiring that $Z_{\rm T}$ lie within the smaller angle of $\ell^+_{\rm T}$ and $\ell^-_{\rm T}$.) Distributions of $m(\tau^+, \tau^-)$ after cut (v) are displayed in Fig. 5.8 for those events with $P_+, P_- > 0$. We make the cut

$$(vi) \quad m(\tau^+, \tau^-) < 50 \text{ GeV or } m(\tau^+, \tau^-) > 150 \text{ GeV}$$

where we define $m(\tau^+, \tau^-) = 0$ if either $P_\pm \leq 0$. Essentially all of the $Z \to \tau^+\tau^-$ events have $P_+, P_- > 0$, while only about 40% of the signal events do. Table 5.2 shows the results of applying cut (vi), where we see that only 2% of the $Z \to \tau^+\tau^-$ background survives, while about 5/6 of the signal is retained.

Even after this cut, the signal is still below the 5σ level of observability. To achieve a further purification we note, as in the previous channel, that the presence in the background of two real Ws undergoing two-body decays $W \to \ell\nu$ will typically

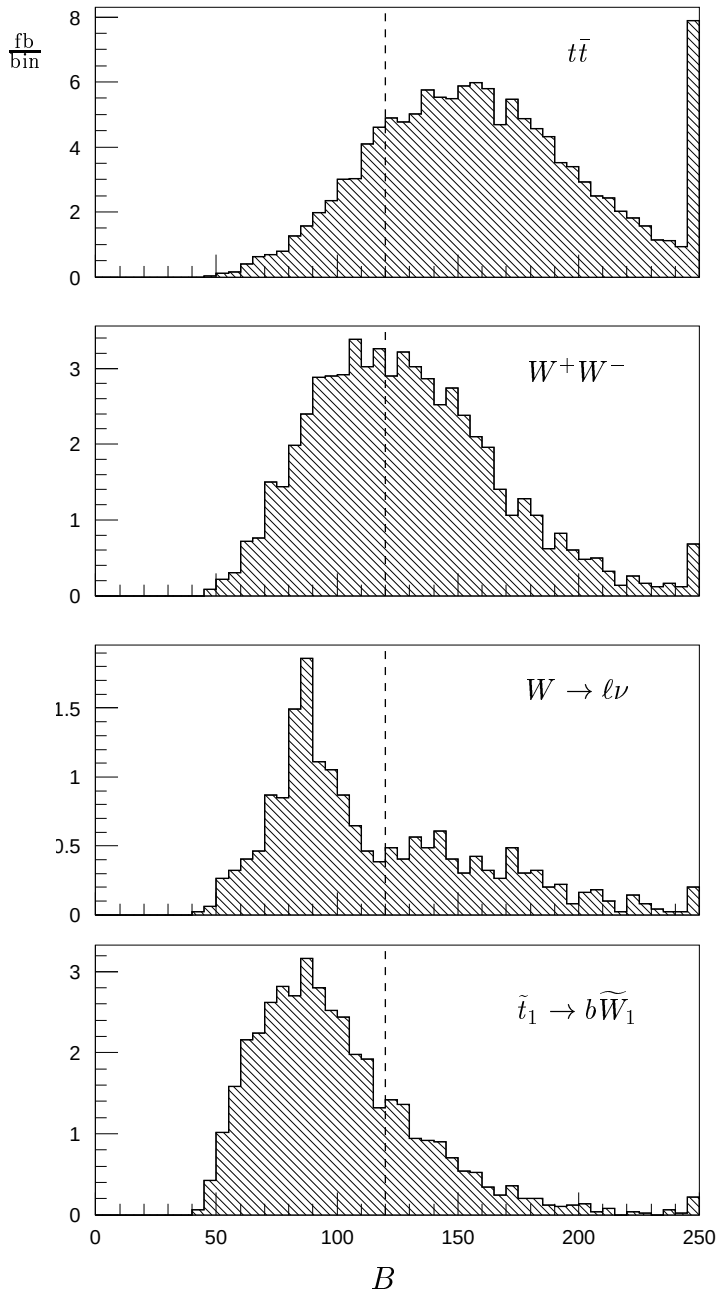

Figure 5.9: Distribution of B in the dilepton channel, after cut (*vi*). The signal case is a 130 GeV $\tilde{t}_1$ decaying to a 100 GeV $\widetilde{Z}_1$. The vertical axes are in fb/bin. Dashed lines at $B = 120$ indicate cut (*vii*).

result in harder lepton momenta. We also find, for the $\tilde{t}_1/\widetilde{W}_1/\widetilde{Z}_1$ masses accessible in this channel, that the backgrounds generally have higher $\not\!\!E_{\rm T}$. The background events are thus "bigger" than the signal events, and a convenient quantity summarizing these features is "bigness"

$$B \equiv p_{\rm T}(\ell^+) + p_{\rm T}(\ell^-) + \not\!\!E_{\rm T} \tag{5.8}$$

which was first introduced in our Run I work [28]. Figure 5.9 shows distributions of B after cut (vi). We find that the discovery reach over the parameter space is maximized with the cut

$$(vii) \quad B < 120 \text{ GeV}.$$

Table 5.2 demonstrates the utility of this cut: only 20% of the $t\bar{t}$ and 50% of the WW backgrounds survive, while we keep 60–75% of the signal.

The reach in the dilepton channel after cut (vii) is still substantially less than that of the b-jet + lepton channel. The situation is improved a bit by considering the total jet transverse energy $J_{\rm T} \equiv \sum_{\rm jets} \left| E_{\rm T} \right|$ whose distributions are shown in Fig. 5.10. $J_{\rm T}$ for the W and Z backgrounds is rather lower than that of the signal, while $J_{\rm T}$ for $t\bar{t}$ is higher. We use the cut

$$(viii) \quad 25 < J_{\rm T} < 175 \text{ GeV}$$

which cuts 1/3 of the background at a cost of less than 1/6 in signal, as shown in Table 5.2.

Figure 5.11 displays contours of the cross-sections after cut $(viii)$ in the $m_{\tilde{t}_1}$–$m_{\widetilde{W}_1}$ plane with $m_{\widetilde{Z}_1} = m_{\widetilde{W}_1}/2$ and $\mathcal{B}(\widetilde{W}_1 \to \ell) = \mathcal{B}(W \to \ell)$. The total background is 49 fb. The 5σ discovery limit for 2 fb^{-1} is 25 fb, shown as a heavy solid line in the figure. The dashed line is at 12 fb = 25% of background. The reach in this

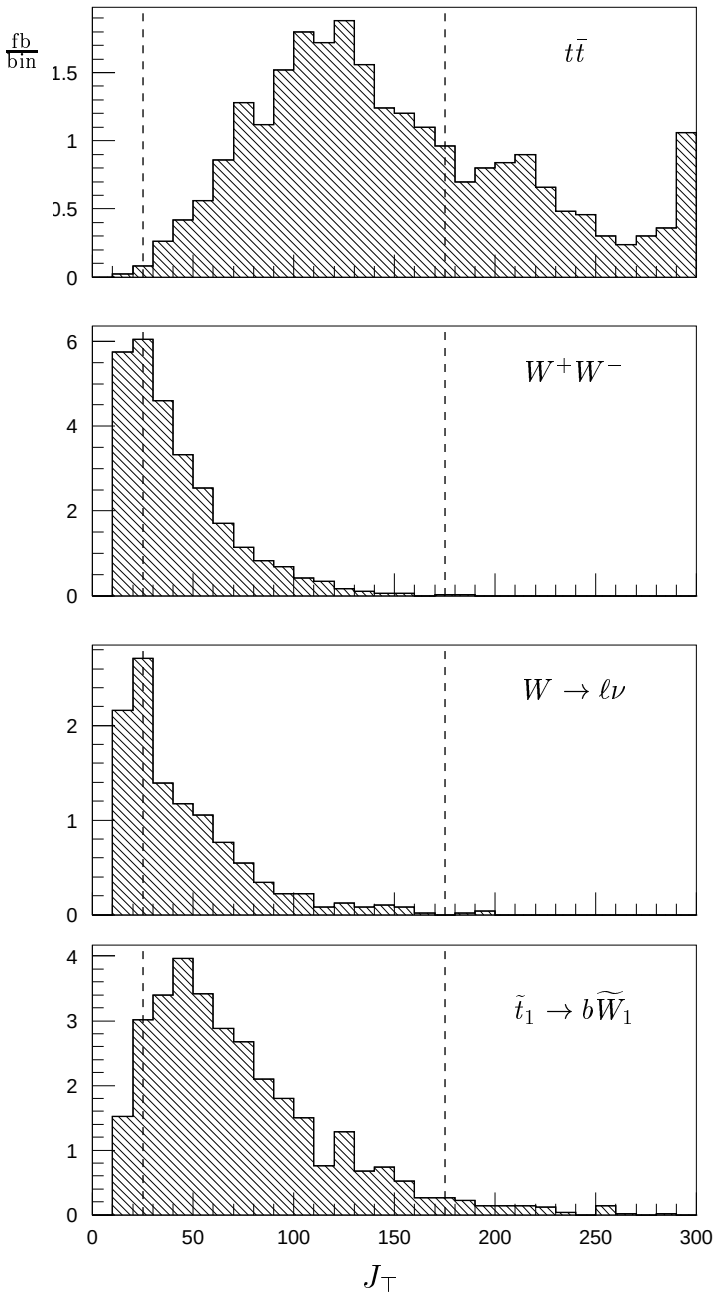

Figure 5.10: Distribution of $J_{\rm T}$ in the dilepton channel, after cut (*vii*). The signal case is a 130 GeV $\tilde{t}_1$ decaying to a 100 GeV $\widetilde{Z}_1$. The vertical axes are in fb/bin. Dashed lines show cut (*vii*) as $25 < J_{\rm T} < 175$ GeV.

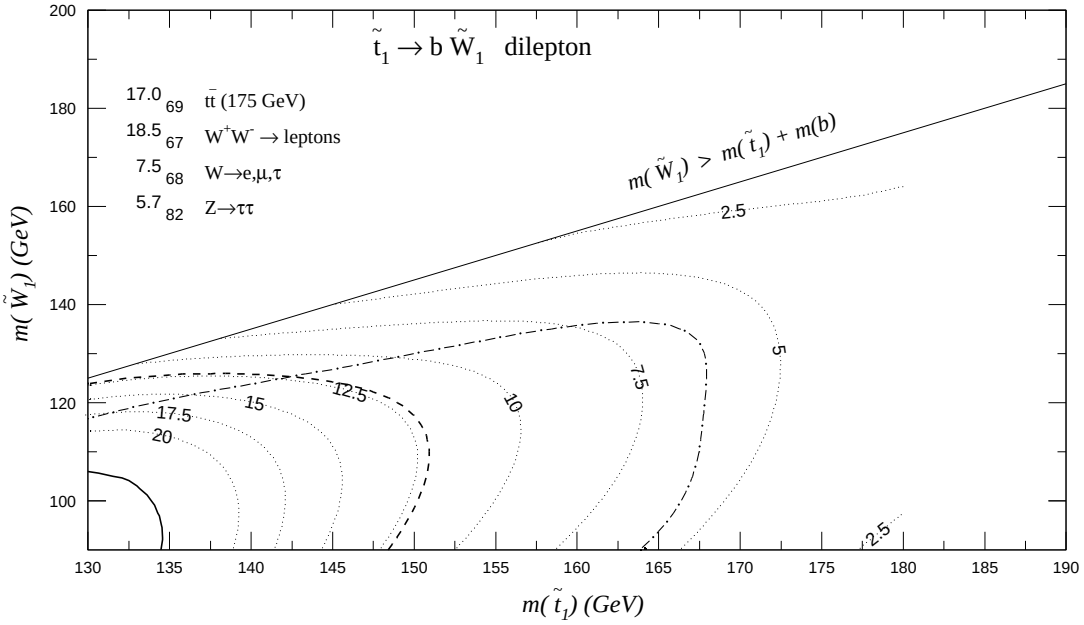

10

Figure 5.11: Cross-section contours, in fb, for the dilepton channel after cut (*viii*) as described in the text. The heavy solid line at 24.7 fb is the 5σ discovery limit for an integrated luminosity of 2 fb^{-1}. The dashed line is 12.1 fb of signal, which is 25% of background. The dot-dashed line shows the reach at 25 fb^{-1} after cut (*ix*).

channel is significantly less than that of the b-jet + lepton channel; $\tilde{t}_1$s heavier than 135 GeV are not accessible via this search.

Relaxing the assumption $\mathcal{B}(\widetilde{W}_1 \to \ell) \approx \mathcal{B}(W \to \ell)$

Because the cross-section for dilepton events goes as the square of $\mathcal{B}(\widetilde{W}_1 \to \ell)$, substantial improvement is possible. The situation will continue to improve as the enhancement factor r of eqn. (5.6) discussed in the previous section increases to its limit $r = 3$, at which point the signal cross-section in this channel would go up by an order of magnitude. In such a case even just 2 fb^{-1} of data could find any stops with $m_{\tilde{t}_1} \lesssim m_t$, even if the chargino is very close to the kinematical limit $m_{\widetilde{W}_1} < m_{\tilde{t}_1} + m_b$. Also, should a stop be discovered in the b-jet + lepton channel of the previous section, then a search in the dilepton channel might yield useful information about $\mathcal{B}(\widetilde{W}_1 \to \ell)$ which, together with basic facts about the $\widetilde{W}_1$ discernible from the discovery, could shed some light on other SUSY parameters.

5.2.3 Run II+

This channel is severely rate limited. We can reach the dashed 25% contour at 12.1 fb in Fig. 5.11 by using cuts $(i) - (viii)$ on an 8.3 fb^{-1} data sample, by eqn. (3.6). This gives us stops out to $m_{\tilde{t}_1} \lesssim 150$ GeV and charginos to $m_{\widetilde{W}_1} \lesssim 120$ GeV. We are background limited here and another cut is required to go further. For the 25 fb^{-1} Run II+ sample, we can eliminate much of the W and Z background by insisting on a tagged b quark:

$$(ix) \quad \text{at least one tagged } B.$$

We did not impose a b-tag requirement for the Run II cuts, since there is not enough signal at 2 fb^{-1} to sustain such a cut. Also, Fig. 5.11 shows that one pays a penalty

for the b-tag, in that an unobservable region of small $m_{\tilde{t}_1} - m_{\widetilde{W}_1}$ is created where the b does not have enough energy to generate the tag. Table 5.2 exhibits the results of this cut. With (ix), the 25 fb^{-1} 5σ discovery limit is extended to the dot-dashed line shown in Fig. 5.11, which pushes the stop mass reach to just over 165 GeV, and increases the region where the SUSY signal can be identified in more than one channel. Detection in both channels helps to identify that the signal is indeed a stop, and can also yield useful information on other SUSY parameters relevant to branching fractions and masses.

Chapter 6

Summary and Conclusions

In this work we have studied two important stop decay modes, $\tilde{t}_1 \to c\widetilde{Z}_1$ and $\tilde{t}_1 \to b\widetilde{W}_1$, in the context of the Run II Tevatron experiments. We have identified useful kinematical quantities for distinguishing the stop signal events from SM backgrounds. We found that these backgrounds could be controlled well enough to expose the stop over a significant range of the parameter space of many models, so that Tevatron experiments in the Main Injector era will probe models not accessible to LEP II.

Our results are summarized in Fig. 6.1. Both the $m_{\tilde{t}_1} \times m_{\widetilde{Z}_1}$ and $m_{\tilde{t}_1} \times m_{\widetilde{W}_1}$ planes are displayed, after the fashion of Fig. 2.6. As with that figure, the vertical axes for $m_{\widetilde{Z}_1}$ and $m_{\widetilde{W}_1}$ will coincide in case $m_{\widetilde{W}_1} = 2m_{\widetilde{Z}_1}$ (indeed, the $\tilde{t}_1 \to b\widetilde{W}_1$ contours correspond to $m_{\widetilde{W}_1} = 2m_{\widetilde{Z}_1}$).

For the $\tilde{t}_1 \to c\widetilde{Z}_1$ mode we show the discovery limits at 2 fb^{-1} and 25 fb^{-1}, for both the $\not\!\!E_{\rm T}$ channel and the c-tagged channel. The irregular hatched region is excluded at the 95% confidence level by LEP II and Tevatron Run I experiments. Figure 6.1 shows the c-tagged channel channel to be clearly superior to the $\not\!\!E_{\rm T}$ channel for this decay mode. While the reach in $\tilde{t}_1$ mass is comparable for the two,

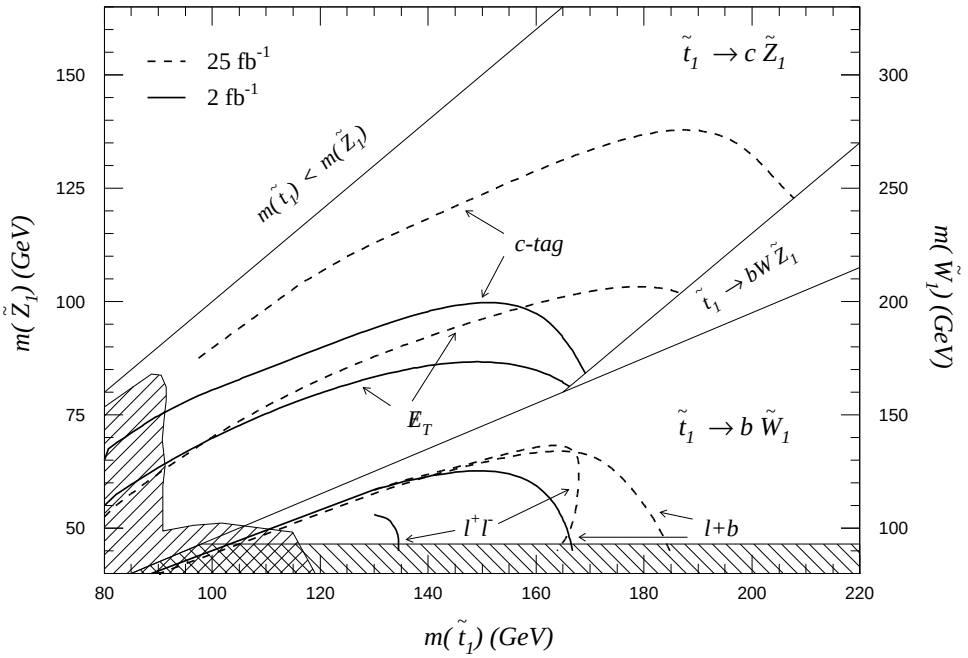

Figure 6.1: Summary of 5σ discovery limits for the light stop. The vertical axis on the left is neutralino mass, and that on the right is chargino mass. In case $m_{\widetilde{W}_1} = 2m_{\widetilde{Z}_1}$, these axes coincide as illustrated. Solid contours show the reach at 2 fb^{-1}; dashed lines are for 25 fb^{-1}. The irregularly shaped hatched region at the left is excluded at the 95% confidence level in the $\tilde{t}_1 \to c\widetilde{Z}_1$ mode by LEP II and Tevatron Run I experiments. The hatched region under $m_{\widetilde{W}_1} = 93$ is excluded by LEP II chargino mass limit.

c-tagging allows heavier $m_{\widetilde{Z}_1}$ to be probed. This is chiefly due to the large jet $E_{\rm T}$ requirement in the $\not\!\!E_{\rm T}$+ jets search which means that $m_{\tilde{t}_1} - m_{\widetilde{Z}_1}$ must be large to yield hard c-jets. In either channel, we may find stops with masses below 165 GeV in Run II. The c-tagged channel generally gives an extra 15 GeV of reach in $\widetilde{Z}_1$ mass.

For higher integrated luminosities, the stop mass may be pushed well past the top mass, and c-tagging with 25 fb^{-1} of data allows discovery of stops heavier than 200 GeV. In the Run II+ scenario, c-tagging extends the $\widetilde{Z}_1$ mass reach by 20 to 30 GeV over the $\not\!\!E_{\rm T}$ channel. Note however that as the $\tilde{t}_1$ becomes heavier the four-body decay discussed in Section 2.2 may have a substantial branching fraction.

Results for the $\tilde{t}_1 \to b\widetilde{W}_1$ decay mode are shown in the lower right portion of Fig. 6.1. The $\ell + b$-jet and dilepton channels are illustrated, under our usual assumptions $m_{\widetilde{W}_1} = 2m_{\widetilde{Z}_1}$ and $\mathcal{B}(\widetilde{W}_1 \to \text{leptons}) = \mathcal{B}(W \to \text{leptons})$. The hatched region $m_{\widetilde{W}_1} < 93$ GeV has been excluded by LEP II at the 95% confidence level.

For this mode, with W-like chargino branching fractions, the dilepton signal is of scant use compared to the $\ell + b$-jet channel with just 2 fb^{-1}. However, when $\mathcal{B}(\widetilde{W}_1 \to \text{leptons}) \gg \mathcal{B}(W \to \text{leptons})$ the dilepton channel rapidly improves. A detection in either or both of these channels could, by differential analysis of the two, yield valuable information about other sectors of the MSSM, particularly if kinematical evidence could be used to constrain the SUSY masses. Even supposing $\mathcal{B}(\widetilde{W}_1 \to \text{leptons}) = \mathcal{B}(W \to \text{leptons})$, we could probe stops out past 165 GeV with the data of Run II, and push this another 20 GeV or so with the higher integrated luminosity of Run II+.

Note that the Run II+ discovery frontiers plotted in Fig. 6.1 for the $\ell + b$ and dilepton channels coincide for $m_{\tilde{t}_1} < 165$ GeV at the high $m_{\widetilde{W}_1}$ end of the range. This reflects the fact that the $\ell + b$ signal is strongly attenuated in the limit

$m_{\tilde{t}_1} \to m_{\widetilde{W}_1}$ as the available energy for a hard identifiable b-jet decreases, while the dilepton suffers less in this limit. Since the statistical significance of the two channels is comparable in this region, the two could be statistically combined to gain a bit more reach in $m_{\widetilde{W}_1}$.

In conclusion, we have demonstrated that the Fermilab Tevatron can probe significant and interesting portions of the light stop parameter space with experiments conducted during the initial and extended Run II operating phases. Particularly important, the procedures we have developed here should allow the Tevatron to test most of the region $m_{\tilde{t}_1} \lesssim 165$ GeV favored by electroweak baryogenesis within mSUGRA models with minimal low-energy particle content.

The large top Yukawa coupling and the availability of substantial LR mixing due to the trilinear scalar coupling make the stop the lightest sfermion in many models, and it may, in principle, be the lightest charged supersymmetric particle. The fact that the Tevatron can subject this hypothesis to a strong test holds out the exciting possibility that supersymmetry may make its first appearance in the discovery of the stop.

Bibliography

[1] *Physics Analysis Workstation 2.12/10 Reference Manual*, CERN Program Library (1999)

[2] S. Abachi et al. (D0 Collaboration), "The D0 Detector" Nucl. Instrum. Meth. **A324**, 185 (1995)

[3] S. Abachi et al. (D0 Collaboration), "Search for squarks and gluinos at $\sqrt{s} =$ 1.8 TeV" Phys. Rev. Lett. **75**, 618 (1995)

[4] S. Abachi et al. (D0 Collaboration), "Search for light top squarks in $p\overline{p}$ collisions at 1.8 TeV" Phys. Rev. Lett. **76**, 2222 (1996)

[5] S. Abachi et al. (D0 Collaboration), "Direct measurement of the top quark mass" Phys. Rev. Lett. **79**, 1197 (1997)

[6] S. Abachi et al. (D0 Collaboration), "Search for top squark pair production in the dielectron channel" Phys. Rev. **D57**, 589 (1998)

[7] B. Abbot et al. (D0 Collaboration), "Measurement of the top quark mass using dilepton events" Phys. Rev. Lett. **80**, 2063 (1998)

[8] S. Abachi et al. (D0 Collaboration), "Search for squarks and gluinos in events containing jets and a large imbalance in transverse momentum" Phys. Rev. Lett. **83**, 4937 (1999)

[9] B. Abbot et al. (D0 Collaboration), "Direct measurement of top quark mass" Phys. Rev. **D58**, 052001 (1998)

[10] G. Abbiendi et al. (OPAL Collaboration), "Search for scalar top and scalar bottom quarks at $\sqrt{s} = 189$ GeV at LEP" Phys. Lett. **B456**, 95 (1999)

[11] G. Abbiendi et al. (OPAL Collaboration), "Search for chargino and neutralino production at $\sqrt{s} = 189$ GeV at LEP " CERN-EP/99-123, to appear in Eur. Phys. J. C (1999)

[12] F. Abe et al. (CDF Collaboration), "The CDF detector: an overview" Nucl. Instrum. Meth. **A271**, 387 (1988)

[13] F. Abe et al. (CDF Collaboration), "Measurement of the top quark mass" Phys. Rev. Lett. **79**, 1992 (1997)

[14] F. Abe et al. (CDF Collaboration), "Search for gluinos and squarks at the Fermilab Tevatron collider" Phys. Rev. **D56**, R1357 (1997)

[15] F. Abe et al. (CDF Collaboration), "Measurement of the top quark mass with the Collider Detector at Fermilab" Phys. Rev. Lett. **80**, 2779 (1998)

[16] F. Abe et al. (CDF Collaboration), "Kinematics of $t\bar{t}$ events at CDF" Phys. Rev. Lett. **80**, 2767 (1998)

[17] M. Acciarri et al. (L3 Collaboration), "Searches for scalar quarks in e^+e^- interactions at $\sqrt{s} = 189$ GeV" Phys. Lett. **B471**, 308 (1999)

[18] M. Acciarri et al. (L3 Collaboration), "Search for charginos and neutralinos in e^+e^- collisions at $\sqrt{s} = 189$ GeV" Phys. Lett. **B472**, 420 (2000)

[19] T. Affolder et al. (CDF Collaboration), "Search for scalar top and scalar bottom quarks in $p\overline{p}$ collisions at $\sqrt{s} = 1.8$ TeV" hep-ex/bf 9910049, to appear in Phys. Rev. Lett. (1999)

[20] T. Affolder et al. (CDF Collaboration), "Search for scalar top quark production in $p\overline{p}$ collisions at $\sqrt{s} = 1.8$ TeV" FERMILAB-PUB-99/340 hep-ex/bf 9912018 submitted to Phys. Rev. Lett. (1999)

[21] S. Ahmed et al. (CLEO Collaboration), CLEO Report CONF 99-10 (1999)

[22] U. Amaldi, W. de Boer and H. Furstenau, "Comparison of grand unified theories with electroweak and strong coupling constants measured at LEP" Phys. Lett. **B260**, 447 (1991)

[23] H. Baer, M. Diaz, P. Quintana and X. Tata, "Impact of physical principles at very high energy scales on the superparticle mass spectrum" JHEP **0004**, 016 (2000)

[24] H. Baer, M. Drees, R. Godbole, J. Gunion and X. Tata, "Phenomenology of light stops at the Fermilab Tevatron" Phys. Rev. **D44**, 725 (1991)

[25] H. Baer, K. Cheung and J. Gunion, "A heavy gluino as the lightest supersymmetric particle" Phys. Rev. **D59**, 075002 (1999)

[26] H. Baer, F. Paige, S. Protopopescu and X. Tata, in *Proceedings of the Workshop on Physics at Current Accelerators and Supercolliders*, edited by J. Hewett, A. White and D. Zeppenfeld, Argonne National Laboratory (1993)

[27] H. Baer, F. Paige, S. Protopopescu and X. Tata, "ISAJET 7.48: A monte carlo event generator for pp, $\bar{p}p$, and e^+e^- interactions" hep-ph/bf 0001086 (2000)

[28] H. Baer, J. Sender and X. Tata, "Search for top squarks at the Fermilab Tevatron collider" Phys. Rev. **D50**, 4517 (1994)

[29] R. Barate et al. (ALEPH Collaboration) "Searches for sleptons and squarks in e^+e^- collisions at 189 GeV" Phys. Lett. **B469**, 303 (1999)

[30] R. Barate et al. (ALEPH Collaboration) "Search for charginos and neutralinos in e^+e^- collisions at centre-of-mass energies near 183 GeV and constraints on the MSSM parameter space" Eur. Phys. J. **C11**, 193 (1999)

[31] R. Barbieri and G.F. Giudice, "$b \to s\gamma$ decay and supersymmetry" Phys. Lett. **B309**, 86 (1993)

[32] V. Barger, M.S. Berger and P. Ohmann, "Implications of supersymmetric grand unification" MAD/PH/826 (1994)

[33] V. Barger and R. Phillips, *Collider Physics* Addison Wesley Publishing (1988)

[34] A. Bartl, H. Eberl, S. Kraml, W. Majerotto and W. Porod, "Scalar top quark production at $\mu^+\mu^-$ colliders" hep-ph/bf 9712412 (1997)

[35] A. Bartl, H. Eberl, S. Kraml, W. Majerotto and W. Porod, in *Proceedings of the 2nd Joint ECFA/DESY Study on Physics and detectors for a linear electron-positron collider* (2000)

[36] W. Beenakker, M. Krämer, T. Plehn, M. Spira, P.M. Zerwas, "Stop production at hadron colliders" Nucl. Phys. **B515**, 3 (1998)

[37] E.L. Berger, B.W. Harris and Z. Sullivan, "Single top squark production via R parity violating supersymmetric couplings in hadron collisions" Phys. Rev. Lett. **83**, 4472 (1999)

[38] C. Boehm, A. Djouadi and M. Drees, "Light scalar top quarks and supersymmetric dark matter" Phys. Rev. **D61**, 095006 (2000)

[39] C. Boehm, A. Djouadi and Y. Mambrini, "Decays of the lightest top squark" Phys. Rev. **D61**, 095006 (2000)

[40] A. Bouquet, J. Kaplan and C.A. Savoy, "Low-energy constraints on supergravity parameters" Nucl. Phys. **B262**, 299 (1985)

[41] CDF Collaboration, FERMILAB-Pub-96/390-E (1996)

[42] F. de Campos et al., in *Proceedings of the Workshop "Physics at Run II: Supersymmetry/Higgs Fermilab, Feb. - Nov. 1998"* (1998)

[43] M. Carena, M. Quiros and C.E.M. Wagner, "Electroweak baryogenesis and Higgs and stop searches at LEP and the Tevatron" Nucl. Phys. **B524**, 3 (1998)

[44] L. Clavelli, "New possibilities for a light gluino" hep-ph/bf 9908342 (1999)

[45] S. Coleman and J. Mandula, "All possible symmetries of the S matrix" Phys. Rev. **159**, 1251 (1967)

[46] D0 Collaboration, FERMILAB Pub-96/357-E (1996)

[47] A. Datta, M. Guchait and K.K. Jeong, "Stop squark search at Tevatron in the light slepton scenario" Int. J. Mod. Phys. **A14**, 2239 (1999)

[48] D. Delepine, J.-M. Gerard, R. Gonzalez Felipe and J. Weyers, "A light stop and electroweak baryogenesis" Phys. Lett. **B386**, 183 (1996)

[49] S. Deser and B. Zumino, "Consistent supergravity" Phys. Lett. **62B**, 335 (1976)

[50] D. Dicus and V. Mathur, Phys. Rev. **D7**, 3111 (1973)

[51] R. Demina, J.D. Lykken, K.T. Matchev and A. Nomerotski, "Stop and sbottom searches in Run II of the Fermilab Tevatron" hep-ph/bf 9910275 (Submitted to Phys. Rev. D) (1999)

[52] S. Dimopoulos and D. Sutter, "The supersymmetric flavor problem" Nucl. Phys. **B452**, 496 (1995)

[53] P.J. Dornan for the ALEPH Collaboration, "ALEPH status report" at LEPC March 7, 2000, Imperial College, London (2000)

[54] C.B. Dover, T. Gaisser and G. Steigman, "Cosmological constraints on new stable hadrons" Phys. Rev. Lett. **42**, 1117 (1979)

[55] M. Drees and K. Hagiwara, "Supersymmetric contribution to the electroweak ρ parameter" Phys. Rev. **D42**, 1709 (1990)

[56] M. Drees and S. Martin, in *Electroweak Symmetry Breaking and New Physics at the TeV Scale* edited by T. Barklow, S. Dawson, H. Haber and J. Siegrist, World Scientific (to be published)

[57] F. Dyson, Sci. Am. sept. 64, 129 (1964)

[58] J. Ellis and S. Rudaz, "Search for supersymmetry in toponium decays" Phys. Lett. **128B**, 248 (1983)

[59] J. Erler and D.M. Pierce, "Bounds on supersymmetry from electroweak precision analysis" Nucl. Phys. **B526**, 53 (1998)

[60] D. Freedman, S. Ferrara and P. van Nieuwenhuizen, "Progress toward a theory of supergravity" Phys. Rev. **D13**, 3214 (1976)

[61] H. Georgi and S.L. Glashow, "Unity of all elementary particle forces" Phys. Rev. Lett. **32**, 438 (1974)

[62] M.T. Grisaru, W. Siegel and M. Rocek, "Improved methods for supergraphs" Nucl. Phys. **B159**, 429 (1979)

[63] L. Girardello and M. T. Grisaru, "Soft Breaking Of Supersymmetry" Nucl. Phys. **B194**, 65 (1982)

[64] R. Haag, J.T. Łopuszanski and M.F. Sohnius, "All possible generators of supersymmetries of the S matrix" Nucl. Phys. **B88**, 257 (1975)

[65] H. Haber and G. Kane, "The search for supersymmetry: probing physics beyond the standard model" Phys. Rept. **117**, 75 (1985)

[66] K. Hikasa and M. Kobayashi, "Light scalar top at e^+e^- colliders" Phys. Rev. **D36**, 724 (1987)

[67] M. Hosch, R.J. Oakes, K. Whisnant, Jin Min Yang, Bing-lin Young, X. Zhang, "Probing top quark decay into light stop in the supersymmetric standard model at the upgraded Tevatron" Phys. Rev. **D58**, 034002 (1998)

[68] L. Ibanez and C. Lopez, "N=1 supergravity, the weak scale and the low-energy particle spectrum" Nucl. Phys. **B233**, 511 (1984)

[69] K. Inoue, A. Kakuto, H. Komatsu and H. Takeshita, "Aspects of grand unified models with softly broken supersymmetry" Prog. Theor. Phys. **68**, 927 (1982)

[70] D.R.T. Jones, "Introduction to supersymmetry" in S. Raby and T. Walker (eds.) *The Building Blocks of Creation, Proceedings of the 1993 TASI*, World Scientific (1994)

[71] M. Jones, "Top mass measurements" talk given at 1998 Moriond Electroweak Conference (1998)

[72] G. Jungman and M. Kamionkowski, "Supersymmetric dark matter" Phys. Rept. **267**, 195 (1996)

[73] S. Katsanevas and S. Melachroinos, SUSYGEN

[74] V.A. Kuzmin, V.A. Rubakov and M.E. Shaposhnikov, "On the anomalous electroweak baryon number nonconservation in the early universe" Phys. Lett. **B155**, 36 (1985)

[75] H.L. Lai *et al.*, "Global QCD analysis and the CTEQ parton distributions" Phys. Rev. **D51**, 4763 (1995)

[76] B. W. Lee, C. Quigg and H. B. Thacker, "Weak Interactions At Very High-Energies: The Role Of The Higgs Boson Mass" Phys. Rev. **D16**, 1519 (1977)

[77] Chong Sheng Li, R.J. Oakes and Jin Min Yang, "One loop qcd corrections to top quark decay into neutralino and light stop" Phys. Rev. **D54**, 6883 (1996)

[78] G. Marchesini, B.R. Webber, G. Abbiendi, I.G. Knowles, M.H. Seymour and L. Stanco, "HERWIG 6.1" Computer Phys. Commun. **67**, 465 (1992)

[79] S. Mrenna, "SPYTHIA, a supersymmetric extension of PYTHIA 5.7" Comput. Phys. Commun. **101** 232 (1997)

[80] G. Münster, "The role of mathematics in contemporary theoretical physics" in E. Rudolf and I.-O. Stamatescu (eds.) *Philosophy, Mathematics and Modern Physics*, Springer Verlag (1994)

[81] P. Nath, R. Arnowitt and A. Chamseddine, *Applied N=1 Supergravity*, ICTP Series in Theoretical Physics Vol. 1, World Scientific (1984)

[82] H.P. Nilles, "Supersymmetry, supergravity and particle physics" Phys. Rept. **110**, 1 (1984)

[83] Y. Okada, "Light stop and the $b \to s\gamma$ process" Phys. Lett. **B315**, 119 (1993)

[84] J.C. Pati and A. Salam, "Lepton number as the fourth color" Phys. Rev. Lett. **32**, 1083 (1974)

[85] J.C. Pati, in *Superstrings, Compositeness and Cosmology*, edited by S. Gates and R. N. Mohapatra, World Scientific (1987)

[86] W. Porod and T. Wöhrmann, "Higher order top squark decays" Phys. Rev. **D55**, 2907 (1997)

[87] W. Porod, "More on higher order decays of the lighter top squark" Phys. Rev. **D59**, 5009 (1999)

[88] A. Sakharov, "Violation of CP invariance, C asymmetry, and baryon asymmetry of the universe" JETP Lett. **5**, 24 (1967)

[89] J. Sender, "Top to stop branching fraction limits from the Fermilab Tevatron top experiments" Phys. Rev. **D54**, 3271 (1996)

[90] Lian You Shan, Shou Hua Zhu, "Top decays into lighter stop and gluino" hep-ph/bf 9811430 (1998)

[91] A. Sopczak, "Higgs boson searches at LEP up to $\sqrt{s} = 202$ GeV" presented at the Seventh International Symposium on Particles, Strings, and Cosmology, PASCOS-99, Granlibakken, USA, Dec 10-16, 1999 (2000)

[92] L. Susskind, "The gauge hierarchy problem, technicolor, supersymmetry, and all that" Phys. Rept. **104**, 181 (1984)

[93] X. Tata, *What is supersymmetry and how do we find it?*, Lectures presented at the IX Jorge A. Swieca Summer School, Campos do Jordão, Brazil, Report no. UH-511-872-97 (1997)

[94] *Physics at the Tevatron Run II* Plenary talk at Pheno 2000, Madison WI (2000)

[95] S. Weinberg, *The Quantum Theory of Fields, Volume I*, Cambridge University Press (1995)

[96] Eugene Wigner, *Gruppentheorie und ihre Anwendung auf die Quantenmechanik der Atomspektren*, Braunschweig (1931)

[97] Eugene Wigner, "The unreasonable effectiveness of mathematics in the natural sciences" in *Symmetries and Reflections*, Indiana University Press (1967)